

**NUMERICAL AND EXPERIMENTAL ANALYSIS ON THERMAL
STRESS MEASUREMENT OF SPIRAL WELDED PIPES**

BY
KHALID NASEEM

A Thesis Presented to the
DEANSHIP OF GRADUATE STUDIES

KING FAHD UNIVERSITY OF PETROLEUM & MINERALS
DHAHRAN, SAUDI ARABIA

In Partial Fulfillment of the
Requirements for the Degree of

MASTER OF SCIENCE

In

MECHANICAL ENGINEERING

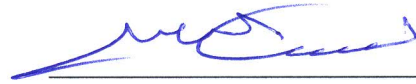
NOVEMBER 2013

**KING FAHD UNIVERSITY OF PETROLEUM & MINERALS
DHAHRAN, SAUDI ARABIA**

DEANSHIP OF GRADUATE STUDIES

This thesis, written by **Khalid Naseem** under the direction of his thesis advisor and approved by his thesis committee, has been presented to and accepted by the Dean of Graduate Studies, in partial fulfillment of the requirements for the degree of **MASTER OF SCIENCE in MECHANICAL ENGINEERING**.

Thesis Committee



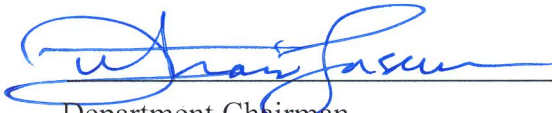
Thesis Advisor

Dr. Yagoub N. Al-Nassar



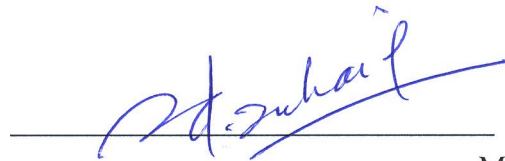
Member

Prof. Abul Fazal M. Arif



Department Chairman

Dr. Zuhair Gasem



Member

Dr. Syed Sohail Akhtar



Dean of Graduate Studies

Prof. Salam A. Zummo

25/2/14

Date





Dedicated to my parents, my brothers and my sisters

ACKNOWLEDGEMENTS

In the Name of Allah, the Most Beneficent, the Most Merciful.

Praise belongs to Allah, the Lord of all the worlds (2) The All-Merciful, the Very-Merciful. (3) The Master of the Day of Requital. (4) You alone do we worship, and from You alone do we seek help. (5) Take us on the straight path (6) The path of those on whom You have bestowed Your Grace, Not of those who have incurred Your wrath, nor of those who have gone astray. (7)

Al-Fatiha

I begin with the name of Allah, the most beneficent, the most merciful. May Allah bestow peace on our beloved Prophet Mohammed (*peace and blessings of Allah be upon him*), and his family. I would not have able to complete this work without the help of Allah who endowed me with health, courage, aptitude and patience.

During this work my parents were a constant source of motivation and support. Their prayers, love and encouragement helped me to arrive at this milestone. I would like to thank my teachers. The things I learnt from are some of the most important lessons of my life.

Acknowledgements are due to *King Fahd University of Petroleum and Minerals* which gave me the opportunity to pursue a graduate degree and also for all the support I received in carrying out this research. I am also grateful to the *Deanship of Scientific Research at KFUPM* (DSR project # SB101009) for providing their support during this research.

I would like to express my gratitude to my thesis advisor Dr. Yagoub N. Al-Nassar for all he taught me, for his patience when I couldn't get things done and for his help when I needed it. I

am especially very thankful to my thesis committee members Prof. Abul Fazal M. Arif and Dr. Sohail Akhtar for their involvement and encouragement. I also like to express gratitude to Mr. Anis for his consistent involvement in the experimental work. I believe that without their consistent help, motivation and interest; I couldn't be able to accomplish this work. I also particularly appreciate the effort of Ahmed Saleh Al-Omari for playing his key role in arranging our visit to Welspun Middle East. I am thankful to this industry and their staff members for providing us the sample to conduct this research.

I sincerely thank my seniors Muhammad Usama Siddiqui and Muhammad Haris Malik for all the help they provided through the course of this work. Not forgotten, special thanks to my friends Muhammad Ibrar Hussain and Osama Hasan for their immense dedication whenever I needed them. Last but not the least, I am very grateful to Sheraz Khalid, Waqas Khalid, Bilal Tanweer, Adnan Saeed, Waqas Akram and all my colleagues in the Mechanical Engineering department for the friendly atmosphere and memorable times.

TABLE OF CONTENTS

ACKNOWLEDGEMENTS	IV
TABLE OF CONTENTS	VI
LIST OF TABLES	X
LIST OF FIGURES	XI
ABSTRACT (ENGLISH).....	XIV
ABSTRACT (ARABIC)	XV
CHAPTER 1 INTRODUCTION	1
1.1 Background of Production of Steel Pipes	1
1.1.1 Seamless Pipe	1
1.1.2 Fusion Weld.....	2
1.1.3 Electric Resistance Weld.....	2
1.1.4 Double Submerged Arc Weld.....	3
1.2 Application & Use Of Spiral Weld Pipes	6
1.3 Spiral Welded Pipe Production Line	6
1.3.1 Welding Process	7
1.3.2 Principle of Arc Welding.....	8

1.3.3	Multi Arc Welding.....	8
1.4	PROBLEM STATEMENT	10
1.5	PROPOSED OBJECTIVES.....	11
CHAPTER 2	LITERATURE REVIEW	12
2.1	Plate Welding.....	12
2.2	Pipe Welding.....	15
2.3	Springback and Split Ring Test.....	20
2.4	Spiral Pipe Welding	24
CHAPTER 3	COMPUTATIONAL MODEL FOR SPIRAL WELDED PIPE.....	27
3.1	Modelling Methodology.....	27
3.2	Thermal Mathematical Model.....	28
3.3	Structural Mathematical Model.....	31
3.4	Heat Source Modelling.....	32
3.5	Implementation of Moving Goldak Heat Source	33
3.5.1	Determining the e_t vector.....	36
3.5.2	Determining the e_n vector	37
3.5.3	Determining the e_b vector	38
3.6	Finite Element Model.....	39
3.7	Filler material Addition.....	43
CHAPTER 4	WELD INDUCED STRESSES AND EFFECT OF TIME LAG	45
4.1	Validation.....	45
4.1.1	Thermal Validation.....	45
4.1.2	Structural Validation.....	47

4.2	Results and Discussion.....	49
4.3	Effect of Time Lag	59
4.4	Conclusion.....	62
CHAPTER 5 HOOP STRESS DISTRIBUTION AND SPLIT RING TEST ANALYSIS		
.....		64
5.1	Hoop stress in a spiral pipe and its comparison	64
5.2	Residual Hoop Stress Field in Spiral Pipe	67
5.3	Split Ring Test.....	72
5.4	Stress Calculation Procedures	73
5.5	Results and Discussion.....	77
5.6	Conclusion.....	81
CHAPTER 6 EXPERIMENTAL ANALYSIS AND MODEL VALIDATION.....		83
6.1	Introduction	83
6.2	Residual Stress Measurement Techniques	84
6.3	Hole-Drilling Method.....	86
6.4	Principle Of Hole Drilling Strain Gage Method	87
6.5	Experimental Setup for Residual Stress Measurement	88
6.5.1	Installation of strain gage and surface preparation	90
6.5.2	Soldering and connections.....	90
6.5.3	RS-200 Milling guide and setup.....	91
6.5.4	RS-200 setup and alignment procedure.....	92
6.6	P3 Strain Indicator and Data Acquisition Recorder	94
6.6.1	P3 strain recorder setup	94

6.7	Experimental Operation	95
6.8	Stress Calculation.....	97
6.8.1	Uniform method for stress calculation	98
6.8.2	Hole drilling for Non-uniform residual stress distribution.....	101
6.8.3	Power series method for stress calculation.....	102
6.8.4	Integral method for stress calculation.....	105
6.9	Results and Discussion.....	110
6.10	Comparison with FE results	115
6.10.1	Finite element with uniform method	115
6.10.2	Finite element with power method	121
6.11	Conclusion.....	123
CHAPTER 7	CONCLUSION AND RECOMMENDATIONS.....	125
REFERENCES	130
VITAE	138

LIST OF TABLES

Table 3.1: Goldak heat source parameters	41
Table 3.2: Temperature Dependent thermal and mechanical properties	42
Table 4.1: HAZ dimensions	47
Table 4.2: Cross sectional positions along the weld seam	50
Table 4.3: Welding times for different distance lag in pitch	60
Table 5.1: Hoop membrane and hoop bending stress	72
Table 5.2: Hoop membrane and hoop bending stress after split	79
Table 5.3: Membrane and bending stress at weld before and after split	79
Table 5.4: Hoop stress using Ref. [76]	81
Table 5.5: Hoop stress using Ref. [60] and Ref. [62]	81
Table 6.1: Strain gage specification	89
Table 6.2: Coefficients of $\bar{a}^o(h)$ and $\bar{b}^o(h)$ for a stress field, $\sigma^o(h) = 1$ [86]	103
Table 6.3: Coefficients of $\bar{a}^1(h)$ and $\bar{b}^1(h)$ for a stress field, $\sigma^1(h) = h$ [86]	103
Table 6.4: Inner gage FE and experimental data	118
Table 6.5: Outer gage FE and experimental data	118
Table 6.6: von Mises stress comparison for Inner gages	121
Table 6.7: von Mises stress comparison for Outer gages	121

LIST OF FIGURES

Fig. 1.1: Production of steel pipes from different methods	3
Fig. 1.2: Block diagram for manufacturing spiral pipes	5
Fig. 1.3: Different types of pipes production [1]	6
Fig. 1.4: Spiral production line [2].....	7
Fig. 1.5: Inside and Outside Multi arc welding [2].....	9
Fig. 3.1: Local and Global coordinate system	34
Fig. 3.2: Finite element mesh.....	40
Fig. 4.1: Comparison of HAZ dimensions.....	46
Fig. 4.2: Cross sectional temperature distribution	47
Fig. 4.3: Tangential stress distribution.....	49
Fig. 4.4: Temperature variation at each cross section.....	52
Fig. 4.5: Transient temperature (a) At the centre of inner cross-sectional lines (b) At the centre of outer cross-sectional lines	54
Fig. 4.6: Temperature distribution during bottom welding on (a) inner and (b) outer side....	55
Fig. 4.7: Temperature distribution during top welding on (a) inner and (b) outer side	55
Fig. 4.8: Binormal Stress distribution.....	56
Fig. 4.9: During bottom welding and intermediate cooling.....	58
Fig. 4.10: During top welding and final cooling.....	59

Fig. 4.11: Welding positions.....	61
Fig. 4.12: For all cases Plastic strain and von Mises stress ⁴	61
Fig. 5.1: Hoop stress in spiral and longitudinal pipe [23].....	66
Fig. 5.2: Stress dependence on the weld angle [24].....	67
Fig. 5.3: Residual hoop stress distribution normal to weld line.....	68
Fig. 5.4: Residual hoop stress along circumferential direction.....	69
Fig. 5.5: Residual hoop stress along thickness	71
Fig. 5.6: Configuration (a) Before splitting (b) After splitting.....	74
Fig. 5.7: (a) Hoop stress before and after split (b) Stress difference before and after split	78
Fig. 6.1: Different residual stress measurement techniques [75].....	86
Fig. 6.2: Strain gage installation on inner and outer sides	89
Fig. 6.3: Different bondable terminal patterns.....	91
Fig. 6.4: Mounted assembly.....	92
Fig. 6.5: Alignment setup assembly [83]	93
Fig. 6.6: High speed drill assembly [83].....	93
Fig. 6.7: P3 strain indicator.....	94
Fig. 6.8: Weld ring sample for residual stress measurement	97
Fig. 6.9: Typical strain gage rosette [85]	100
Fig. 6.10: Residual stress using different methods	109
Fig. 6.11: Principal stresses along depth for Inner gages	111
Fig. 6.12: Principal stresses along depth for Outer gages.....	113
Fig. 6.13: Principal stresses along depth for IG-3 and OG-3	114
Fig. 6.14: Residual stress distribution on inner side using uniform method.....	116

Fig. 6.15: Residual stress distribution on outer side using uniform method.....	116
Fig. 6.16: Comparison for inner gages.....	119
Fig. 6.17: Comparison for outer gages.....	119
Fig. 6.18: Residual stress distribution on inner side using power series method	122
Fig. 6.19: Residual stress distribution on outer side using power series method	122

ABSTRACT (ENGLISH)

NAME: Khalid Naseem
TITLE: Numerical and experimental analysis on thermal stress
measurement of spiral welded pipes
MAJOR FIELD: MECHANICAL ENGINEERING
DATE OF DEGREE: NOVEMBER 2013

In the field of piping industry, spiral welded pipes are manufactured in large diameter with various length and dimension. Such pipes are generally economical in production with properties like good weldability, rapid production rate and resistance to high pressure. It is being used commonly in all types of industries but its application on large scale is mostly seen in petrochemical industries, oil and gas sector. Residual stresses generated by welding during the production of spiral welded pipe causes imperfection in the material. To ensure the safe service life and performance with high durability, welding induced defects such as welding deformation and residual stresses must be estimated. Due to welding, large local plastic strains are produced in the weld metal and the heat affected zone (HAZ). For this purpose finite element model is developed to simulate the residual stresses due to intense heating and subsequent cooling during welding process. Arc is generated in spiral welded pipes by multiple wire electrodes operated on AC/DC current, adjusted at inside and outside of the pipe. In this work, the time lag between the top and bottom wires is varied and its consequent effects on the residual stress distribution have been studied. The split ring test is analyzed numerically and its limitation is highlighted. Experimentation has been performed on X70 grade steel pipe using hole drilling method for validation. Different hole drilling stress calculation procedure are adopted and analyzed for in depth non-uniform stress estimation.

ABSTRACT (ARABIC)

ملخص الرسالة

الاسم: خالد نسيم

عنوان الرسالة: التحليل العددي والتجريبي لقياس الإجهادات الحرارية في الأنابيب الملحومة لولبيا

التخصص العام: الهندسة الميكانيكية

تاريخ لتخرج: 1435هـ - (نوفمبر 2013م)

في مجال صناعة الأنابيب يتم تصنيع الأنابيب الملحومة لولبيا بأقطار كبيرة مع إختلاف في الأطوال والسماكات ، وهذه النوعية من الأنابيب عادة ما تكون إقتصادية في الإنتاج مع خصائص مثل قابليتها الجيدة للحام، ومعدل الإنتاج السريع لها ، ومقاومتها للضغط العالي. كما إن استخدامها شمل جميع أنواع الصناعات ولكن استخدامها على نطاق واسع في الغالب في الصناعات البتروكيماوية وقطاع النفط والغاز . ولما كان تنفيذ اللحام يتم على مسار لولبي لإنتاج هذه الأنابيب فإن اللحام يؤثر في خصائص المادة المحيطة بها ، ولضمان جودة اللحام وخدمة آمنة وطويلة لهذه الأنابيب مع متانة عالية في الأداء فإن التشوهات التي يسببها واللحام والعيوب التي تصاحبه والاجهادات المتبقية يجب أن نقدر . ومعروف أنه نتيجة لعملية اللحام تتخطى المادة موضعيا حاجز المرونة ، ولهذا الغرض فقد تم تطوير نموذج عنصر محدود لمحاكاة عملية اللحام نفسها وذلك للوقوف على تقدير الاجهادات المتبقية نتيجة للحرارة العالية المصاحبة لعملية اللحام وعملية التبريد التي تلحقه . يتم إنشاء قوس اللحام اللولبي في هذه الأنابيب بواسطة سلكين كهربائيين تعمل على AC / DC أحدهما مثبت في داخل والآخر من خارج الأنبوب ، وتتنوع الفترة الزمنية الفاصلة بين هذين السلكين ، وقد خضع هذا التغير الزمني للدراسة لمعرفة الآثار المترتبة عليه في توزيع الاجهادات المتبقية. كما تم في هذه الدراسة تمثيل اختبار الإنقسام الحلقي عدديا كما تم تحديد مدى الإستفادة منه . كما تم أيضا قياس الاجهادات المتبقية بواسطة جهاز الحفر الموضعي وذلك لمقارنتها مع النتائج العددية ، ل قد أجريت هذه التجارب على X70 أنابيب الصلب. كما طبقت عدة طرق مختلفة لقياس الإجهادات لهذا الشأن.

CHAPTER 1 INTRODUCTION

1.1 BACKGROUND OF PRODUCTION OF STEEL PIPES

For understanding the production of steel pipes, it is necessary to have an understanding about the production of steel and its different forms. The primary raw forms of the steel can be billet, ingot, bloom and slabs. A useful product can be obtained by performing process such as reheating, extrusion or squeezing this largely produced volume of raw steel and converting it into the valuable configuration.

Two basic forms of steel are used for the production of steel pipes i.e. Round billet and the slab. A billet is commonly used for the production of seamless pipes while the other types of the steel pipes are produced by the solid slabs which are reheated and processed firstly into the plate and coils. There are different methods for the production of steel pipes. Among these methods the mostly used are: Seamless, Fusion Weld, Electric Resistance Weld and Double submerged arc Weld.

1.1.1 Seamless Pipe

Seamless pipes are made from the round cylindrical heated billet and then pushed and pulled rapidly over a mandrel with the piercing point which is placed at the center of the billet. This process produces a round hollow tube or shell. The required size and wall thickness is achieved

by further finishing. The size range of these pipes varies from 1/8" to 26". These pipes are suitable for thick walled and exotic chemical industries and also used for coiling, flanging and threading. Moreover, these pipes find their usage in construction, oil refinery and petrochemical industries. But these are unavailable in long length.

1.1.2 Fusion Weld

Fusion weld process is also named as continuous weld in which the pipes are produced in the sizes of 1/8" to 4-1/2". Fusion weld pipes are prepared in sizes from the coiled steel of the required width and thickness and the weight of the pipes. The process consists of the continuous end to end welding of the coil to make ribbon. This ribbon is further fed into leveler and then pulled into a furnace where it is heated up to desired temperature. After fusing at high temperature, the forming rolls are used to shape the heated skelp. The edges of the skelp are pressed firmly and tightly by the roller to get the forged weld. At the final the stage the fusion welded pipes of required length are obtained by sizing the rollers.

1.1.3 Electric Resistance Weld

In Electric resistance welded pipes, a coil strip of appropriate width and thickness is used which made from the rectangular slab. This process is the cold formed. The strip is pulled over the rollers and gradually converted into a cylindrical shape with end to end contact. Electric charge is applied on the edges of the contact point and heating it to a proper weld. In this manufacturing process, the pipes can be made with the length of 115 feet. The automated production line provides high speed and continuous products with uniform thickness and outside dimensions are obtained by this process.

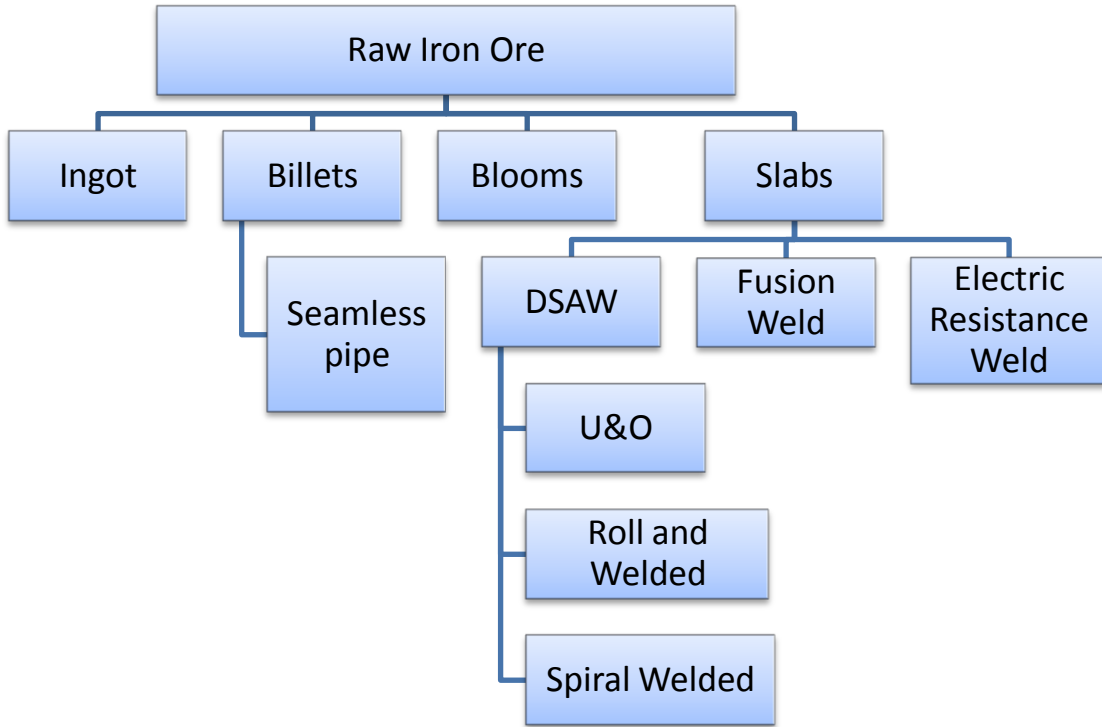


Fig. 1.1: Production of steel pipes from different methods

1.1.4 Double Submerged Arc Weld

Double submerged arc Weld abbreviated as DSAW. Pipes which are produced by this technique are referred as double submerged arc welded pipes. As the name implies welding arc flux is applied. This submerged arc protects the weldment form the impurities present in the air. The steel in heated by welding from both inside and outside. Depending upon the process, the double submerged arc welded pipes are further categorized into three types.

- U&O press
- Rolled and Weld press
- Spiral Weld

U&O press

In this pipe production process, presses are used. These presses are controlled mechanically or hydraulically. It is called expanded and so called U&O press method because first U press is used to make the U- shape of the plate and after this O press is actuated to make a complete cylinder shape. This cylindrical shaped plate is then welded from both inside and outside by submerged arc process in which mostly five wires are used. Pipes are made by this process are exceptionally of high quality with the exact dimensional tolerances.

Rolled and Weld Press

Rolled and Weld press, sometime this process is called as Pyramid roll method. In this method three roller are used which are oriented in configuration to make pyramidal shape. The trimmed edges steel plate of desired thickness and grade is fed into the roller for bending and resulting into shape of a cylinder. This cylindrical bended rolled sheet is transferred to the welding station. These pyramids rollers usually are in length of 20 feet or shorter. It can be capable of producing large diameter pipes with even extremely thick walls. Girth welding is used in production of larger length pipes like 5, 10 or 20 feet.

Spiral Weld

Spiral welded steel pipes are produced by DSAW with the spiral seam along the entire length of the pipe. The angle of the de-coiled steel against the forming head determines the dimension of the outer diameter of the pipe. If the angle between them is more sharp and acute then the resulting pipe will be of larger diameter. The demand of these pipes has been continuously increasing due to its large production from the hot rolled coils of the required length on which the non-destructive testing are performed for the assurance of the quality product. These pipes

can be of large diameter even up to 144 inches with 115 feet in length. The block diagram of the manufacturing spiral welded pipes is shown in Fig. 1.2

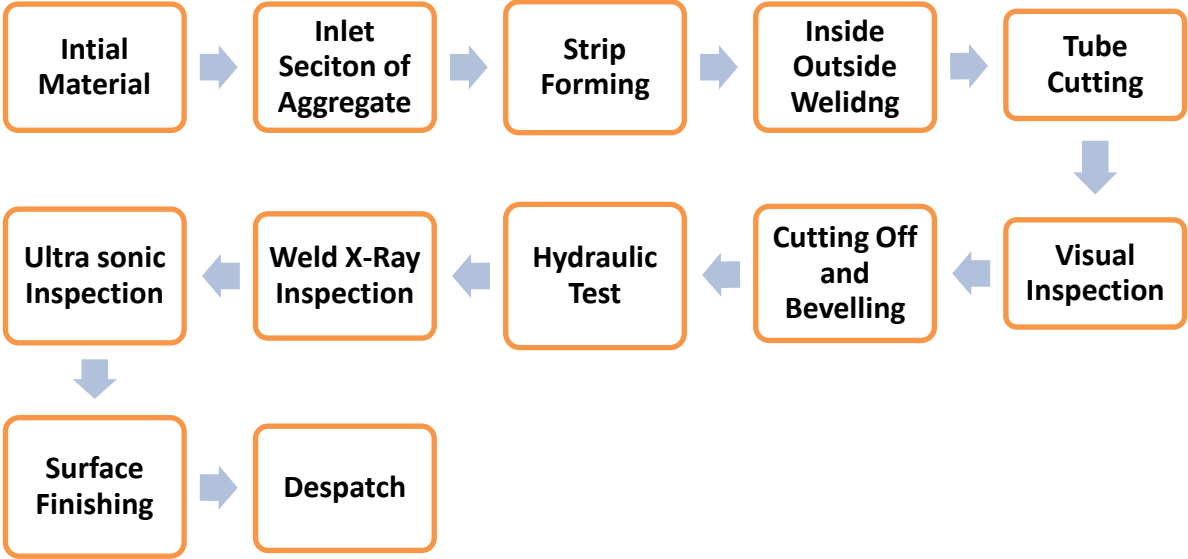


Fig. 1.2: Block diagram for manufacturing spiral pipes

Spiral welded pipes are mostly used in industrial sectors for transferring and conveying the fluids from one location to another. These are actually large diameter pipes and Double submerged arc welding method is employed for their production. High quality pipes are produced economically and in large choice of diameter and thickness. Pipe industries are facing challenge to enhance the service life and durability of their pipes in order to make their products cost effective and economical.

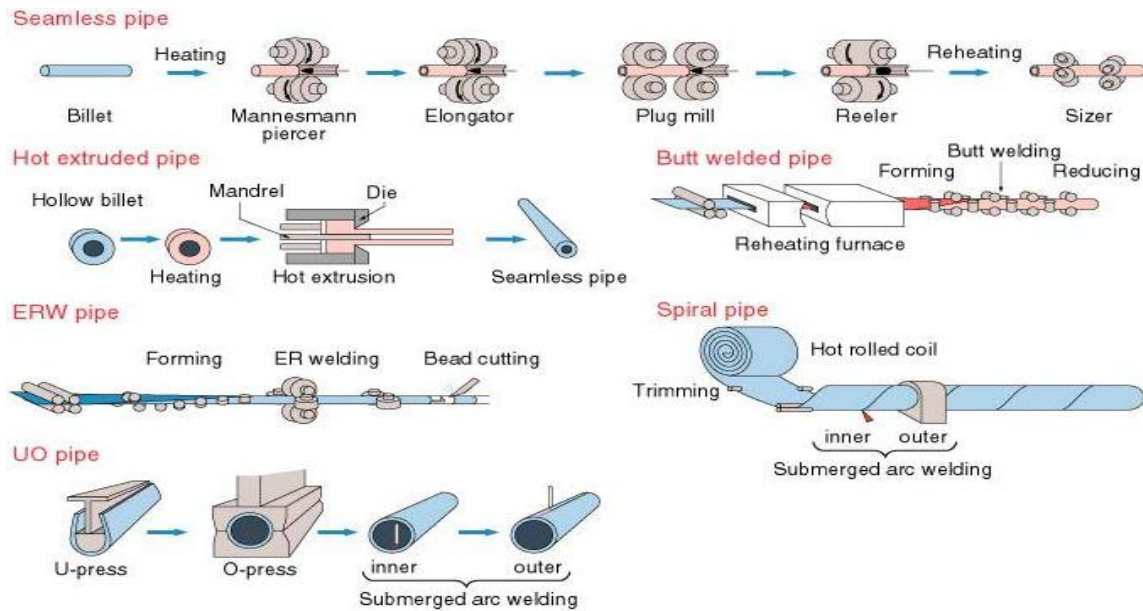


Fig. 1.3: Different types of pipes production [1]

1.2 APPLICATION & USE OF SPIRAL WELD PIPES

Spiral welded pipes are extensively used in different industries such as petrochemical industries, Oil and gas field, waste water and hydropower sectors. They can also be used in pump station piping, force mains, water treatment plant. Fertilizer plant, chemical industries and paint industries are also use these pipes.

1.3 SPIRAL WELDED PIPE PRODUCTION LINE

The spiral welded pipe production line is designed to manufacture spiral welded pipes, either from the same size of the steel strips to different diameters of pipes or from different widths of steel strips to the seam diameter of pipes. Spiral welded pipe production by submerged arc

method is based on using tandem welding technique for joining inside and outside coil edges, which have been trimmed and beveled by carbide milling for high quality weld structure.

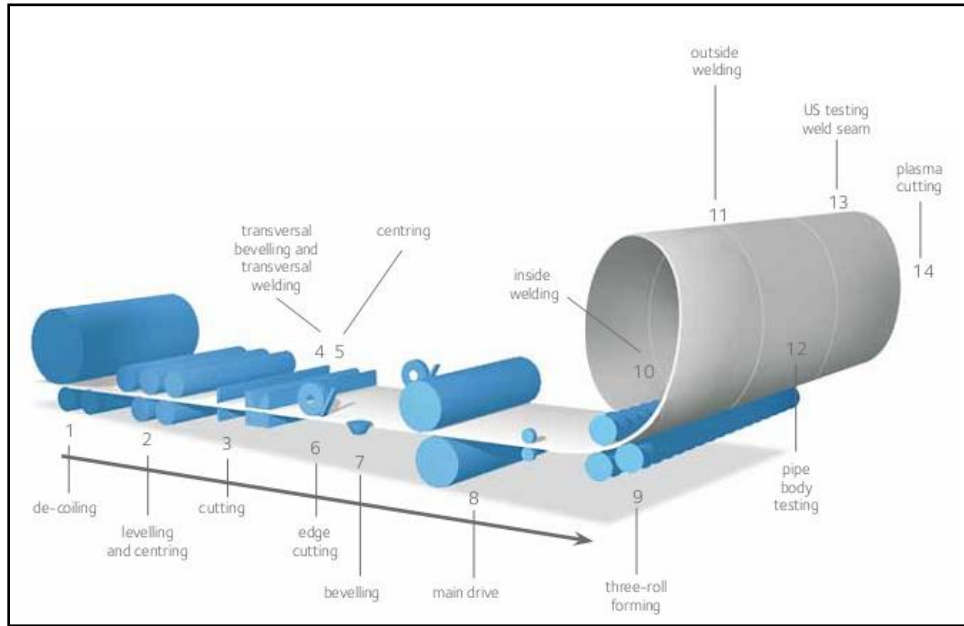


Fig. 1.4: Spiral production line [2]

Welding of hot rolled steel coils takes spiral form after passing through forming rolls. Excellent exterior weld quality at high production speeds is provided by double submerged arc welding process. Manufactured pipes are cut to the desired lengths at the exit of the pipe machine. Pipe ends are beveled by means of carbide machining for accurate on-site welding. After the pipe is conveyed to hydrostatic testing and off-line ultrasonic testing and/or real time X-ray inspection, the pipe will be subject to final inspection for the compliance to customer requirements. Starting from incoming control up to the final inspection stage; entire process is monitored and supported by computerized system. Traceability is achieved by input controls and barcodes through entire production lines.

1.3.1 Welding Process

Welding is process in which two metals are permanently joined. Double submerged arc welding process (DSAW) is used as a fabrication process for the production of spiral welded pipes in the pipe industry.

1.3.2 Principle of Arc Welding

Arc welding is a type of welding that uses a welding power supply to create an electric arc between an electrode and the base material to melt the metals at the welding point. They can use either direct (DC) or alternating (AC) current, and consumable or non-consumable electrodes. During submerged arc welding (SAW) the molten weld and the arc zone are protected from atmospheric contamination by being “submerged” under a blanket of granular fusible flux consisting of lime, silica, manganese oxide, calcium fluoride, and other compounds. When molten, the flux becomes conductive, and provides a current path between the electrode and the work. This thick layer of flux completely covers the molten metal thus preventing spatter and sparks as well as suppressing the intense ultraviolet radiation and fumes.

1.3.3 Multi Arc Welding

Spiral mill mostly uses AC and DC arc in combination for welding. Multi arc principal is used on both of the inside and outside. During the first welding pass, DC arc while for the second pass AC arc is used. Large and concentrated penetration is achieved during the first pass and the purpose for the second pass is to achieve the better deposition rate. As a result, full penetration of weld with high quality is produced during multi-arc welding on both side of the coil in a cost effective way. A large range of coil can be transformed into spiral pipes in the economical way by using this technique, highly flexible with full penetration of weld. The multi arc welding with the purpose of deep penetration, filling and finishing of weld on both side of spirally weld pipe is shown in Fig. 1.5

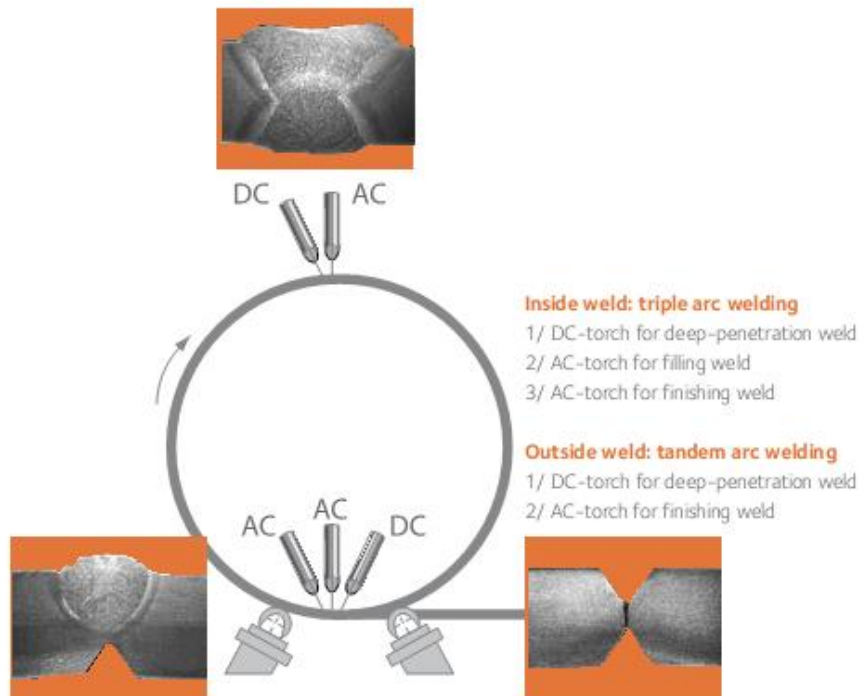


Fig. 1.5: Inside and Outside Multi arc welding [2]

1.4 PROBLEM STATEMENT

Since the spiral welded pipes are being extensively used in numerous industrial sectors. Therefore, to enhance the quality and service life of these pipes are one of the main interests of the researchers. Residual stress field that is generated in the welded structure has always been the key role parameter which severely affects the performance and life of these pipelines. Imperfections like thermal stresses, large local plastic strains after cooling, deformation, distortions and sometimes solidification cracking are highlighted factors of the welded structure. High temperature heating and rapidly cooling generates the large thermal gradient and heat effected zone (HAZ) during the welding process. During the manufacturing of the spiral welded pipes, identifying the process variables are very essential for the required bead size, quality and weldability. Additionally, combined stress fields due to forming, pre-heat, post-heat treatment and welding process are generated. These pipes are also suspected to hydrogen induced stress cracking and environmental hazards. The defects arise during manufacturing and operation must be estimated and should be minimized for the reliable product of spiral pipelines with the consideration of reduced capital cost. This work aims to develop a model which can predict the temperature distribution and consequently induced residual stresses in the spiral welded pipe. Furthermore, it is aimed to study the effect of time lag on the residual stress distribution, dependent upon the positions of adjusted arcs on the top and bottom side. It can also be utilized to determine the failure criteria in the spiral welded pipes. These studies are intended to improve the manufacturing process and as a result enhance the performance of spiral pipes.

1.5 PROPOSED OBJECTIVES

The main proposed objectives of the current research work are highlighted as below.

- (i) To develop a comprehensive FE model, including thermal model, structural model, their coupling along with the filler addition for the prediction of temperature and stress field during double submerged arc welding of spiral line-pipes.
- (ii) Appropriate verification and validation of model have to be conducted for the confidence of simulation results and reliable physical outputs.
- (iii) Investigate the influence of time lag and its consequent effects on stress distribution, tensile stress region, and plastic strains.
- (iv) From the experimental part, measurement and estimation of residual stresses will be done using hole-drilling technique along with the comparison of numerical and experimental results.

CHAPTER 2 LITERATURE REVIEW

In the following sections, a brief literature review has been done on welding and its corresponding influence on the different configuration such as Plate welding, Pipe welding, Spiral pipe welding. Additionally, the related work on the springback and split ring test is also reported.

2.1 PLATE WELDING

Welding as a fabrication process is one of an old subject. An extensive research work has been carried out on this field since 1930. A dominant role in the research is due to the vast increase of computational weld mechanics. To understand the mechanism in plate welding, wide range of research is available. Argyis et al. [3] studied the thermo-mechanical response and resulting residual stresses and distortions in a plate weld with thermoelastic-viscoplastic analysis. It was found that the considerable viscoplastic strain accumulated in the fusion region. The residual stresses in a plate welding reduced the buckling strength and induced brittle fracture. The effect of welding condition on the single pass butt welded plate was studied by Teng and Lin [4]. They studied the effect of travelling speed, external mechanical constraint, specimen size and their preheat

temperature. The peak of residual stress decreased in the central region with the increase of length and also with increase of speed while the thickness had an inverse relation with the tensile residual stress in the fusion regime. The preheating temperature significantly reduced the weld stresses. Furthermore, it was found that the weld bead was in tension with magnitude of yield stress while the far ends were in compression. The effect of temperature dependent material properties on the stress and temperature field in an aluminum weld plate was studied in [5]. The material properties were taken as a function of temperature, room temperature and their averaged value. It was observed that thermal conductivity had some influence on the temperature distribution. In contrast, specific heat and density had a negligible effect and could be considered as an average value over temperature. Young's modulus and thermal expansion coefficient had weak effect on the residual stresses. Instead of average value of Young's modulus, room temperature value could give better prediction. Temperature dependent yield stress was foremost important mechanical property for residual stress and distortion. If room temperature value was provided to it then no permanent deformation and plastic strain would occur thus giving zero residual stress.

The effect of welding sequence such as single pass, multi-pass and also in circular path was studied by Teng et al. [6]. They concluded that different arrangements of weld path order generate residual stresses accordingly. Angular distortions, volumetric shrinkage in a plate during welding was considered in the study [7]. These angular distortions were dependent on the applied constraints and more prominently seen in the thin as compared to thick plate. Lindgren [8] had presented a comprehensive review on

computational weld mechanics, its formulation and interaction on different aspects. The buckling deformation in the weld plate with thermo-elastic-plastic analysis and its comparison with elastic inherent strain deformation method was presented by Wang et al. [9]. It was found that due to nonlinear behavior of buckling, the magnitude of deformation estimated with elastic analysis was significantly small. However, Dean Deng et al. [10] compared the results of elastic FEM with the thermo-elastic-plastic FEM. It was verified that the inherent strain method could effectively predict the deformation in thin butt welded plate. H. Long et al. [11] studied the longitudinal and transverse shrinkage, angular distortion, and residual stresses in a plate. Furthermore, it was reported that the welding speed and thickness had a considerable effect on the weld distortions. Higher longitudinal and transverse shrinkage was observed in the weld area and the mid-section of plate respectively.

The residual stress distribution in SAW (Submerged Arc Welding) and DSAW (Double Submerged Arc Welding) plate was analyzed. Zhang et al. [12] showed that the transverse residual stresses in DSAW were lower than the SAW. The DSAW could have an improved penetration, less thermal distortions and less undercuts as reported in [13]. Yilbas et al. [14] observed the effect of laser welding. They also measured the welding residual stress with XRD technique and found in agreement with numerical prediction. Additionally, optical microscope and SEM were used for metallurgical examination of the welded region. Attarha et al. [15] studied the temperature distribution in similar and dissimilar welded plate by finite element method and compared through experiments by using K-type thermocouples. They found that the decreasing temperature during cooling

had a nonlinear behavior. Deng and Kiyoshima [16] investigated the start or end residual stress distribution in thick plate which were suspected flaw sites. The effect of welding direction and its sequence was also considered.

The residual stresses and strains mainly depend upon the temperature field and heat flow pattern. Kumaresan et al. [17] modified the Goldak heat source model based on infinite plate theory to finite plate theory. Smith et al. [18] studied the effect of material hardening models on the residual stress field in multi-pass weld groove specimen. They demonstrated that the magnitude of tensile stresses were over predicted by isotropic hardening model while under prediction was observed in longitudinal stresses with pure kinematic hardening model. They suggested mixed isotropic-kinematic hardening model for more accurate prediction. Jiang et al. [19] investigated the effect of heat sink on the weld stresses. The averaged value of heat transfer coefficient and contact length was varied. They observed that longitudinal stresses were decreased due to the short dwell cooling time with heat sink. The effect of tacking on the start and end of the plate weld was considered in the study [20]. It was found that the distortion level could be increased by tacking. The longitudinal residual stress through thickness was evaluated by Javadi et al [21] using ultrasonic stress measurement, based on acousto-elasticity. The results had an acceptable agreement with the finite element prediction. However, the concordance was deviated with high frequency transducer.

2.2 PIPE WELDING

Fusion welding is the most common method for joining and manufacturing pipes. A wide range of applications for these pipelines have been found in industries. To meet the industrial demands, their quality and sustainability must be assured in order to have reliable service. It is always a necessary step to analyze the mechanical behavior of pipes under working loads and stresses. Imperfections and distortions in pipes due to welding are the main reasons for their degradation.

Research in this issue has focused on normalizing the effects of welding on pipes. Josefson and Karlsson [22] studied the effect of multi-pass butt welding on different grooves of pipe. The results of single-U groove were compared with narrow groove. Larger deflection and smaller residual stresses were found in the narrow groove. Teng and Chang [23,24] investigated the residual stress in girth butt welded pipes. The effects of these stresses on the diameter and thickness were also considered. It was found that the tensile zone was larger and less residual axial stresses were present in thick pipes. It was also depicted that the tensile hoop stresses were more in thin walled pipes as compared to thick pipes. The influence of wall thickness on welding stress distribution was studied in their research [24]. It was concluded that the tensile and compressive residual axial stresses occurred at the inner and outer surface along the weld line of the pipe, respectively. Brickstad and Josefson [25] described the variation of axial and hoop stresses through the thickness by performing a parametric study. The investigated parameters for different pipe configurations were varying number of passes and magnitude of heat input. Weld induced stresses can be lowered either by post weld heat treatment (PWHT) or mechanical stress relieving (MSR) treatment. Yang and Lee [26]

studied the reduction of residual stresses by MSR treatment with different magnitudes of pressure at the inner, outer, and edges of a pipe. With the increase in the magnitude of inner loading, stresses were released linearly.

Weld metal shrinkage is common phenomena during cooling and ultimately local plastic strains occur. Basavaraju [27] investigated the shrinkage in butt welded pipes with an axisymmetric model. It was found that axial and circumferential strains were more in larger sized pipes having thick wall as compared to smaller size with thin wall. Runnemalm and Hyun [28] suggested an adaptive meshing scheme for coupled thermo-mechanical analysis of welding. It reduced the problem size with increased accuracy. Sabapathy et al. [29] studied the in-service welding of pipelines using a numerical technique. Heat source model was modified in terms of shape and size accordingly for vertically upward or vertically downward arc welding for the accurate penetration, weld bead. The approximate burst pressure was also determined by translating the temperature field into the pipe wall's cavity.

Abid and Siddique [30] analyzed the effects of tack welding and root gap in the pipe flange joint. Weld residual stress fields and their corresponding deformations at four different tacking locations were studied. The appropriate location of tacking was 90° and 270° from weld start position. However tacking had no significant overall effect but locally it might be a cause of stress raiser or reducer. With different root gaps, it was found that larger gap increase the lateral shrinkage and smaller gap were preferred for better penetration. Yaghi et al. [31] discussed the modeling of axisymmetric butt welding steel pipe. Element Kill and birth option had been used for 4 and 36 multi-weld passes for

different nominal sizes of pipes. It was found that the residual axial and hoop stresses on the outside surface were independent on diameter. Deng et al. [32,33] developed three dimensional (3-D) and two dimensional (2-D) thermo-mechanical model of pipe welding. The results of these models were compared with experimental measurements and found in good agreement. However, 3-D model could give detailed distribution of temperature and stresses while 2-D model was computationally inexpensive. In [33] the influence of yield strength of weld metal and its effect on residual stress distribution were seen and comparison with experiments were given. It was found that the yield strength had a significant effect on stresses in weld zone. The initial stresses during cold working could increase the yield strength of base metal so higher residual stresses were expected.

Lee and Chang [34] considered the circumferential welding with inside radius to wall thickness ratio ranging from 10 to 100. The effects of diameter on the residual stress field had been investigated. It was also concluded that welding distribution at start/end violated the axisymmetric assumption so FE model should be three dimensional for accurate prediction. The effects of welding sequence and its consequent influence on distortions on V-joint pipe were studied by Sattari-Far et al.[35]. It was also cleared that the suitable welding sequence could considerably decrease the welding distortions. However, these could be unexpectedly increased with unfavorable sequence. Barsoum [36] studied the influence of residual stresses on weld root and weld toe for multi-pass tubular weld and their effect on the fatigue strength. The maximum penetration was considered with single-U shape joint and minimum penetration with fillet weld. Torsion

fatigue test was performed for crack propagation. Linear elastic fracture mechanics (LEFM) was used for investigation of crack growth due to lack of penetration in root.

Malik et al. [37] investigated the residual stress distribution in circumferentially arc welded thin walled pipe. It was concluded that axial residual stress fields were not sensitive to angular location however, contrary effects were observed on hoop residual stresses. The effects of tacking on axial stresses were observed on the inner surface but these were not prominent on hoop stresses. Akbari and Sattari-Far [38] analyzed the effects of heat input magnitude on the stress distribution in dissimilar pipes. They found unbalanced residual stresses on both side of weld centre line. The peaks of hoop stresses did not differ significantly with the change of heat input. Lee et al. [39] also investigated the dissimilar steel girth welded pipe. The results revealed that the residual stress magnitudes and distributions are different from their corresponding similar steel pipes and the stress variation were more pronounced in hoop stress as compared to the axial stress.

Chang et al. [40] examined the effect of axial tension loading on the circumferentially welded pipe. The reduction in the pipe diameter due to shrinkage at the weld zone and the applied load caused a secondary bending moment thus resulting in redistribution of stresses. Deng and Kiyoshima [41,42] investigated the stress distribution near the weld start/end location. The sharp gradients of residual stresses were found near to the vicinity of starting and ending position. They also concluded that the last pass had the large contribution to the final stress distribution. In their research [42] the initial stresses were introduced in the model with special heating cycle and its influence on laser

welded pipe was observed. It was analyzed that in the vicinity of weld location, the residual stress were determined by welding but the effects of initial stresses on residual stress field were observed away from the weld centre line. Liu et al. [43] developed an axisymmetric model for the investigation of the residual stresses during multi-pass in narrow gap thick walled pipe. They found that axial stress distribution were of bending nature at the weld centre line and the HAZ line. The hoop residual stress was tensile through the wall. Moreover, the axial and hoop stresses did not change after the filling of groove up to a certain height.

2.3 SPRINGBACK AND SPLIT RING TEST

With the increase in the demand of high strength and light weight steel in the last few decades, especially in the automotive industries for the purpose of improving the strength, the challenge of springback is being faced [44]. Springback is considered as an elastic recovery of the metal when the load has been removed after the finishing of the forming process [45]. This behavior can also be seen in the metal stamping and sheet metal bending processes [46,47]. When the metal is bent or stamped, the elastic recovery as springback changes the final shape, as a result of not meeting the design specification and fails to execute its purpose. Since a large number of parts are produced during manufacturing processes by sheet metal forming, it is of the utmost concern that the knowledge of the springback behavior is comprehended and judged so that the final shape of the product remains intact and process parameters can be controlled for effective quality.

In the case of deep drawing from the sheet metal, the Demeri split ring test can set as a benchmark for evaluating the springback [48,49]. This test involves four sequential steps. Firstly, a deep cup is drawn from a sheet, placed in blank holder and pushed with punch. Secondly, a circular ring is cut from the midsection. Thirdly, the ring is split longitudinally and the fourth step is to measure the opening and closing of the ring. During the forming processes, residual stress are produced in the component. These residual stresses are responsible for accumulating the plastic strains at different locations. When the ring is split, stresses integrated over the thickness cause a bending moment and finally changes the shape [45,46]. The curved beam and plate bending theories has been adopted to predict the springback. On the basis of the Hook's law, the elastic part is recover from the total strain which is ratio of the stress to strain and mainly dependent on the elastic stiffness.

A progressive research has been carried out in last ten years for the accurate prediction of the springback during the split ring test. Experiments as well as finite element codes have been developed for appropriate selection of the control parameters. Chen [44] studied the split ring test analysis in cup drawing sheet metal forming by using finite element analysis. A sensitivity analysis was performed by taking seven different simulation variables such as mesh, integration points, contact force, settle down time etc. The results were compared with the experimental results and it was concluded that the simulation agreed to the experimental results in the range of 10%.. Foecke and Gnaeupel-Herold [45] investigated the effect of error misalignment through experimental setup on the opening of the split ring. It was found that the opening of the split ring was chiefly

effected by the adjustment errors of the initial blank over the punch and in vertical cutting location.

The springback behavior is mainly dependent upon the residual stresses in the component after large strain deformation. Synchrotron X-ray measurement in [50] was done along the thickness and non linear axial and tangential stress gradient was measured. Through the averaged thickness stress value, springback measured by split ring cut in a cup agrees accurately up to 3%. Due to the bauschinger effect in high strength steels (HSS), the complex material modeling was required for estimating the springback. Yoshida-Uemori material model was implemented in [51] and its results were compared with LS-DYNA standard material models. It was found that the Yoshida-Uemori model reliably predicts the opening in HSS but the most expensive model.

Laurent et al. performed a series of research on the springback of split ring test [48,52–55]. In [52,53] the warm forming condition of alumina alloys and its consequent effects were considered. It was found that the opening after splitting depends upon temperature. The stress distribution gradient in the thickness decreased with increase in temperature and as a result less opening was observed .Furthermore, the distribution of the tangential stress had a main influence for the shape change. While in [48,55] the effect of hardening laws and yield criteria were considered. Material models, isotropic and kinematic hardening were combined with plastic flow yield criteria like von Mises,Hill'48 and Barlat'91. It was declared that yield criteria could have more effect on springback than the hardening law and kinematic hardening with Barlat'91 gave more

accurate prediction. In [54] the influence of element formulation, element type, mesh density and plastic yield criteria were studied.

It was essential that the Bauschinger effect had to be captured precisely in metal sheet forming due to the reverse of strain. The research [56] dealt with material modeling by using non-quadratic anisotropic yield function ANK Yld2000-2d . It closely matched the experimental results as compared to the combined isotropic-kinematic hardening law. Xia [57] conducted an experimental research on number of rings taken from a cup drawn. It was observed that the ring cut out near the bottom of cup showed negative opening and exhibiting conversely to all other rings. A comprehensive review based research on the issues of springback is done by Wagoner et al. [58]. In this work he categorized the previous work into five distinctive topics. Those were related to material representation, material class and numerical procedure. An investigation was made in [59] in which the dependence of springback on the axial and tangential stress was studied by using the neutron diffraction and it was found that the neutral plane had been shifted towards inside which was consistent with the bending theory.

In pipe and tubing, the residual stresses are induced during manufacturing process. The amplitude of the bending stress field could be related to the opening and closing of the split ring[60] . In ASTM standard practice E1928, similar approach based on split ring test is used for calculating the circumferential residual stresses in thin walled tubing. These formulas were based on Sachs and Espey method which were related to the change in diameter upon splitting. In this practice linear stress distribution along the wall thickness was assumed and reasonably justified. The release of the bending moment after

split was related to the release of the bending stress. Therefore, minimum and maximum values occurred at the surfaces [61]. The same procedure was depicted for the quenched tube [62].

In the production of spiral pipes, weld residual stresses are generated due to the thermal gradient caused by heating and cooling cycles. Dong et. al [63] presented the three dimensional welding simulation and also performed splitting on a welded pipe ring. It was found that different hoop deformation could occur depending upon the location of cut, near or away from the weld seam.

2.4 SPIRAL PIPE WELDING

Spiral pipes are fabricated in large diameter with double submerged arc welding (DSAW) at inner and outer side location. The manufacturing technique of these pipes based on continuous process, feeding of sheet by rollers after bending and then welding. Pipes of larger length as of desired specification can be produced by this advent way of forming. These pipes are used in various chemical, petrochemical, Oil and gas sector, all type of process industries etc. Knoop [64] in his report discussed the modern technology of two step process in the manufacturing of spiral pipes described by Salzgitter in 1985. He also explained its qualitative and economical advantage over the conventional procedure.

The research studies have been carried out to understand the interaction of welding and its subsequently induced residual stresses during the manufacturing of line pipes for the improvement of their qualities. Arif et al. [65] analyzed the spiral laser welding of a mild steel tube. They modeled moving volumetric heat distribution as a laser heat source. The effects of different welding speeds were also studied. The experimentally residual stresses were measured by XRD technique (X-Ray Diffraction) and results were found in good agreement with the numerical simulation. The metallurgical examination was done by optical microscope and SEM (Scanning Electron Microscope). It was found in their study that high value of von Mises stress occurred in weld region after cooling and hardness in weld region was higher as compared to base metal. Forouzan et al. [66] studied the submerged arc welding of spiral welded pipes. The Goldak heat source distribution was applied by using un-furl mapping technique in which pipe was considered as a flat plate. The computational cost was reduced by using solid and shell element and the transition between them were defined by multipoint constraint technique. The hole drilling measurement was performed for validation purpose. The hydrostatic test was also simulated through ramp loading of internal pressure and it was concluded that the reduction of high tensile stresses and von Mises stresses were found.

Dong et al. [63] used three dimensional shell model for predicting the residual stresses in a long spiral pipe. Forming induced residual stresses, plate forming and radial expansion were determined by using plane strain model. Furthermore, their interaction with welding was studied. Finally, cold expansion and its effects were studied. It was

found that the cold expansion had a beneficial effect on the hoop residual stress while detrimental effects was observed on residual longitudinal stress in weld component.

CHAPTER 3 COMPUTATIONAL MODEL FOR SPIRAL

WELDED PIPE

In the following section, the computational model for spiral welded pipe is discussed briefly. The number of processes is involved in the manufacturing of spiral welded pipes. The developed model is effectively predicts the weld residual stress due to submerged arc welding. This chapter is about the implementation of the structural and thermal models into the Finite-Element (FE) using ANSYS software.

3.1 MODELLING METHODOLOGY

Physics of welding involves an intricate mathematical modelling due to thermal, mechanical, metallurgical interactions. The non linear three dimensional thermo-mechanical transient analysis is performed. Furthermore, temperature field is considered as an independent from the stress field and obtained separately from the stress analysis and the combination of both these analyses are associated by using sequentially field coupling. The localized heat gradient and temperature field is obtained by thermal loading. The thermal elasto-plastic analysis is performed for the determining the resultant

residual stresses. The temperature dependence of material properties are incorporated. Additionally weld elements are added sequentially for the deposition of filler material.

3.2 THERMAL MATHEMATICAL MODEL

The temperature distribution during thermal analysis in welding can be obtained by using heat diffusion equation. The derivation of heat diffusion equation based on the conservation of energy law which states that the time rate of change of kinetic energy plus internal energies is equal to the sum of the rate of the work from all forces and couples plus a summation of all external energies that enter or leave a control volume per unit of time.

$$C_p \rho \frac{\partial T}{\partial t} + \nabla \cdot \Phi - Q = 0 \quad (3.1)$$

According to Fourier Law,

$$\Phi = -k \nabla T$$

The incorporation of the conservation of energy and Fourier law results into the three dimensional transient heat diffusion equation as shown in Eq.(3.2)

$$C_p \rho \frac{\partial T}{\partial t} = \nabla \cdot (k \nabla T) + Q \quad (3.2)$$

where C_p the temperature dependent specific heat of the material, ρ is the temperature dependent density $T(x,y,z,t)$ is the temperature of the material at any location (x,y,z) at

time t . $Q(x,y,z,t)$ the amount of heat generated per unit volume per unit time at location of (x,y,z) at time t . Φ is the heat flux at location (x,y,z) and k the temperature dependent thermal conductivity of the material.

The transient non uniform temperature field T during arc welding can be obtained by solving the nonlinear heat conduction equation with sufficient and proper initial and boundary conditions. The surface convection and radiation are modeled as thermal boundary conditions which are representing the heat losses of the domain. The following set of equations are solved along with the Eq. (1) to get the temperature distribution over the whole region.

$$q_c = h(T - T_\infty)$$

$$q_r = \xi \times \Sigma(T^4 - T_\infty^4)$$

where h representing the convective heat coefficient. T_∞ is considered as an ambient room temperature. ξ is the emissivity of the body surface and Σ is the Stefan Boltzmann constant. The value of the Stefan Boltzmann constant is $5.67 \times 10^{-8} \text{ W/m}^2 \text{ K}$.

During the transient heat transfer problem in which temperature field is changing with time, ambient temperature is considered as an initial boundary condition over the model at time $t=0$.

$$T_\infty = T(x, y, z, 0)$$

The finite element formulation of heat diffusion equation can be obtained by applying the weighted residual weak form approach using Galerkin method and it yields as

$$\rho \int (C_p [N][N']) \{\dot{T}_e\} dV + \int [B'] [D] [B] \{T_e\} dV = \int [N] Q dV + \int_A [N] h (T_\infty - [N'] \{T_e\}) dA \quad (3.3)$$

Eq. (3.3) give the nodal temperature and can be summarized into

$$[C] \{\dot{T}_e\} + [K] \{T_e\} = [F_e] \quad (3.4)$$

where, [N] is the element shape function matrix, [D] is the constitutive or material stiffness matrix, C is the specific heat matrix, T_e is vector containing nodal temperature, K is the conductivity matrix and F_e is the vector containing the internal heat sources and the boundary conditions and serves as the nodal loads. The mathematical formulation of these matrices is as follow

$$[C] = \rho \int (C_p [N][N']) dV$$

$$[K] = \int [B'] [D] [B] dV + \int_A h [N][N'] dA$$

$$[F_e] = \int_V Q [N] dV + \int_A h T_\infty [N] dA$$

The temperature field is obtained in thermal analysis by using the Eq.(3.4) in which assembled element equations are simultaneously solved for the whole divided volume into number of elements for the unknown nodal temperatures. The gain of the internal energy is associated with the latent heat of fusion. The sharp increase in the heat capacity

at the fusion temperature due to the latent heat of fusion during the phase change causing the convergence issues. Therefore, enthalpy method is used for the transient thermal analysis and provided along the enthalpy of the material as a function of temperature.

3.3 STRUCTURAL MATHEMATICAL MODEL

The formulation of the structural analysis is based on the principle of virtual work that the virtual change in internal strain energy must be offset by an identical change in the external work due to applied loads. Considering the strain energy due to the thermal stresses resulting from the constrained motion of body during the a temperature change and the principal of virtual work and the divergence theorem, the equilibrium equation and the constitutive equations can be written as

$$\begin{aligned} & \{\delta u\}' \int_V [B'] [D] [B] \{u\} dV - \{\delta u\}' \int_V [B'] [D] \{\varepsilon^{th}\} dV \\ & = \{\delta u\}' \int_A [N'] \{P\} dA + \{\delta u\}' \{f\} \end{aligned} \quad (3.5)$$

Since $\{\delta u\}'$ vector is common in all terms and represent the virtual displacements.

The condition required to satisfy above equation reduces to

$$[K]\{u\} = \{F^{th}\} + \{F^{pr}\} + \{F^n\}$$

where $[K] = \int_V [B'] [D] [B] dV$ is the element stiffness matrix,

$\{F^{th}\} = \int_V [B'] [D] \{\varepsilon^{th}\} dV$ is the element thermal load vector, $\{\varepsilon^{th}\} = \{\alpha\} \Delta T$ is the

thermal strain vector, $\{\alpha\}$ is the vector of coefficient of thermal expansion,

$\{F^{pr}\} = \int_A [N]^T \{P\} dA$ is the element pressure vector and $\{f\}$ is the nodal force vector.

3.4 HEAT SOURCE MODELLING

Modelling of heat source plays a vital role in the simulation of welding analysis because it serves as a thermal load. The non uniform temperature field generated due to intense local heating causes Fusion Zone (FZ) and Heat Affected Zone (HAZ), change in microstructure, molten weld pool. Deformations, stress and strain fields, and resulting residual stresses are due to transient temperature distribution which in turn dependent upon the heat applied and heat distribution pattern. The moving volumetric heat distribution proposed by Goldak is used to determine the temperature history and weld bead profile. The Goldak double ellipsoidal heat input model, based on the Gaussian heat distribution power in space, has capability of shallow and deep penetration. The power density of double ellipsoidal body heat distribution can be mathematically formulated as.

$$q(x, y, z) = \frac{6\sqrt{3} fQ}{abc \pi \sqrt{\pi}} e^{(-3\frac{x^2}{a^2})} e^{(-3\frac{y^2}{b^2})} e^{(-3\frac{z^2}{c^2})} \quad (3.6)$$

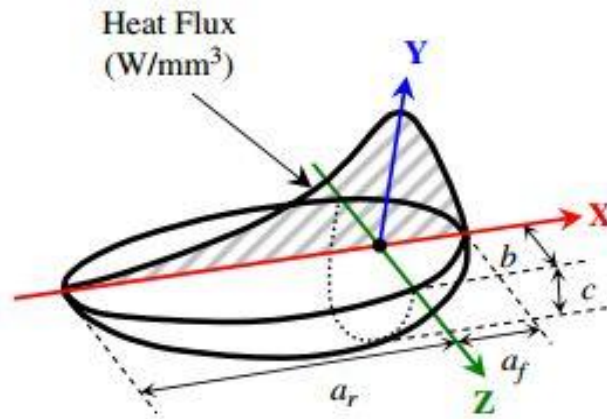


Fig. 3.1: Heat source model

where a, b, c are the shape parameter of the Goldak heat source for the weld pool geometry as in Fig. 3.1. In Goldak double ellipsoidal heat density distribution, the front half and rear half are the quarter of two different ellipsoids where f determines the fraction of heat deposition in the front and rear region. The fractional heat is specified by the following relation.

$$f_f + f_r = 2$$

3.5 IMPLEMENTATION OF MOVING GOLDAK HEAT SOURCE

The moving Goldak heat source is the most commonly used model for the flat plates. However, it can be used for spatial curved seam just like in the spiral welded pipes. The position of any point from the welding tip source is described with reference to local coordinates system with the help of Frenet's formulas[67]. The relation between the

moving local and fixed global coordinate system has been developed. The orientation of moving local coordinate system with three mutually perpendicular axes is continuously changing along the spiral path with respect to the global coordinates system. The Goldak heat source distribution is associated with local coordinate system with origin describing the contact of welding wires which are producing arc. The origin O of fixed global coordinate system xyz is at the centre of pipe with $\hat{i}, \hat{j}, \hat{k}$ orthogonal set of unit vectors. Similarly, the origin O' of moving local coordinate system $x'y'z'$ is on the spiral path at any time t with $\bar{e}_t, \bar{e}_n, \bar{e}_b$ as orthogonal set of unit vectors. Fig. 3.2 shows the fixed global and moving local coordinate system.

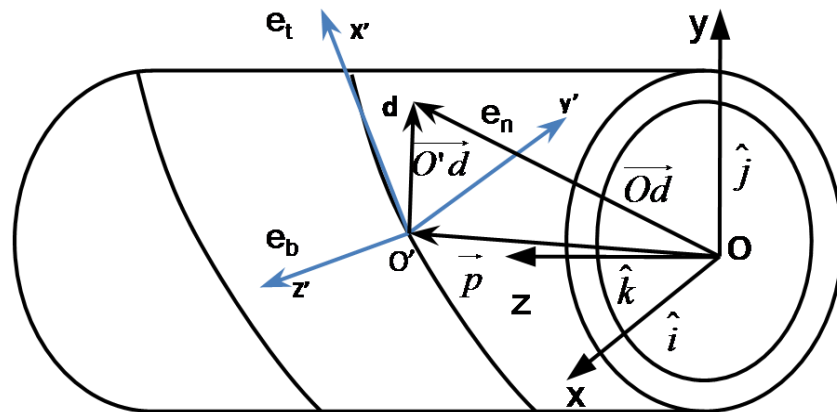


Fig. 3.2: Local and Global coordinate system

The position vector \vec{p} of any point on the spiral line can be described with reference to global coordinate by the following equation.

$$\vec{p} = x\hat{i} + y\hat{j} + z\hat{k} = r\cos\theta\hat{i} + r\sin\theta\hat{j} + r\theta\tan\alpha\hat{k} \quad (3.7)$$

where r is the radius of spiral seam, α is the spiral helix angle, θ is the rotational advancement. The relationship of the rotational advancement with the manufacturing feed velocity v can be obtained by taking the time derivate of the position of vector \vec{p} Eq.(9).

$$\frac{d\vec{p}}{dt} = -r\sin\theta\frac{d\theta}{dt}\hat{i} + r\cos\theta\frac{d\theta}{dt}\hat{j} + r\tan\alpha\frac{d\theta}{dt}\hat{k} \quad (3.8)$$

The rate of change in the rotational advancement defines the angular velocity ω . So by using the definition of $\omega = d\theta/dt$ it gives

$$\vec{v} = \frac{d\vec{p}}{dt} = -r\omega\sin\theta\hat{i} + r\omega\cos\theta\hat{j} + r\omega\tan\alpha\hat{k} \quad (3.9)$$

Taking the magnitude of Eq.(3.9) , it gives the relation of rotational advancement and feed velocity.

$$|\vec{v}| = v = \sqrt{(-r\omega\sin\theta)^2 + (r\omega\cos\theta)^2 + (r\omega\tan\alpha)^2} \quad (3.10)$$

$$|\vec{v}| = v = \sqrt{(r\omega)^2\{\sin^2\theta + \cos^2\theta + \tan^2\alpha\}} \quad (3.11)$$

By applying the trigonometric identities $\sin^2\theta + \cos^2\theta = 1$ and $1 + \tan^2\alpha = \sec^2\alpha$, it can be reached to

$$v = r\omega \sec \alpha \quad (3.12)$$

$$d\theta = \frac{v \cos \alpha}{r} dt \quad (3.13)$$

Solving the above differential equation by taking integration

$$\int_0^\theta d\theta = \int_0^t \frac{v \cos \alpha}{r} dt \quad (3.14)$$

$$\theta = \frac{vt \cos \alpha}{r} \quad (3.15)$$

3.5.1 Determining the e_t vector

From the Frenet's Formula, the rate of the change in the position vector with respect to the infinitesimal small arc ds describes the tangent vector on the curve with unit magnitude..

$$\bar{e}_t = \frac{d\bar{p}}{ds} = \frac{d\bar{r}}{d\theta} \frac{d\theta}{ds} \quad (3.16)$$

$$\bar{e}_t = \frac{d\theta}{ds} \left\{ -r \sin \theta \hat{i} + r \cos \theta \hat{j} + r \tan \alpha \hat{k} \right\} \quad (3.17)$$

$$\bar{e}_t = \frac{r}{s'} \left\{ -\sin \theta \hat{i} + \cos \theta \hat{j} + \tan \alpha \hat{k} \right\} \quad (3.18)$$

From the magnitude of $|\bar{e}_t|=1$, we have

$$\left(\frac{r}{s'}\right)^2 \{(-\sin \theta)^2 + (\cos \theta)^2 + (\tan \alpha)^2\} = 1^2 \quad (3.19)$$

$$\left(\frac{r}{s'}\right)^2 \sec^2 \alpha = 1 \quad (3.20)$$

$$s' = r \sec \alpha \quad (3.21)$$

Putting Eq.(3.21) into Eq.(3.18) we get \bar{e}_t

$$\bar{e}_t = -\cos \alpha \sin \theta \hat{i} + \cos \alpha \cos \theta \hat{j} + \sin \alpha \hat{k} \quad (3.22)$$

3.5.2 Determining the e_n vector

The normal unit vector on the spatial curve is equal to the product of radius of curvature and the rate of change of unit tangent vector with respect to the infinitesimal small arc ds . Mathematically it can be written as

$$\bar{e}_n = \rho \frac{d\bar{e}_t}{ds} = \rho \frac{d\bar{e}_t}{d\theta} \frac{d\theta}{ds} \quad (3.23)$$

$$\bar{e}_n = \frac{\rho}{s'} \left\{ \frac{r}{s'} \left(-\cos \theta + \frac{\sin \theta}{s'} s'' \right) \hat{i} - \frac{r}{s'} \left(\sin \theta + \frac{\cos \theta}{s'} s'' \right) \hat{j} - \frac{r}{s'^2} s'' \tan \alpha \hat{k} \right\} \quad (3.24)$$

From Eq. (3.21), taking again derivative of s' with respect to $d\theta$

$$s'' = \frac{ds'}{d\theta} = 0 \quad (3.25)$$

Putting Eq. (3.25) in Eq. (3.24), we get

$$\bar{e}_n = -\frac{\rho r}{s'^2} \{ \cos \theta \hat{i} + \sin \theta \hat{j} \} \quad (3.26)$$

From the magnitude of $|\bar{e}_n| = 1$, we have

$$\left(-\frac{\rho r}{s'^2}\right)^2 \{ \cos^2 \theta + \sin^2 \theta \} = 1^2 \quad (3.27)$$

$$\rho r = s'^2 \quad (3.28)$$

Putting Eq. (3.28) in Eq. (3.26)

$$\bar{e}_n = -\{ \cos \theta \hat{i} + \sin \theta \hat{j} \} \quad (3.29)$$

3.5.3 Determining the \bar{e}_b vector

The direction perpendicular to the osculating plane (plane containing the \bar{e}_t and \bar{e}_n vector) is binormal unit vector on the curve. So it can be given by

$$\bar{e}_b = \bar{e}_t \times \bar{e}_n \quad (3.30)$$

$$\bar{e}_b = \sin \alpha \sin \theta \hat{i} - \sin \alpha \cos \theta \hat{j} + \cos \alpha \hat{k} \quad (3.31)$$

The Eq.(3.22), Eq.(3.29) and Eq.(3.31) can be expressed into matrix form as

$$\begin{Bmatrix} e_t \\ e_n \\ e_b \end{Bmatrix} = \begin{bmatrix} -\cos \alpha \sin \theta & \cos \alpha \cos \theta & \sin \alpha \\ -\cos \theta & -\sin \theta & 0 \\ \sin \alpha \sin \theta & -\sin \alpha \cos \theta & \cos \alpha \end{bmatrix} \begin{Bmatrix} \hat{i} \\ \hat{j} \\ \hat{k} \end{Bmatrix} \quad (3.32)$$

The local coordinate system $x'y'z'$ consist of tangent, normal and binomial unit vector on the spiral curve, determined at any instant of time by using above set of equations. The body heat distribution is applied as thermal load to any point d on the spiral pipe by calculating the Goldak's distances from the tip of the heat source. The position vector of point d from the wire tip with reference to global coordinate system is calculated and projected on the local coordinate system at that instant of time to compute the Goldak's distances.

$$\overline{O'd} = \overline{Od} - \overline{p} \quad (3.33)$$

$$\begin{aligned} x' &= \overline{e_t} \cdot \overline{O'd} \\ y' &= \overline{e_n} \cdot \overline{O'd} \\ z' &= \overline{e_b} \cdot \overline{O'd} \end{aligned} \quad (3.34)$$

3.6 Finite Element Model

For the analysis of three dimensional nonlinear transient thermo-mechanical phenomena, a geometrical model consisting of ring is developed which is actually the portion of spiral welded pipe. The spiral ring with outer diameter of 711mm with the wall thickness of 16mm is modeled. The length of spiral ring is about 10 times less than the pitch of spiral pipe which is 1460 mm. The spiral seam rolled on the pipe is define by the

helix angle α which is the function of parameters as the pitch and the diameter of the pipe and can be calculated by.

$$\alpha = \tan^{-1}\left(\frac{P}{\pi D}\right)$$

where P is the pitch of spiral pipe and D is the pipe diameter. A 3-D finite element model is developed using ANSYS as finite element package and shown in Fig. 3.3

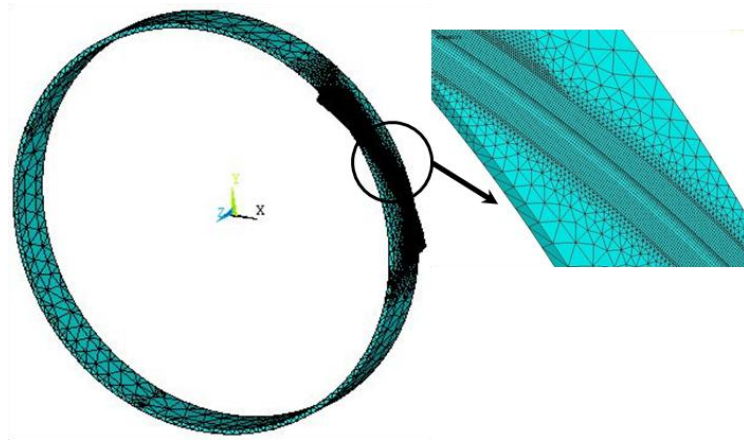


Fig. 3.3: Finite element mesh

In order to predict the accurate temperature history due to thermal loading involving heating and cooling cycles, uncoupled heat transfer transient analysis is performed to solve the heat conduction problem with convection and radiation as boundary conditions. The combined heat loss on the surface due convection and radiation is modeled. Thermal loading due to the welding moving heat source is applied as the volumetric heat density with the double ellipsoidal model proposed by Goldak et al. [68]. A user subroutine is written for the moving body heat source in which position, time and Goldak parameters

are passed through the routine to evaluate the heat flux. The welding heat source power Q which is dependent upon the efficiency η of the welding process, and the applied voltage and current and given by relation below.

$$Q = \eta VI$$

where, V and I stand for the voltage and current, respectively. The efficiency of submerged arc welding process is taken as 85% . The characteristic of Goldak parameters are related to the bead profile and shown in Table 3.1.

Table 3.1:Goldak heat source parameters

Goldak Parameters	Value
Width of the heat source, b (mm)	11
Depth of the heat source, c (mm)	12
Front heat source distance, a_f (mm)	16
Rear heat source distance, a_r (mm)	24
Front ellipsoidal heat fraction f_f	0.4
Rear ellipsoidal heat fraction, f_r	1.6
Velocity, v (mm/sec)	19.17

The thermo-physical properties of the material depending upon temperature are provided. The large change in the internal energy due to intense heating is causing the phase change in the model. Therefore, enthalpy as a function of temperature is provided to account for the latent heat over the range of the solidus and liquidus temperature. Intense heat of the moving arc generates the melted zone in specimen. The thermal conductivity of the material is assumed higher than its value at room temperature in those region to initiate the fluid flow when the temperature reaches above the solidus

temperature [32,66]. The welding is performed first on the bottom side and then on the top side with the subsequent intermediate cooling cycle, related to position of the torches. Most commonly the latter arc unit is placed at half of the pitch before 12 o'clock as compared to the prior arc unit. Therefore an equivalent intermediate cooling time is given between the first and last welding pass on the bottom and top side respectively.

A rate independent bilinear isotropic hardening material is considered for the material constitutive behavior which implies the Mises yield surface, associated flow rule and the von Mises yield criterion for the material plasticity. The thermal and mechanical temperature dependent material properties for both base and filler metal are assumed to be the same which are provided in the Table 3.2.

Table 3.2: Temperature Dependent thermal and mechanical properties

Temperature (°C)	Thermal Conductivity (W/mK)	Specific Heat (J/kgK)	Enthalpy $\times 10^9$ (J/m ³)	Poisson's ratio	Yield Stress (MPa)	Young's Modulus (GPa)	Thermal Expansion Coefficient $\times 10^{-6}$ (°C ⁻¹)
0	51.9	450	1	0.2786	290	200	10
100	51.1	499.2	2	0.3095	260	200	11
300	46.1	565.5	2.65	0.331	200	200	12
450	41.05	630.5	3.8	0.338	150	150	13
550	37.5	705.5	4.1	0.3575	120	110	14
600	35.6	773.3	4.55	0.3738	110	88	14
720	30.64	1080.4	5	0.3738	9.8	20	14
800	26	931	5.23	0.4238	9.8	20	15
1450	29.45	437.93	9	0.4738	-	2	-
1510	29.7	400	11	-	-	0.2	-
1580	29.7	735.25	11	-	0.0098	0.00002	-
5000	42.2	400	12.5	0.499	0.0098	0.00002	15.5

A sequentially coupled analysis is performed in which the thermal results are applied on the mechanical model for the prediction of the residual stress field. The mesh during

the thermo-mechanical elastic plastic model is same as that in the thermal analysis. The boundary conditions are applied for the numerical convergence and restricting the rigid body motion in the model. For this reason the model is constrained far away from the welding region so that boundary conditions may not affect the stress field. Finite element discretization and meshing in both thermal and structural formulations are such that they can capture the accurate stress and temperature gradient. Therefore, dense mesh is achieved near the weld portion while the region away from it has comparatively coarse mesh. A combination of solid brick elements and tetrahedral elements are used to built up the model with eight and four nodes, respectively. For thermal analysis, SOLID 70 is used because of its thermal conduction capability to solve steady and transient problem with single degree of freedom. The equivalent structural element SOLID 185 is used for 3D structural analysis. It has three degree of freedom with capabilities such as plasticity, large deflection, large strain, stress stiffening, swelling and creep. Furthermore, these elements are also support birth and death option for filler deposition.

3.7 FILLER MATERIAL ADDITION

In the current simulation, the addition of filler material deposition is also considered. Initially, the whole finite element model is generated. For thermal analysis, all elements belonging to the weld pool are deactivated by assigning very low thermal conductivity. The weld elements are added on both sides depending upon whether welding is being done on the top or bottom side. The weld bead elements are activated as the welding progresses and these elements must be under the influence of heat source. To avoid the ill

conditioning and float, the nodes not attached to the active elements are remained fixed at ambient temperature till the birth of respective elements.

In the structural, the reference temperature for zero thermal strain calculation is set as melting and ambient temperatures for the filler and base metal, respectively. In order to avoid the numerical instabilities, it is revealed that elements are not born until the heat source has passed. At such instant, elements have reached to their peak temperature and consequently experience cooling. Furthermore, the property of temperature dependent secant coefficient of thermal expansion is also modified according to prescribed reference temperature of deactivated filler elements and their material properties are also switched at the time of activation. The Full Newton-Rapshon iterative scheme along with the modified material property table is used for improved convergence and reformulated stiffness matrix.

CHAPTER 4 WELD INDUCED STRESSES AND EFFECT OF TIME LAG

The non uniform temperature and stress field is produced due to welding. The results obtained from the developed model as discussed in pervious chapter are analyzed in this section. Temperature and stress evolution in spiral is at different locations and times are presented. The effects of stress by introducing the time lag in the weld torches are also described.

4.1 VALIDATION

4.1.1 Thermal Validation

The high temperature and flux gradient due to the heat input per unit volume by the arc generated between the wire and base metal due to the heat source interaction with material cause severe thermal excursions which result into fusion and HAZ region. The thermal loading of heating and cooling cause the melting, re-melting and solidification of the weld pool and generates the boundaries of fusion and HAZ. For the validation purpose, the comparison of numerically obtained boundaries and dimension of HAZ is

made with welding data sheet [69] of spirally weld pipes of same dimension and grade. A reasonable good and close agreement is found between them as shown in Fig. 4.1.

The fusion zone and heat affected zone exhibits different mechanical and metallurgical behavior as compared to the base metal. This is because that in these regions, the attained peak temperature is well above the solidus temperature which changes the microstructure. The phase transformation, changes in microstructure and mechanical properties are mainly dependent upon the heat input, peak temperature and cooling rate. The cross-sectional temperature distributions for different times along the location 2 are shown for inner and outer welding in Fig. 4.2: These temperature distribution characterize the weld bead shape and also responsible for the change in micro-structural properties in the vicinity of FZ (fusion zone) and HAZ.

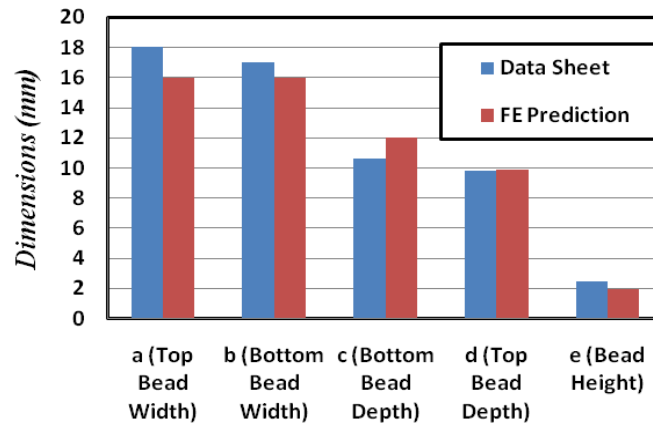


Fig. 4.1: Comparison of HAZ dimensions

Table 4.1: HAZ dimensions

dim.	SPIRAL		FE PREDICTION (mm)	
	a	b	a	b
a	18	± 3 mm	16	16
b	17	± 3 mm	16	16
c	8.9	10.6 mm	12	12
d	9.8	11.4 mm	9.9	9.9
e	0.5	2.6 mm	2	2

(Comparison with data sheet)

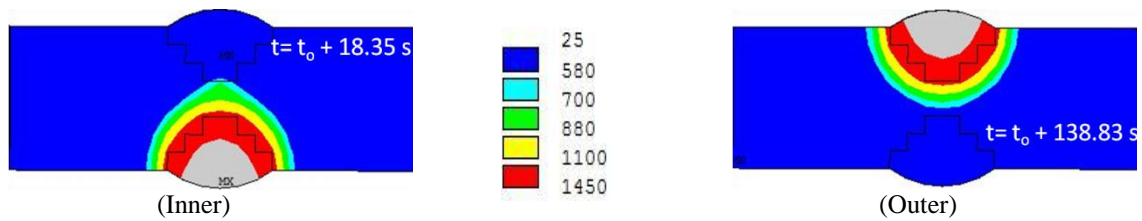
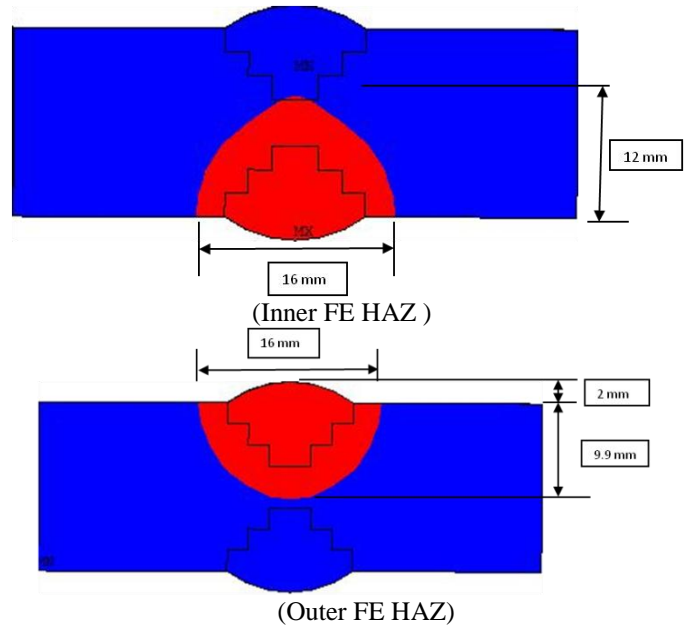


Fig. 4.2: Cross sectional temperature distribution

4.1.2 Structural Validation

It is well reported that the high tensile residual stresses usually exist near to the weld region and parallel to the direction of weld line. These tensile stresses are high enough that they may even surpass the yield stress. The weld metal fracture and weld cracking are the detrimental effects of the tensile stresses. Further away from the weld line, the residual stresses are compressive which are counter balanced of the tensile stresses. The tangential stress whose direction is always parallel to the rolling weld direction and

change accordingly to the weld line in case of spiral welding. Therefore, the tangential residual stresses cause high tensile stresses in the locality of weld zone. The transformation of stresses at location 2 is performed for both inner and outer side by using the Eq. (4.1) and shown in Fig. 4.3. The distribution of stresses, as suggested by Masubuchi and Martin [70] by Eq. (4.2) and Tada and Paris [71] by Eq. (4.3), are also plotted for justification. Here, σ_m is the maximum stress in the weld zone, b is the half of the width of tension zone and y is the distance in transverse direction to the weld.

$$\sigma' = A_{ik} \sigma_{kl} A_{jl} \quad (4.1)$$

$$\sigma = \sigma_m \left(1 - \left(\frac{y}{b} \right)^2 \right) \exp \left(-\frac{1}{2} \left(\frac{y}{b} \right)^2 \right) \quad (4.2)$$

$$\sigma = \sigma_m \left(1 - \left(\frac{y}{b} \right)^2 \right) / \left(1 + \left(\frac{y}{b} \right)^4 \right) \quad (4.3)$$

It is evident that the tensile tangential stress in spiral ring is higher in outer side as compared to the bottom side and their values are 308.4 MPa and 283.5 MPa, respectively. The percentage increase with reference to the bottom surface is found to be 8.78%. The tensile residual stress area is wider on outer surface than inner surface. This is because of post heating by the outer side welding which reduces the tensile stresses and tensile area on the inner surface. The distribution as suggested by Masubuchi and Tada showed the slight variation away from the weld zone but still reasonable agreement is observed in weld region. Away from the weld zone, the deviation of compressive stresses is due to the curvature of pipe and double sided welding.

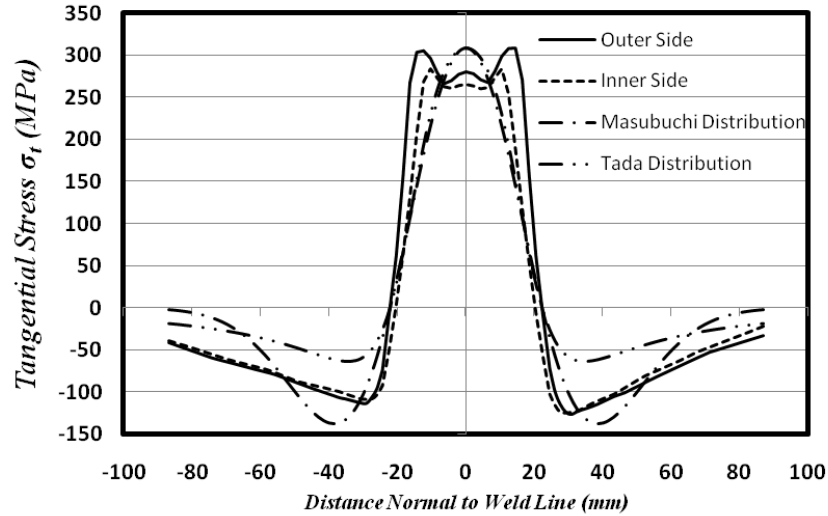


Fig. 4.3: Tangential stress distribution

4.2 RESULTS AND DISCUSSION

The double submerged arc welding of spiral pipe ring is performed. The residual stress field is mainly dependent upon the nonlinear temperature distribution in the whole domain.

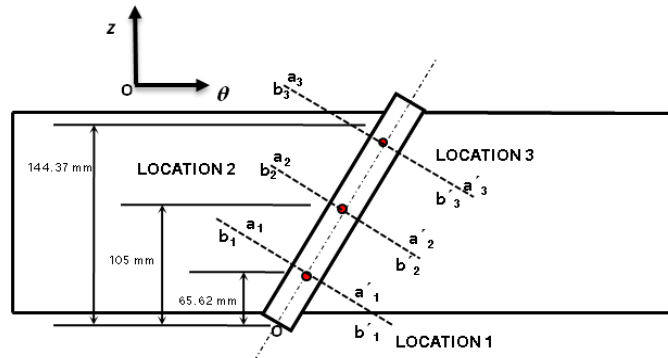
Three different locations are taken for investigation of temperature profile along the cross-section of welding line. The details of these positions in cylindrical coordinates for both inner and outer sides are shown in Table 4.2. The outer and inner sides are denoted by a-a' and b-b' while the subscripts 1, 2, and 3 represent the corresponding locations.

The temperature profiles at each cross section for different times are plotted in the Fig. 4.4. At each cross-section, four different times are taken which are corresponding to

the time required to reach at each cross-section on the inner and outer side, while remaining times are at the end of intermediate and the final cooling.

The temperature rises suddenly to very high value even above the melting temperature on the centre of each cross section. The temperature on the inner surface rises at 11.87 s, 18.35 s and 24.83 s. The moving heat source reaches progressively on all these locations at these values of time. Since the center of heat source is along the weld line, the maximum value of temperature is at the 0 mm on the cross-sectional line.

Table 4.2: Cross sectional positions along the weld seam



Position No.	Outer /Inner	Radial distance r (mm)	Azimuth Angle θ (deg)	Axial Position z (mm)
Location 1	Inner	695	16.18	65.62
	Outer	711	16.18	65.62
Location 2	Inner	695	25.89	105
	Outer	711	25.89	105
Location 3	Inner	695	35.59	144.37
	Outer	711	35.59	144.37

It can also be seen that the distribution of temperature normal to the weld lines have a sharp gradient. As moving away from the center, the temperature decreases till it almost reaches to the room temperature. The shape of temperature profile normal to rolling

direction of welding is similar to the distribution observed in circumferentially weld pipe [37]. Moreover, the similar shape of temperature profile is also seen in the plate welding [72].

It is also clear from the distribution that the temperature on the both side of the centre line varies symmetrically irrespective of the spiral welding and also the exponential decay of temperature on both side is same which justified by the Rosenthal analytical solution of heat flow [73]. The temperature peak is higher on the outer side than on the lower side. The high peaks of temperature on the outer side are observed at 132.22 s, 138.83 s and 145.44 s. The heat source reaches to corresponding locations at each instant of time. There is no significant change in the maximum temperature value and profile at each location which is because of the constant speed and heat input process parameters. At the end of intermediate and final cooling, the temperature profile drops down to the lower values due to the heat conduction and heat loses in the form convection and radiation.

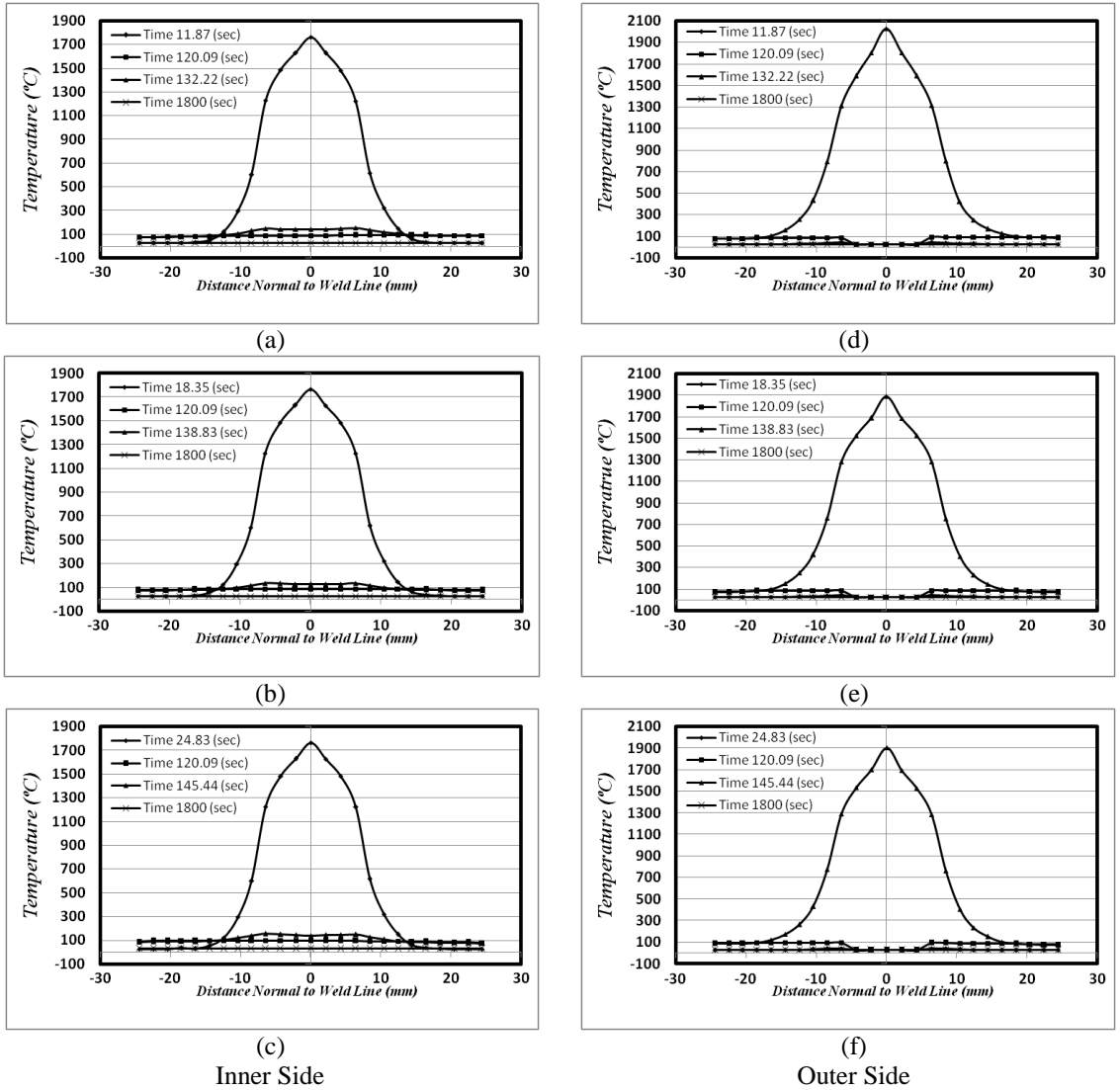
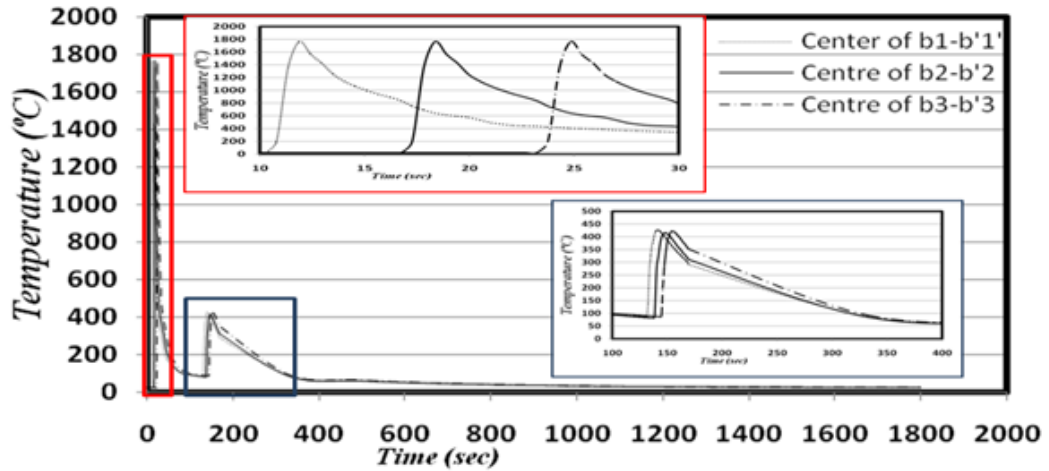


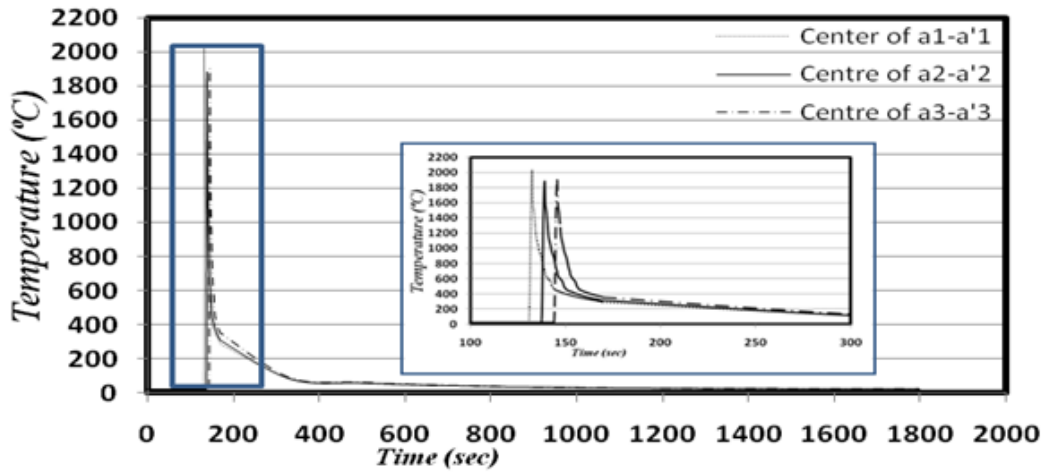
Fig. 4.4: Temperature variation at each cross section

The transient temperature histories at the centre of inner and outer cross-sectional lines are plotted in the Fig. 4.5. which is similar in trend to [37,65,66] The sharp rise of temperature is seen as the heat source passes through the each point with the corresponding value of time. The temperature decreases rapidly after the passing of the arc. The intermediate cooling time is much lower than the final cooling time. During the final cooling, the temperature value returns gradually to the room temperature. When the

top welding starts, after finishing of the intermediate cooling, the temperature of inner side again increases from lower temperature value to almost 450 °C, as shown in Fig. 4.7. The welding on the outer side acts as post weld heat treatment for the inner side weld. The influence of top welding on the bottom side weld can also be seen in the stress distribution.



(a)



(b)

Fig. 4.5: Transient temperature (a) At the centre of inner cross-sectional lines (b) At the centre of outer cross-sectional lines

The temperature distribution at inner and outer weld seam during the bottom and top welding are shown in the Fig. 4.6 and Fig. 4.7. The temperature is high enough in weld pool during the bottom welding but on the opposite side the torch is not yet passed and

the weld bead is still not laid therefore; the temperature on the top weldment is at room temperature. The variation of temperature on the top is seen away from the weld bead during the bottom welding. The isotherms of temperature evolve and spread behind the heat source which is due to the conduction of heat towards the lower temperature region.

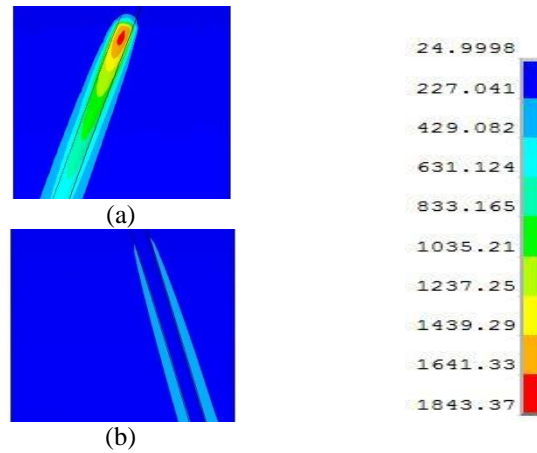


Fig. 4.6: Temperature distribution during bottom welding on (a) inner and (b) outer side

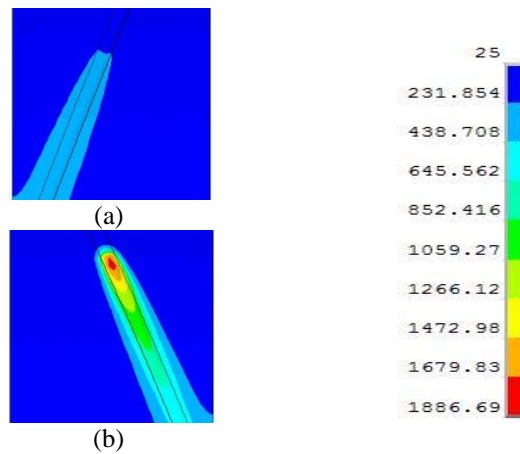


Fig. 4.7: Temperature distribution during top welding on (a) inner and (b) outer side

The binormal stress distribution which is perpendicular to the direction of weld seam and representing the transversal stress of spirally weld path. The binormal stress distributions are plotted for inner and outer spiral weld line in the Fig. 4.8 by performing the transformation of stresses along the weld direction. The stress for the outer side at both start and end is compressive and least compressive at the middle. The inner side stress is tensile at start and end location. The final states of residual stresses are dependent upon the temperature distribution attained in last welding pass. Therefore, The trend of the binormal stress on the top side has a close resemblance with the study [4,6].

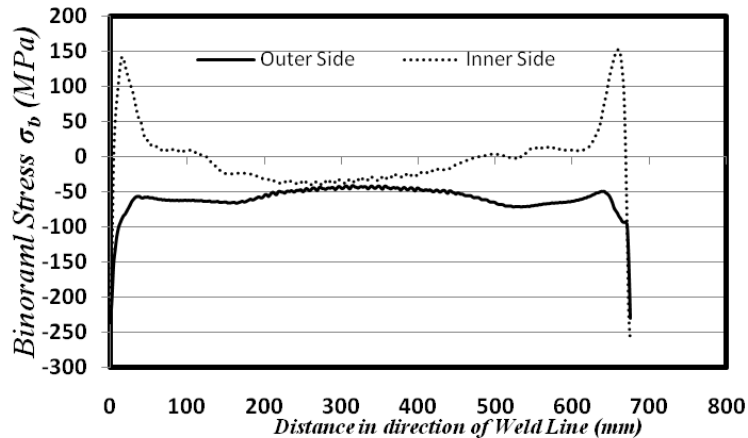
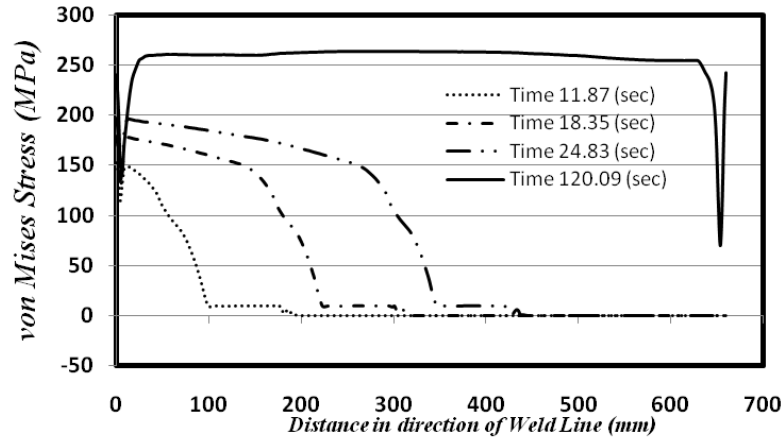


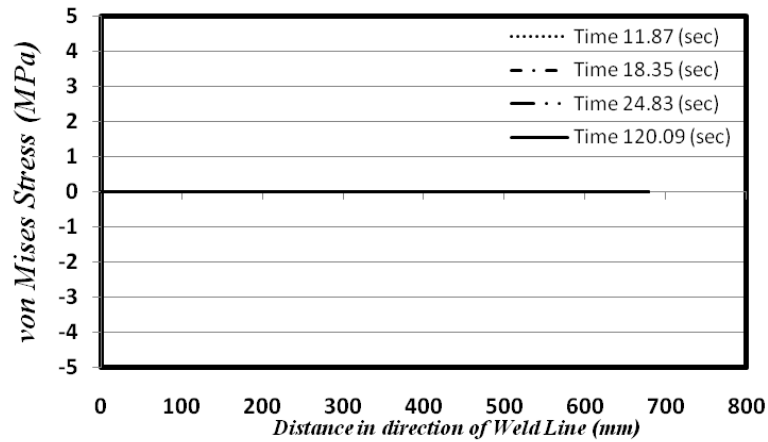
Fig. 4.8: Binormal Stress distribution

The von Mises stress distribution for both inner and outer spiral weld lines for bottom welding are shown in the Fig. 4.9. With the passage of time, the von Mises stress starts to develop behind the heat source and at the end of intermediate cooling it becomes the residual stress on the inner weld line. This is due to the lowering of temperature gradient behind the heat source position and attainment of thermal strain as the temperature decreases with time. Therefore, high value residual is reached at the end of intermediate

cooling due to the metal shrinkage and developed thermal strain. The value of von Mises stress is zero ahead to heat source position and also on outer weld line. Thus, the residual stresses are not yet build up there because weld fusion is not occurred. Residual stress of low value is present at the position of heat source centre and surrounding because of high temperature gradient in this region. The attained high temperature results in melting of weldment in this area. Moreover, the insignificant contribution of von Mises stress is due to the low value elastic modulus at a high temperature.



(Inner weld line)



(Outer weld line)

Fig. 4.9: During bottom welding and intermediate cooling

After the completion of bottom welding and intermediate cooling, the top welding starts and then final cooling step occurs. The residual distributions are shown for outer and inner weld line during the top welding in Fig. 4.10. The von Mises stress develops on the outer weld line as the welding proceeds, similar to the bottom welding on inner line. The residual stress on inner weld line has already been attained by the completion of bottom welding and intermediate cooling. Therefore, the temperature distribution by top welding redistributes the stresses on the inner weld line. The sudden drop in the stress

value is due to the penetration of heat towards the bottom side during the top welding and it moves to the next location according to the heat source position with time.

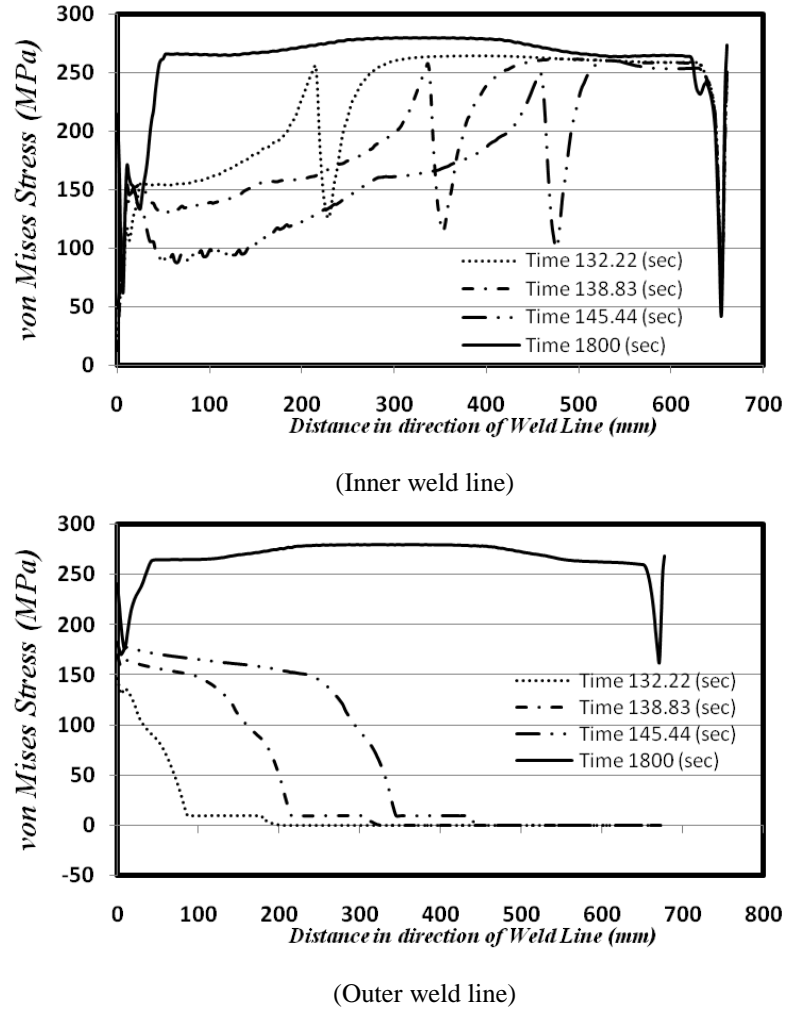


Fig. 4.10: During top welding and final cooling

4.3 EFFECT OF TIME LAG

The top and bottom welding heads are situated at such a position which produces the welding time gap. Therefore, an intermediate cooling of bottom weldment occurs before

the initiation of top welding. Usually the adjusted bottom and top submerged arc units are before 6 o'clock and 12 o'clock respectively. The rolled strip passes through the bottom welding unit before reaching to the top welding unit. The inclination of torch positions effects the weld bead shape due to the rotation of pipe and weld metal pool. Therefore, the concave and convex weld beads are produced somehow on bottom and top respectively. However, the current study does not incorporate the flow of weld metal and the rotation of pipe instead the heat source is moved along the weld path. The intermediate time is varied for six different corresponding pitch positions of top welding relative to the bottom welding as in Table 4.3. The different configurations of top welding at various pitch position are shown in the Fig. 4.11.

Table 4.3: Welding times for different distance lag in pitch

No.	Distance lag in Pitch	Bottom Welding Time (sec)	Intermediate Cooling Time (sec)	Top Welding Time (sec)	Final Cooling Time(sec)
1	0.25	34.54	25.49	35.26	1800
2	0.5	34.54	85.54	35.26	1800
3	0.75	34.54	145.59	35.26	1800
4	1	34.54	205.64	35.26	1800
5	1.25	34.54	265.68	35.26	1800
6	1.5	34.54	325.73	35.26	1800

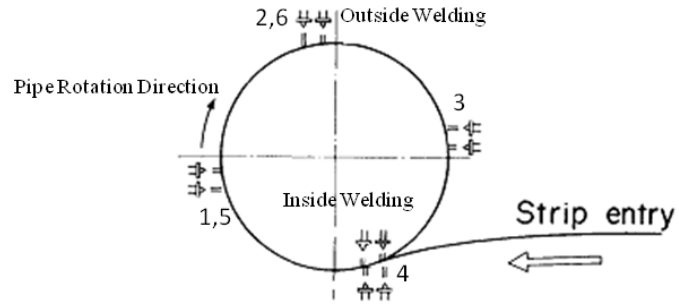
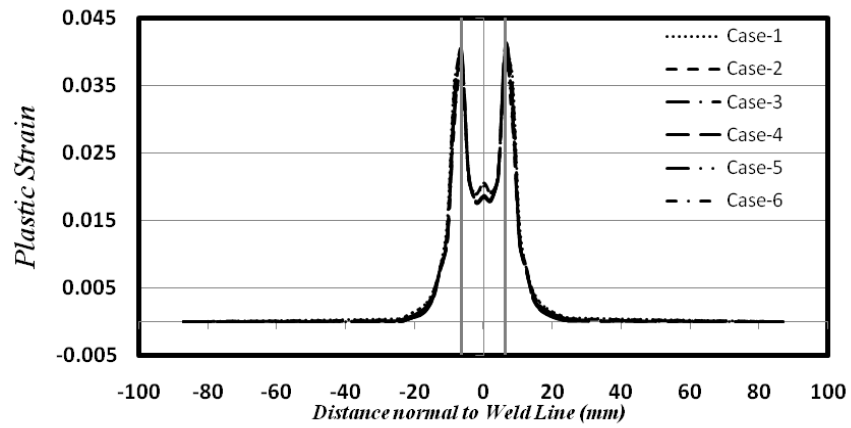
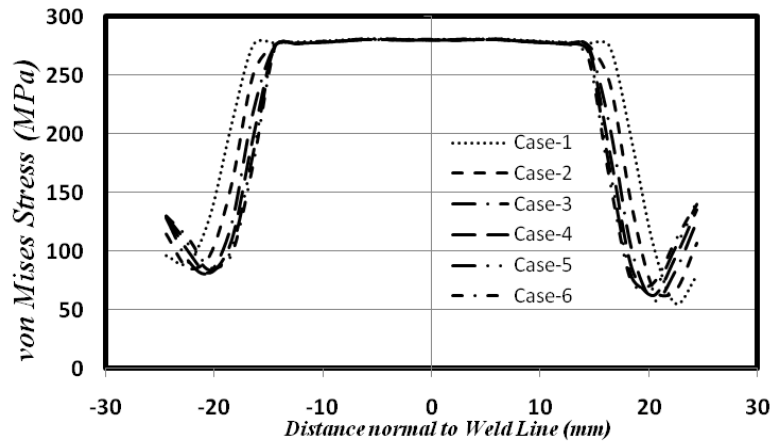


Fig. 4.11: Welding positions



(Outer side)



(Outer side)

Fig. 4.12: For all cases Plastic strain and von Mises stress

The equivalent plastic strain and von Mises stress for all cases are plotted at location 2 on the outer side for all cases. It is found that the maximum value of plastic strain does not change appreciably with varying the lag time between the welding torch units. However, it is observed that the maximum value of plastic strain occurs at the interface of filler material with side wall and minimum at the center of the welding line. Further away from the side walls it reduces sharply till it vanishes. The molten state of filler metal in the weld groove and its restriction in material flow path is due to side the walls. The fusion of side walls at high temperature and subsequent contraction on cooling results in the maximum value of plastic strain at the contact surfaces. It is also observed that the level of von Mises stress distribution is also same in all cases near to the weld line. The position of case-1 is at 0.25 of pitch which is closest to the bottom welding source and has least intermediate cooling time. The isotherm generated by the top welding is affected more in this case. Therefore, prolonged area of high stress is observed and least area is in the case-6 which is 5 times away from the case-1. Thus, there is an insignificant change in the residual stress level in the vicinity of weld which is approaching to 280 MPa for all pitch positions. However, the small variation is observed away from the weld in all cases.

4.4 CONCLUSION

A comprehensive model for spiral welded pipe has been developed to investigate the distribution of temperature welding. By sequentially coupling the structural model with

the thermal model, welding residual stress field has been analyzed to draw out the following conclusions:

- The stress field distributions of spiral welding in the tangential and binormal space are similar to that of plate welding.
- The tensile stress on the bottom side of the weld bead is lower than the upper side because of redistribution of stresses during top welding.
- The maximum plastic strain occurs at the walls of the groove adjoining the base metal.
- Time lag has an insignificant effect on the residual stress level and maximum estimated value of plastic strain. However, change in the time lag increase or decrease the high stress area.

CHAPTER 5 HOOP STRESS DISTRIBUTION AND SPLIT RING TEST ANALYSIS

Residual hoop stress induced due welding in the pipe has the significant effect and its one of the criterion for designing of pipelines to suit their purpose. The weld induced hoop stress distribution is analyzed in the spiral pipe in the current chapter. The study is also conducted whether the split ring test estimates the weld induced hoop stress or not.

5.1 HOOP STRESS IN A SPIRAL PIPE AND ITS COMPARISON

During the working service pressures, resulting stresses are developed. These pipelines are normally designed for the load of hoop stress of 72% of minimum specified of the yield strength (SMYS) of the base material. The Barlow approximation [74] for the circumferential hoop stress and longitudinal axial stress are given by.

$$\begin{aligned}\sigma_{\theta} &= \frac{1}{2} \left(\frac{D}{t} \right) P_i \\ \sigma_z &= \frac{1}{4} \left(\frac{D}{t} \right) P_i\end{aligned}\tag{5.1}$$

where D is the nominal diameter of pipe, t is the wall thickness. It is quite interesting from the Eq.(5.1) that the magnitude of the resulting hoop stress is twice the axial stress. Due to this reason the longitudinal burst often occur during the pressure test which determines the failure mode of the pipe. Therefore, the design criterion of hoop stress is necessarily met for the safe and reliable application of the pipe.

The actual stresses in the pipe can be higher than the applied hoop stress, as generally, the residual stresses are not accounted for design. These stresses are additive and contributing in stress field. Therefore, fabrication induced stresses have gained interest for more structural integrity assessment procedure which required more information of residual stress state for accurate design approach of the pipe.

The spiral welded pipes can withstand more hoop stress as compared to the longitudinal welded pipes. The basic reason is the deviation of the spiral seam relative to the pipe axis. The longitudinal pipes experience the maximum hoop stress while the spiral pipes are subjected to some of its fraction as shown in Fig. 5.1. Therefore, these pipes can withstand more hoop stress relative to the longitudinal pipes. The relationship of the weld normal stress acting perpendicular to the weld seam and the helix angle are related by the following equation [75].

$$\sigma_n = \sigma_z (\cos^2 \alpha) + \sigma_\theta (\sin^2 \alpha) \quad (5.2)$$

where, σ_z and σ_θ are longitudinal and hoop stress respectively, α is the helix angle relative to pipe axis.

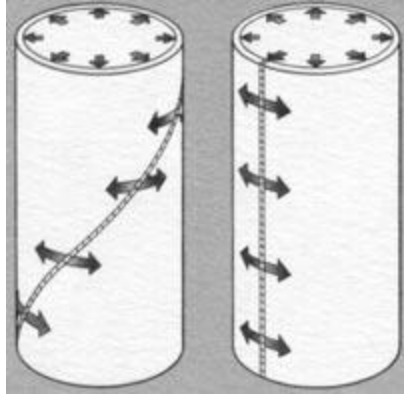


Fig. 5.1: Hoop stress in spiral and longitudinal pipe [76]

The stress dependence on the weld angle is explicitly explained by Knoop and Sommer [77]. For the three cases of loading, the ratio of normal stress to the circumferential stress as a function of the weld angle is shown in Fig. 5.2. It is clear that when neglecting the longitudinal stress, the more normal stress acting perpendicular to the weld seam decreases with the deviation of seam angle from the pipe axis. It is found from all loading cases, the longitudinal weld seam are subjected to highest stress, and circumferential weld seam to the lowest stress. The spiral pipes are placed in between them. Therefore, in these pipes the weld normal stress lies between the 50 to 75 % of the longitudinal weld.

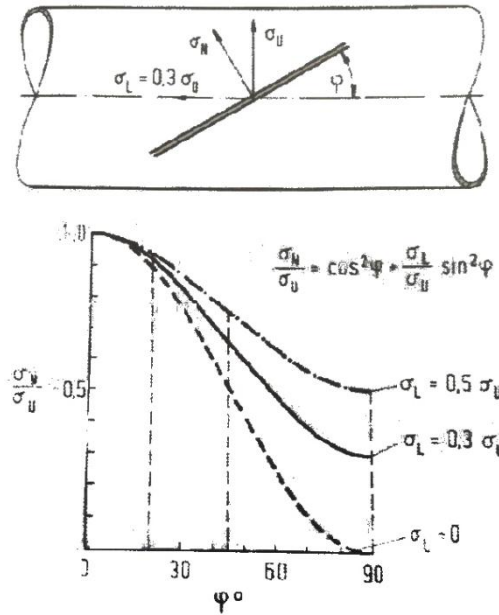


Fig. 5.2: Stress dependence on the weld angle [77]

5.2 Residual Hoop Stress Field in Spiral Pipe

The residual hoop stress develops in spiral pipe due to the weld metal contraction and expansion after the weld heating and its subsequent cooling. The hoop stress distribution normal to the weld line on the inner and outer side is shown in Fig. 5.3. The tensile hoop stress exists near the weld zone while the compressive stress is present far away from the weld center line. The compressive stress away from weld line at distance of 25 mm on outer side is comparatively higher than the inner side. The magnitude of the tensile hoop is high and reaches near to the yield strength. On the outer side, hoop stress is relatively low on the weld center line than just near in its vicinity. The similar distribution of stress in spiral pipe is depicted in [63].

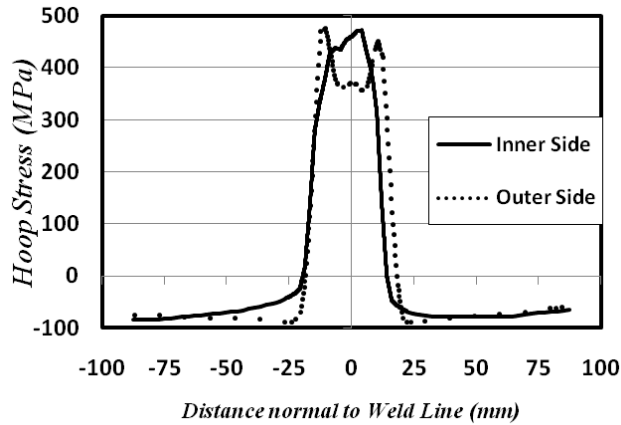


Fig. 5.3: Residual hoop stress distribution normal to weld line

Since the hoop stress plays dominant role in service when the pipe is subject to the high working internal pressure. For the required safe operation, the estimation of its hoop stress must be assured. The hoop stress distribution along circumferential direction for inner and outer side is shown in the Fig. 5.4. The peak hoop stress on both outer and inner side is observed at the position of weld line. However, the maximum hoop stress on the outer side is higher as compared to the inner side. The nature of stress at the weld line is highly tensile. The magnitude of hoop stress on outer side is 470 MPa while on the inner side is 420 MPa. The hoop stress decreases sharply just very near to weld line on positive and negative angular positions at both outer and inner sides. The maximum compressive stress is observed to be -100 MPa. The compressive stress zone is present till 36° and -36° on both sides of pipe. The major portion of pipe doesn't have significant hoop residual stress. The value of stress is nearly zero on negative angular position from -36° to -180° and also on positive angular position from 36° to 180° on both inner and outer side. The hoop stress shows variation in circumferential direction i.e. tensile peak

and compression zone. Therefore, weld residual stress distribution are not axisymmetric in circumferential direction.

The hoop stress generates the bending moment stress along the thickness of the pipe. The hoop shrinkage is the main cause of the well known tourniquet effect that is due to the local inward deformation in the vicinity of weld [25]. The through wall Hoop stress from outer side towards the inner side of pipe can be seen for different circumferential location in the pipe in Fig. 5.5. The increasing direction of spirally welded helix is the increasing circumferential direction. The 0° position where welding has been took place while 90° , 180° and 270° positions are corresponding in the increasing circumferential direction.

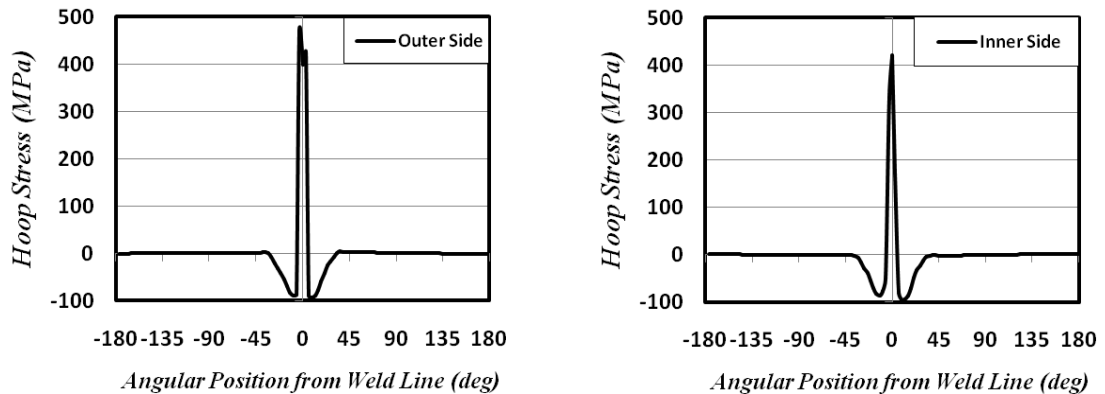


Fig. 5.4: Residual hoop stress along circumferential direction

The hoop stress is varying linearly along the thickness direction at 90° , 180° and 270° positions. The bending nature of stresses is observed at these positions. The magnitude of hoop stress far away from the weld location is very low which are only generated in result of highly stressed region near weld. At 90° position, the outer side stress is found to be 1MPa and on inner side it is -1.12 MPa. The stress is linearly decreasing at 90° and

270 ° positions with very low magnitudes. However, at 180° of weld position, the stress is increasing from -0.51 MPa to 0.58 MPa from outer towards inner side. The stress variation along thickness direction at weld 0° position is highly tensile of large magnitude. The maximum hoop stress of 525 MPa is observed in the range of 7.6 mm to 10.4 mm. The similar distribution is observed in [33] along the thickness for the case in which yield strength of weld and base material are considered to be same. The different values of tensile hoop stresses are observed at 0 mm and 20 mm i.e at outer and inner side of pipe.

There is always corresponding simple structural stress distribution in the form of membrane and bending components for a given local through thickness stress distribution of obtained finite element model which satisfy the equilibrium conditions [78]. Therefore, equilibrium-equivalent components to the local stress distribution can be obtained. The structurally equivalent stress distribution in the form of membrane and bending stress is written as, $\sigma_s = \sigma_m + \sigma_b$ where σ_m is the membrane and σ_b is the bending component. Generally, the membrane residual stresses are prevailing in the hot rolled fabricated sections whereas the bending residual stresses are dominant in cold formed sections [79]. The bending stress is assumed as linearly varying along the thickness while the membrane stress is uniform tensile or compressive stress which is constant through thickness.

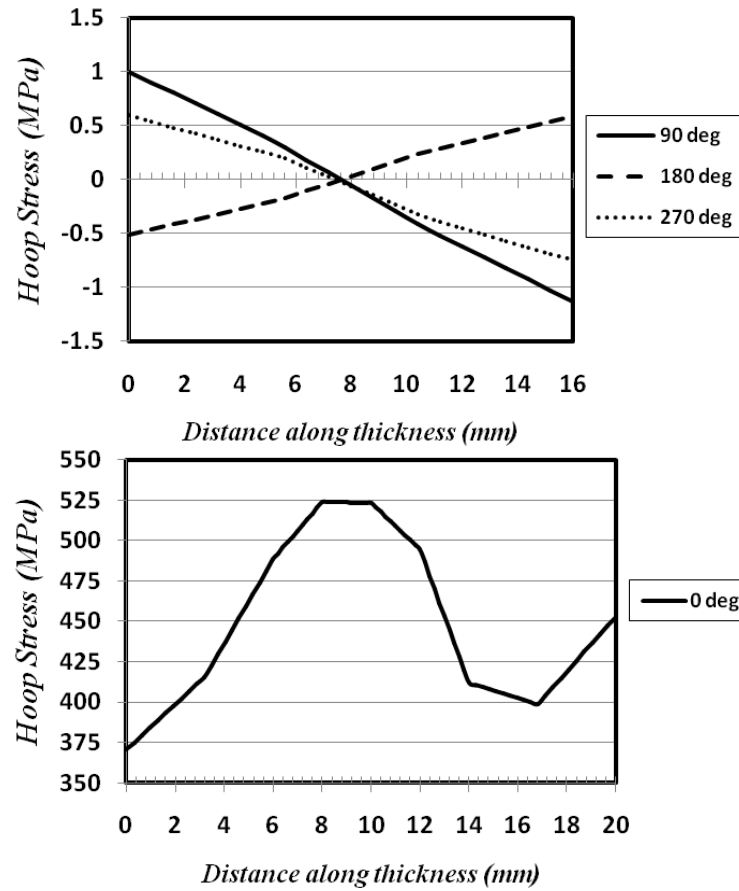


Fig. 5.5: Residual hoop stress along thickness

The hoop membrane and hoop bending stress through thickness are calculated at different positions along the circumferential directions as show in Table 5.1. The membrane stress values at 90, 180 and 270 positions are very low. At these positions, the total stress has major bending stress component which is also comparatively small in magnitude. At the 0°, the local plastic deformation due excessive heat at the weld position causing high tensile hoop stress. Therefore, the membrane stress of large tensile magnitude of 393 MPa is observed at this position. The bending stress value is found at this position is comparatively much higher to the other far away positions from weld. The

bending stress is linearly varying -22.5 MPa to 22.5 MPa from outer to inner side with zero stress at the centre of thickness.

Table 5.1: Hoop membrane and hoop bending stress

0°			90°			
	Membrane (MPa)	Bending (MPa)	Total (MPa)	Membrane (MPa)	Bending (MPa)	Total (MPa)
Outer		-22.54	370.60		1.09	1.00
Centre	393.10	0.00	393.10	-0.06	0.00	-0.06
Inner		22.54	415.70		-1.09	-1.13
180°			270°			
	Membrane (MPa)	Bending (MPa)	Total (MPa)	Membrane (MPa)	Bending (MPa)	Total (MPa)
Outer		-0.58	-0.51		0.71	0.60
Centre	0.03	0.00	0.03	-0.07	0.00	-0.06
Inner		0.58	0.58		-0.71	-0.75

5.3 Split Ring Test

The manufacturing processes such as welding, thermal processing, sheet bending and extrusion have the tendency to developed locked in residual stresses in the tubes and pipes. These stresses exist in the part without the external load being applied. When the part is subjected to external load, the residual stress state is superimposed on the resulting stress state due to applied external load. The structural failure is possible if the combined total stress state exceeds the design stress limit of the component. Therefore, it is necessary to determine the residual stress in pipes to avoid the failure and crack propagation.

A straight forward experimental method for deducing residual stress in pipes is commonly used named as split ring test. As this method is based on splitting and relatively simple from other techniques such strain gage, X-Ray diffraction, Optical techniques. Therefore, it is mostly adopted for the industrial inspection of the components. The approach in this method is to measure the deflection in component after sectioning. The deformation measurements then combine with an elasticity solution to obtain the residual stresses in a tube or pipe. Usually, the residual circumferential stress plays significant role in the welded pipes as the highly tensile stress exists near to the weld. Additionally, due to the external load, the hoop stress is doubled of the longitudinal stress. Therefore, in case of tubing and piping, the interest in estimation of hoop stress is of major concern.

5.4 Stress Calculation Procedures

Many researchers have analyzed the split ring test and provide different equations for the estimation of residual hoop stress in a pipe. In the splitting method, a longitudinal cut is made in a ring of pipe through the wall thickness. The equilibrium is attained again after splitting due to the redistribution of stress. The resulting deformation causes either ring opening or closing. The formulation provided in [80] relates the residual hoop stress in the component using theory of elasticity.

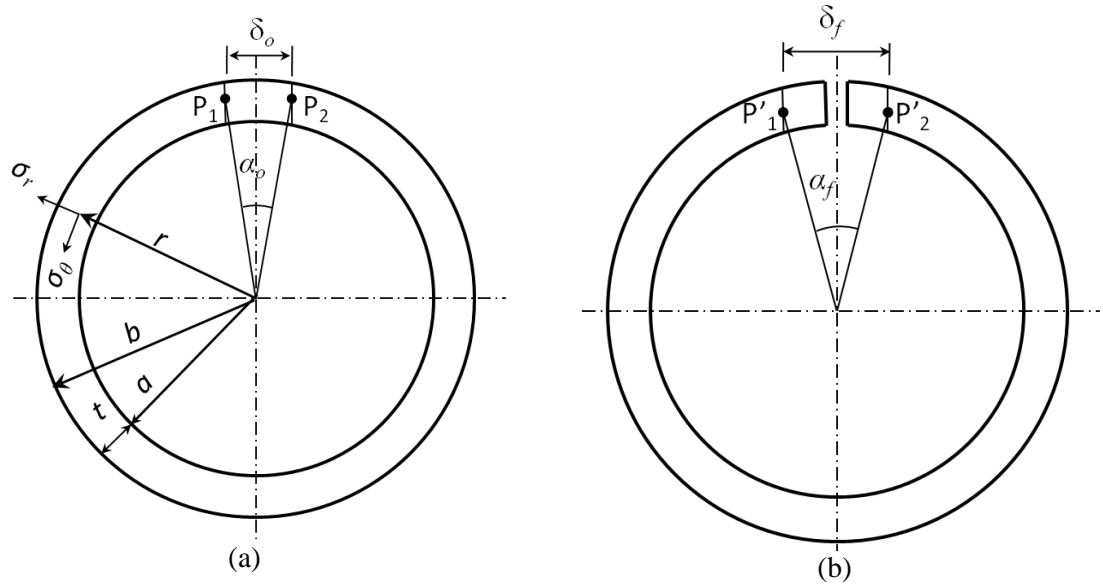


Fig. 5.6: Configuration (a) Before splitting (b) After splitting

In Fig. 5.6, a pipe ring is considered with inner and outer radii, a and b respectively. The ring has been marked before splitting. After splitting, the marked points are displaced due to the release of residual stress which causes to open or close the ring. A moment has to be applied at two ends to retain the ring to its original position. The moment would be equivalent and opposite in direction to the residual moment which caused the deformation after splitting. The general solution of the problem is given in [80] with assuming the stress distribution is symmetric about the pipe axis.

$$\Phi = A \log r + Br^2 \log r + Cr^2 + D \quad (5.3)$$

The stress function depends upon r . and A, B, C and D are constants determined from the boundary conditions. The corresponding stress function is given by.

$$\sigma_r = \frac{1}{r} \frac{\partial \Phi}{\partial r} = \frac{A}{r^2} + B(1 + 2 \log r) + 2C \quad (5.4)$$

$$\sigma_\theta = \frac{\partial^2 \Phi}{\partial r^2} = \frac{A}{r^2} + B(3 + 2 \log r) + 2C \quad (5.5)$$

$$\tau_{r\theta} = 0 \quad (5.6)$$

The required boundary conditions are taken for a ring of unit length as $\sigma_r = 0$ for $r = a$ and $r = b$, $\tau_{r\theta} = 0$ at the boundaries and $\int_a^b \sigma_\theta r dr = M_r$.

Applying these boundary conditions yield the following expression for the hoop stress above equations with manipulation, results the hoop stress into

$$\sigma_\theta = -\frac{4M_r}{n} \left(\frac{-a^2 b^2}{r^2} \log \frac{b}{a} + b^2 \log \frac{r}{b} + a^2 \log \frac{a}{r} + b^2 - a^2 \right) \quad (5.7)$$

Where the value of n is given by

$$n = (b^2 - a^2)^2 - 4a^2 b^2 (\log(b/a))^2 \quad (5.8)$$

and the residual moment, M_r is calculated as:

$$M_r = -\frac{\alpha E}{8\pi} \left\{ \frac{(b^2 - a^2)^2 - 4a^2b^2 (\log(b/a))^2}{2(b^2 - a^2)} \right\} \quad (5.9)$$

where, E is the modulus of elasticity, α is the measured angle of displacement between the two marked ends. The total displacement between the points is defined as the difference between the displacement of marks before and after splitting i.e. $\delta = \delta_o - \delta_f$ and the angle α is related by $\alpha = \delta/r$.

According to the crampton's method [81], the circumferential stress in a tube and pipe can be estimated due to change in diameter on splitting by using the following equation based upon the linear bending along the thickness.

$$\sigma_\theta = \frac{Et}{1-\nu^2} \left(\frac{1}{D_o} - \frac{1}{D_f} \right) \quad (5.10)$$

where D_o and D_f are initial and final diameter before and after the split respectively. The equation is modified with approximation of the final diameter depending upon the ring gap ΔC [62].

$$\sigma_\theta = \frac{Et}{1-\nu^2} \left(\frac{1}{D_o} - \frac{1}{\left(\frac{\Delta C}{\pi} + D_o \right)} \right) \quad (5.11)$$

Another equation given in [60] also relates the ring gap angle with the residual hoop stress as .

$$\sigma_{\theta} = \frac{Et}{4\pi R} \alpha \quad (5.12)$$

where R is the mean radius. For rings longer than $0.1D$, E is replaced by $E/(1-\nu^2)$.

5.5 RESULTS AND DISCUSSION

In the current work, spiral welded pipe is longitudinally split at the position of 180° to the weld. After splitting the residual stress is released which causes the redistribution of stresses and new equilibrium position is achieved. The release of the stress causes the corresponding release of associated residual bending moment in the pipe. The throughout thickness, residual hoop stress before and after split is shown in Fig. 5.7(a) and the difference in the stress state is given in Fig. 5.7(b). It is observed that the on the outer side the residual stress of 6 MPa has been relieved and the gradually along the thickness stress release is linearly decreasing upto 11.2 mm. However, from the thickness 11.2 to 2 mm, the difference in state before and after split is negative which shows that the stress has been increased slight. The maximum stress increase of 1.55 MPa is found at 14 mm. It can also be seen that after splitting, the hoop residual stress at the weld position is dropped slightly.

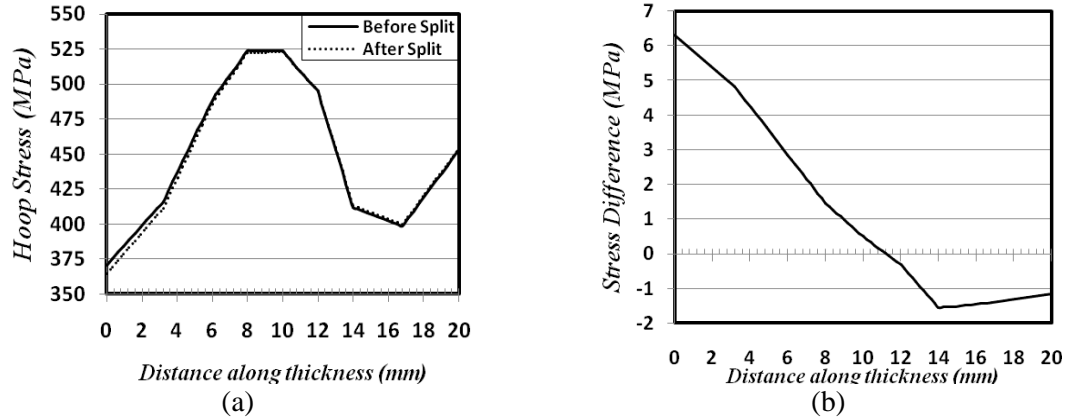


Fig. 5.7: (a) Hoop stress before and after split (b) Stress difference before and after split

The hoop membrane and hoop bending stress after splitting is shown in Table 5.2. The major portion of the pipe, except in the vicinity of welded zone, has low value of bending hoop stress along the thickness. The small portion of hoop stress is released at 90° and 270° after splitting of pipe. It is observed that at the location of cut, the membrane and bending hoop stresses are zero which depicts hoop stress is completely relieved. It is because of the reason that the cutting position is far away from welding and before splitting insignificant magnitude of hoop stress was present. At the weld location membrane stress is released from 393.10 MPa to 387.60 MPa but the bending stress is increased by 0.75 MPa along the thickness.

Table 5.2: Hoop membrane and hoop bending stress after split

	0°			90°		
	Membrane (MPa)	Bending (MPa)	Total (MPa)	Membrane (MPa)	Bending (MPa)	Total (MPa)
Outer		-23.29	364.30		-0.50	-0.50
Centre	387.60	0.00	387.60	-0.03	0.00	-0.03
Inner		23.29	410.90		0.50	0.45
	180°			270°		
	Membrane (MPa)	Bending (MPa)	Total (MPa)	Membrane (MPa)	Bending (MPa)	Total (MPa)
Outer		0.00	0.00		0.51	0.49
Centre	0.00	0.00	0.00	-0.01	0.00	-0.01
Inner		0.00	0.00		-0.51	-0.52

At the weld location, after splitting the membrane stress is released as shown in Table 5.3. The difference between before and after stress release is found to be 5.5 MPa. The average relieved stress along thickness at weld is calculated to be 5.53MPa. The maximum stress in the pipe is released at the weld location which is opposite to the location of cut. The weld thermal stresses are not completely relieved due to longitudinal splitting because the membrane stress of high value 387.6 MPa is still present after the splitting. Only a small portion of membrane stress is observed to be released due to splitting.

Table 5.3: Membrane and bending stress at weld before and after split

	Before split stress (MPa)			After split (MPa)			Difference (MPa)			Avg (MPa)
	Membrane	Bending	Total	Membrane	Bending	Total	Membrane	Bending	Total	
Outer		-22.54	370.60		-23.29	364.30		0.75	6.30	
Centre	393.10	0.00	393.10	387.6	0.00	387.60	5.5	0.00	5.50	5.53
Inner		22.54	415.70		23.29	410.90		-0.75	4.80	

The hoop stress along thickness is calculated in Table 5.4 using ref. [80] which employs elastic theory for curved bars in pure bending. It is evident that the calculated hoop stress varies almost linearly along the thickness. The stress on the outer and inner radius is estimated to be 4.07 MPa and -4.23 MPa respectively whereas in FEA model, the stress on outer and inner side is found to be 6.30 MPa and 4.80 MPa respectively. The hoop stress is also calculated using ref. [62] and ref. [60] as shown in Table 5.5. The calculated hoop stress using mentioned references are found to be 4.56 MPa and 4.45 MPa respectively. After splitting, the ring opening of 7.8 mm is observed in the pipe due to displacement of the ends. The average hoop stress through FE model is calculated to be 5.53 MPa which is nearly close to theoretically estimated values. It is clearly analyzed that the split ring test does not calculate the residual hoop stress due to welding at the weld location but it can only capable for determining the release in hoop stress after splitting in the pipe. The localized residual stresses are produced due to non-uniform heating and cooling during welding process. Therefore, split ring test unable to determine the localized stresses due to welding as only a small portion of stress is released from the weld location.

Table 5.4: Hoop stress using Ref. [80]

r (mm)	α (rad)	n	σ_θ (MPa) Ref. [80]
695	0.01125	8.74E-08	-4.23
696.8	0.01122	8.74E-08	-3.27
698.6	0.01119	8.74E-08	-2.32
700.3	0.01116	8.74E-08	-1.38
702.1	0.01113	8.74E-08	-0.45
703.9	0.01111	8.74E-08	0.48
705.7	0.01108	8.74E-08	1.39
707.4	0.01105	8.74E-08	2.29
709.2	0.01102	8.74E-08	3.19
711	0.01099	8.74E-08	4.07

Table 5.5: Hoop stress using Ref. [60] and Ref. [62]

ΔC (mm)	t (mm)	α	$\sigma_\theta = \frac{Et}{4\pi R} \alpha$ Ref. [60] (MPa)	$\sigma_\theta = \frac{Et}{1-\nu^2} \left(\frac{1}{D_o} - \frac{1}{\left(\frac{\Delta C}{\pi} + D_o \right)} \right)$ Ref. [62] (MPa)	FEA Average (MPa)
7.816	16	0.011119	4.56	4.45	5.53

5.6 CONCLUSION

The residual stresses in spiral pipe have been modeled due to welding process. The hoop residual stress field is estimated which is generated due to intense heating of welding. The split ring test is incorporated in the current model. The following conclusions have been drawn out from the current work.

- In the inner and outer side of the pipe, the residual hoop stresses are highly tensile at the welded pipe but compressive in the vicinity of the weld zone. The stresses in the major portion of pipe are not significant. Therefore, the angular distribution of stress is not symmetrical.
- The hoop membrane and hoop bending stress are high at the weld location but not significant at 90° , 180° and 270° to weld position.
- The major portion of the pipe, except in the vicinity of welded zone, has low value of bending hoop stress along the thickness.
- The split ring test does not determine the residual hoop stress at the weld location. However, it determines the released in stress due to the longitudinal cut. The maximum stress released is found at the weld location.

CHAPTER 6 EXPERIMENTAL ANALYSIS AND MODEL

VALIDATION

In the current chapter, the experimental background, theory and procedures are mentioned. The finite element simulation of spiral submerged arc welded ring is conducted but the reliability and the validation of the model is necessary for the residual stress distribution. Therefore, experimentation is performed using hole drilling method for residual stress calculation. The comparison between the experimental results and finite elements are made for verification purpose.

6.1 INTRODUCTION

Finite element simulation has been also conducted for a spirally welded ring. The FEA solution is based on the number assumptions such as the quasi-stationary heat source moves with constant speed and magnitude of distributed flux intensity. However, variation in the speed and variable flux intensity is present during the actual manufacturing process. Other assumptions can be the material model and its properties at

high elevated temperature. Despite of these, reliable results can be obtained through FE simulation.

The usefulness of FE based model relies completely upon the verification with the experimental work. The homogeneity between them guarantees the correctness of FE solution. The accuracy of model is judged on the basis of their comparison.

6.2 Residual Stress Measurement Techniques

Residual stresses are internal locked stresses in the component which are generated as the result of manufacturing process. Such process can be welding, heat treatment, shot peening, shape change and forming, grinding and machining, and material deformation. . Mostly, residual stresses are undesirable because of their detrimental effects on the product's life. The significant influences of stresses can be distortion and deformation, metal shrinkage, dimensional instability, change in microstructure, brittle fracture, cold cracking. The fatigue life of the product is directly affected because of such stresses.

The nature of residual stresses is different in each of the manufacturing process, depends upon its origin and the cause. Welding is the most common process in industry, generates residual stress of remarkable level. Weld metal solidification causing the differential shrinkage and deformation due to contraction results into the undesirable stress distribution in the structure. The origin of these stresses is the non-uniform thermal heat distribution, causing plastic deformation and phase transformation in the material.

The measurement of the stresses is necessary to identify that whether it can fit for the required purpose or cause the failure damage. Different methods, procedure and techniques have been adopted for the assessment of these stresses in the component. Each of the method has its certain limitation, capability, advantage and accuracy depending upon the nature of stress. The methods for residual stress measurement are based on the destructive, non-destructive and semi-destructive techniques which are shown in Fig. 6.1. The destructive and semi-destructive methods are referred as mechanical methods. The original stress field is anticipated by the cause of stress relaxation due to complete or partial removal of material.

The hole drilling strain gage technique is adopted for calculating the weld thermal stress in the spiral welded ring of X70 grade steel. It is quiet useful and handy method for identification of nature, orientation and measurement of weld induced stresses. It is categorized as semi-destructive method because of a small hole is inserted in the component for the estimation which is usually tolerable and can be easily repairable.

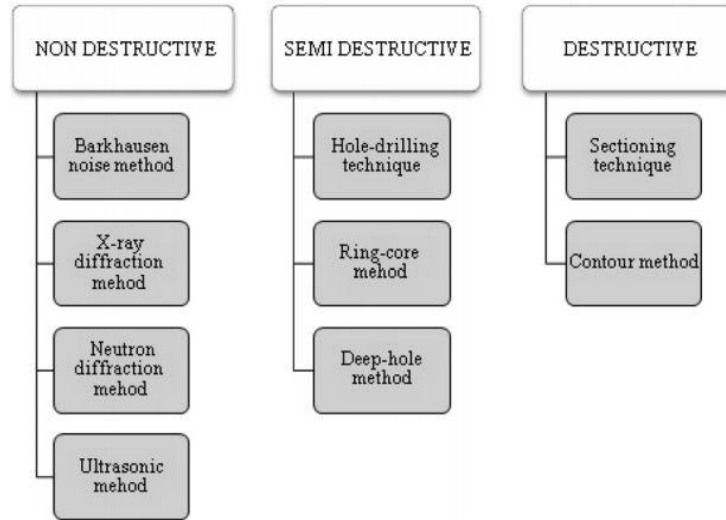


Fig. 6.1: Different residual stress measurement techniques [79]

6.3 HOLE-DRILLING METHOD

Hole- drilling is an advent technique for measuring the residual stress. It is relatively simple and quick. Due to insertion of very small hole in component, it is characterized as a semi-destructive technique. The continuous research is growing to implement this method for identifying the new measures for calculating the residual stress such spline, intergral and power series method [82]. The investigations are being carried out to make this method more accurate and reliable with less uncertainty errors. The drilled hole is assumed to be absolute center of the strain gage rosette. Wang [83] studied the misalignment errors associated with eccentric hole during the experimentation. The error analysis was performed and it was found the 10% off-centre would cause the variation of stress by five percent. Ajovalasit [84] obtained formulae to calculate the actual residual stress with incorporating the eccentric parameters of the hole due to the misalignment.

The application of this method is widely seen in welding technology to estimate the residual stress field and validation of finite element model. Akbari and Sattari-Far [38] experimentally measured the surface residual stress for dissimilar weld pipes and the effect of magnitude of heat input on the stress distribution is studied. Deng et al. [33] analyzed the multi-pass welding in the austenitic stainless steel. The hoop and axial stresses are measured using electric resistance strain gage mounted on both inner and outer side of the pipe to verify the 2D axisymmetric model. The similar strategy is adopted for the authenticity of stress distribution in three dimensional circumferentially arc welded pipe [37]. The regression based model was developed in [85], for minimization of the residual stress in the heat affected zones of AISI 304 plate in which principle stress magnitude and directions were calculated in HAZ using hole drilling method. The residual stresses, before and after the hydrostatic test, in spirally welded pipe were predicted by Forouzan et al. [66] using numerical technique. The justification and validation of results are made through experiments using this technique.

6.4 Principle Of Hole Drilling Strain Gage Method

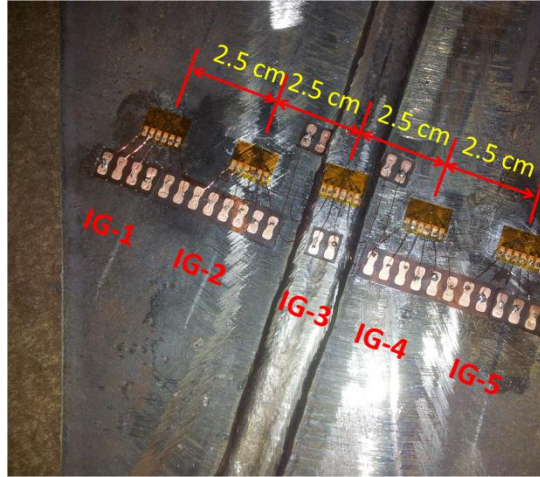
Various methods and procedure are proposed for determining the initial stress field in a structural member by disturbing its stress equilibrium through mechanical device and measuring the resulting deformation. Hole-drilling method of residual stress measurement is laid on the same principle and its foundation was first laid by Mathar [86].

The residual stressed body is subjected to the small diameter hole. This introduction of hole in relaxes the stresses at the location of hole and it's around. This is because that every perpendicular to the free surface is necessarily a principal axis on which the shear and normal stresses are zero. The disturbance in stress equilibrium due to relieved stresses in the locality of hole region causes the local strains to correspondingly change. The resulting deformation on the surface of the test object is measured for residual stress calculation.

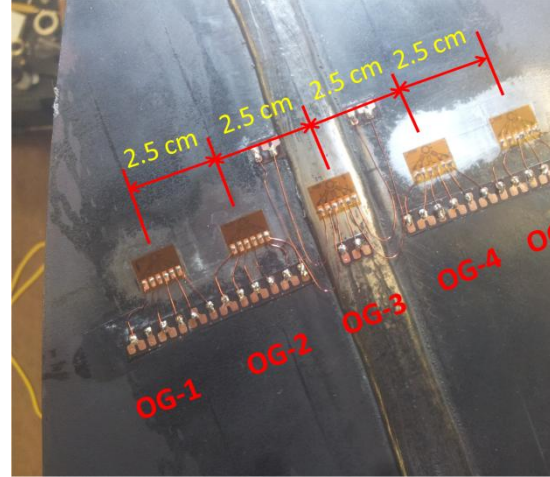
The calibration and empirical coefficient are used to determine the residual stress form the obtained measured strains after drilling. These suitable constant are dependent upon the hole type, i.e through hole or blind hole, type of strain gage rosette etc. This method has an advantage that it can be conveniently and practically implemented with fair accuracy and reliability.

6.5 Experimental Setup for Residual Stress Measurement

An experimental setup is established in the KFUPM Mechanical Stress Lab, for the residual stress measurement in spirally welded API 5L X70 high grade steel pipe ring. Initially strain gages are mounted on the inner side and, then by turn, are placed on the outer side of the ring. The five strain gage rosettes of type CEA-XX-062UM-120 are positioned, in line such as these are perpendicular to the weld seam. One of the strain gage is on the weld centre line while the others two are attached on the both side of the seam. The equally distance of 2.5 cm is maintained between the rosettes. The pictorial view of the mounted gages on inner and outer side can be seen in Fig. 6.2.



Inner side

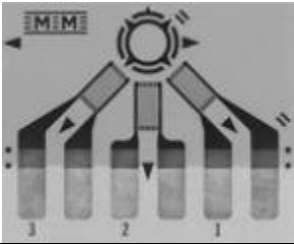


Outer side

Fig. 6.2: Strain gage installation on inner and outer sides

The rosette type CEA-XX-062UM-120 in the current experimental work is used. The advantage of these rosettes can be taken because of their small gage length. Therefore, with this geometrical shape, hole can be placed near to the weld and on the seam without any irregularity. The specification of the gage can be seen in Table 6.1.

Table 6.1: Strain gage specification

Gage pattern and designation of CEA-XX-062UM-120	Resistance Ω	Dimensions					
		Gage Length	Grid Centre line Dia.	Typical hole dia.		Matrix	
				Min.	Max.	Length	Width
	120 ± 4%	0.062 (inch)	0.202 (inch)	0.06 (inch)	0.08 (inch)	0.38 (inch)	0.48 (inch)
		1.57 (mm)	5.13 (mm)	1.5 (mm)	2.0 (mm)	9.6 (mm)	12.2 (mm)

6.5.1 Installation of strain gage and surface preparation

Prior to the bonding of gage on pipe, well properly prepared surface is achieved, according to the instruction Bulletin B-129-8 of micro-measurement system. The purpose of surface preparation is to obtain uncontaminated and a clean surface with the strong stable bond for the consistent results. Mostly openly exposed to environment surfaces contains some kind contamination, therefore surface preparation is a first and necessary step.

The following basic five steps are followed for surface preparation.

- 1) Solvent degreasing
- 2) Abrading
- 3) Application of gage layout line
- 4) Conditioning
- 5) Neutralizing

The strain gage rosette is installed firmly with M-bond 200 Adhesive on after the surface preparation according to the installation instructions provided in bulletin B-127-4.

6.5.2 Soldering and connections

After the insertion of gage, soldering and connection are made with the bondable terminals. Soldering is simple procedure for wiring and can be conveniently used for the lead wires connection. The application notes TT-603, TT-606 and TT-609 are followed for the connection of strain gage with the bondable terminals and further with lead wires.

The resistance of strain gages should be checked after the completion of connections. The resistance value should be in the range of $120 \pm 4\% \Omega$.

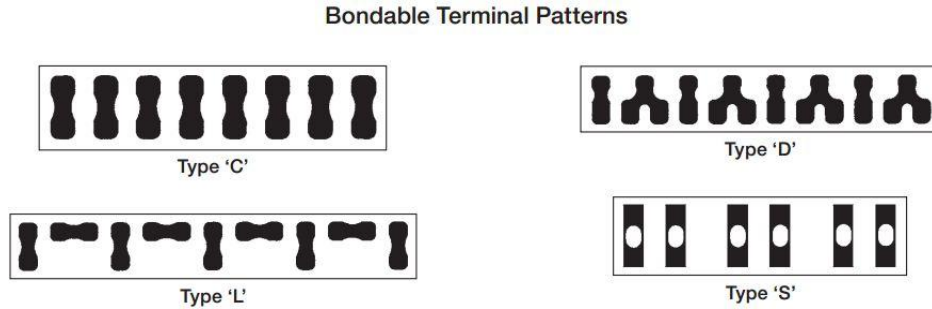


Fig. 6.3: Different bondable terminal patterns

6.5.3 RS-200 Milling guide and setup

The RS-200 milling guide is highly precise instrument for measuring the stresses. The setup is mounted on the strain gage. Its flexibility makes it more handy and suitable for usage. The whole assembly comes in a protective carrying case. The main components are milling guide assembly, microscope, high speed turbine, depth setting gauges with other useful components such as illuminator assembly, anti-rotation adapter, alignment template, tubing and pneumatic valve. The whole assembly is stationed on the pipe as shown in Fig. 6.4. After finishing of measurements, the swivel pads of milling guide assembly are removed with the help of pad removal tool.

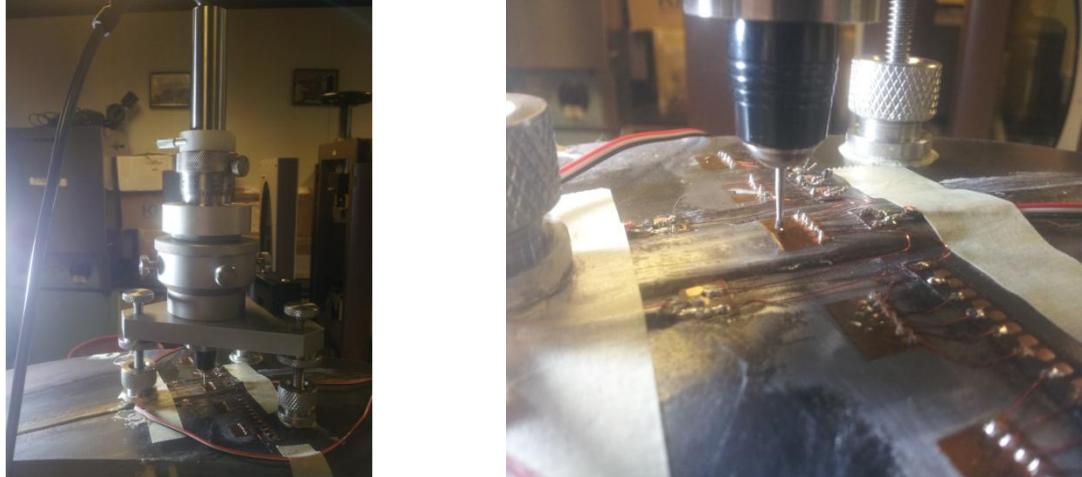


Fig. 6.4: Mounted assembly

6.5.4 RS-200 setup and alignment procedure

The whole assembly is aligned according to the RS-200 milling guide instruction manual. For setting and alignment of the instruments, the following steps are executed

- Alignment template center hole is placed on the rosette and fiducial marks are drawn with the help of pencil for the swivel pads.
- Milling guide assembly is to be placed over the marked holes and leveled according to the surface with the help of leveling screws. The whole assembly should be perpendicular to the test surface. After the adjustment, assembly is returned back.
- Cement mixture is made and applied on the marked circles. Carefully, place the guide assembly over the cemented area. It should be assured that the pads are on the marked circles within the tolerable limit of 3 mm. Wait till the assembly is affixed.

- Whole assembly is mounted as shown in alignment setup in Fig. 6.5. Microscope is adjusted for the clear view of the rosette.
- The most important and crucial step which should be done carefully while aligning. Microscope is used for this reason. The cross hairs which are seen through microscope are adjusted with rosette cross hairs. Adjusting screws are used for this purpose. When they are accurately aligned, firmly lock the screws. It must be assured that exact centre has been achieved.
- High speed component assembly is installed as shown in Fig. 6.6 for drilling the hole. It is assured that drill bit is revolving with high speed and all pneumatic and electrical wire connections are complete. Micrometer screw is rotated for the insertion of hole into the part at very fast rotating speed.
- The measured strains through strain indicator, hole depth through micrometer and hole diameter using microscope can be recorded, respectively.

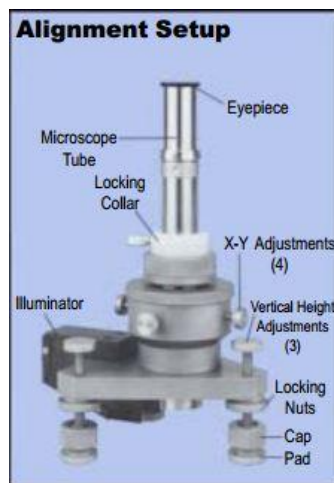


Fig. 6.5: Alignment setup assembly [87]

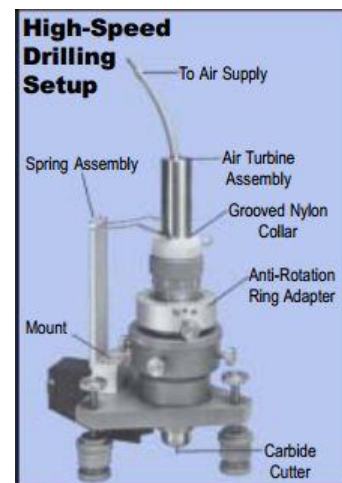


Fig. 6.6: High speed drill assembly [87]

6.6 P3 Strain Indicator and Data Acquisition Recorder

P3 strain indicator from Vishay measurement group is a highly accurate instrument as shown in Fig. 6.7, used with resistive strain gages and strain-gage-based transducers. It works as a bridge amplifier, static strain indicator, and digital data logger in a wide stress measurement application. The indicator has capability to attain signal from full- half- and quarter-bridge inputs with 120-, 350- and 1000- bridge completion resistance.

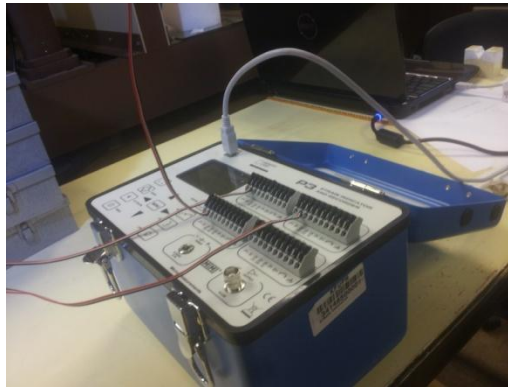


Fig. 6.7: P3 strain indicator

6.6.1 P3 strain recorder setup

The following main steps are taken to use the P3 strain recorder.

- Lead wires connection in quarter bridge circuit is made. Each wire of the gage is connected to channel-1, channel 2 and channel 3 of the indicator.
- Laptop/ Computer interface can be made through the USB wire connection for data recording on the Laptop/computer
- Balance the strain gage reading on the indicator to the initial zero strain.

6.7 EXPERIMENTAL OPERATION

Experimental procedure is quiet easy for the residual stress measurement using hole drilling method. The experimental operation can be summarized in the following steps:

- Carefully, mount the three grid strain gage rosette on the surface at the location where residual stresses are need to be determine.
- P3 strain indicator is connected cautiously to each grid of the strain. Before introducing hole into the part, P3 strain indicator must be balanced to zero strain for each rosette reading.
- Accurate placement and adjustment of the RS-200 milling guide assembly on the strain gage with perfect hole centering for drilling. This step is most critical for correct stress measurement. Therefore, it should be performed with care.
- Precision hole is drilled through the centre of rosette into the test part. High speed turbine is used for this purpose.
- Measurement of relaxed strains are obtained and recorded.
- Using special data reduction relationships (according to the ASTM E837) are used to determine principal stresses from the measured strain.

A small blind hole in cylindrical shape of known configuration, diameter and depth is introduced into the test part. For the blind hole, no closed form solution exists from the theory of elasticity. Therefore, the coefficients are obtained through calibration or empirical procedure [87]. These coefficient are depend upon the geometrical shape,

diameter of hole, depth of hole, type of strain gage and material on which test is being conducted. However, through different approaches, the material dependency on the calibration coefficient is excluded and leaving only the geometrical dependent, proposed by Schajer [88]. Finite element techniques or experimental methods are mostly employed to calculate these coefficients. These coefficients can also be found in ASTM E837 [89] for standard testing procedure for residual stress measurement. In the case of non-uniformity in the stress field distribution, power series and integral methods are formulated to determine stress from strain relaxation data [90]. In the current work, the H-drill commercially available software is used for stress field evaluation.

The objective of the current work to inspect the residual stresses in a spiral welded ring sample using hole drilling method as show in Fig. 6.8. Furthermore is to develop a finite element model and validate it with the experimentally calculated residual stresses. The principal residual stresses are measured using H-drill from the measured strains. The FE based solution of spiral welding is compared with the experimental results.



Fig. 6.8: Weld ring sample for residual stress measurement

6.8 Stress Calculation

There are different developed methods for residual stress calculation. The nature and distribution of residual stress to be measured are not known in advance. Therefore, it is always a good practice to try all methods. The appropriate selection of the method depends upon the good judgment, engineering approach, combined with knowledge of stresses expected. The following three methods for residual stress calculation are extensively used.

Uniform method

This method assumes uniform residual stress along depth from the surface of the specimen and provided in ASTM 837 [89]. It does not offer spatial resolution and least sensitive to the experimental errors when measured residual stresses are uniform.

Power method

This method offers limited amount of spatial resolution by assuming the linearly varying residual stress along the depth. It is good choice when the measured residual stresses are varying smoothly with depth. However, this method is relatively more sensitive to experimental errors than uniform method.

Integral method

It provides the evaluation of residual stress within each depth during measurement. This method has highest spatial resolution form other methods. It is for measuring varying residual stresses. This method is severely sensitive to small experimental errors.

6.8.1 Uniform method for stress calculation

A blind hole is drilled in the centre of the each rosette with increments. The stress field disturbs because of the insertion of hole and redistribute. The correspondingly released strain components are measured with the strain gages. The linear elasticity theory relates the relieved component of strains with the maximum and minimum

principle residual stress and their angle β using following expressions. A schematic diagram showing the typical configuration of strain gage of general type, with mean diameter D , is illustrated in Fig. 6.9

$$\sigma_{\max} = \frac{\varepsilon_1 + \varepsilon_3}{4\bar{A}} - \frac{1}{4\bar{B}} \sqrt{(\varepsilon_2 - \varepsilon_1)^2 + (\varepsilon_3 + \varepsilon_1 - 2\varepsilon_2)^2}$$

$$\sigma_{\min} = \frac{\varepsilon_1 + \varepsilon_3}{4\bar{A}} + \frac{1}{4\bar{B}} \sqrt{(\varepsilon_2 - \varepsilon_1)^2 + (\varepsilon_3 + \varepsilon_1 - 2\varepsilon_2)^2}$$

$$\beta = \frac{1}{2} \tan^{-1} \left(\frac{\varepsilon_1 - 2\varepsilon_2 + \varepsilon_3}{\varepsilon_1 - \varepsilon_3} \right)$$

The non-dimensionalized new calibration coefficients \bar{a} and \bar{b} are introduced by Schajer [88]. The purpose for these coefficients is to exclude the material dependency on the calibrated constant and make them solely dependent upon the geometrical feature of the hole and type of the used rosette. The expression relating the calibration constant is given as.

$$\bar{A} = -\frac{1+\nu}{2E} \bar{a}$$

$$\bar{B} = -\frac{1}{2E} \bar{b}$$

where the σ_{\max} and σ_{\min} are the maximum and minimum principal stress with β angle of orientation, ε_1 , ε_2 and ε_3 are measured relieved strains, E is the modulus of elasticity, ν is the Poisson ratio, \bar{A} , \bar{B} , \bar{a} and \bar{b} are the calibration coefficients.

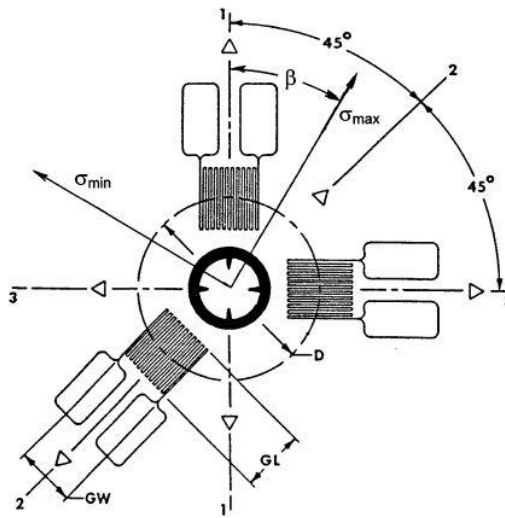


Fig. 6.9: Typical strain gage rosette [89]

The calibration coefficients have been calculated by number of researchers through numerical or experimental methods for different rosette configurations. These coefficients can be easily found in the available literature [88,90,91]. However, for the current study, commercially available program developed by Vishay Measurement Group Inc. and G.S. Schajer is used for the estimation of residual stresses. This program is highly specialized for its task and named as H-Drill. It requires simple user input to find the calibration constants based on the gage type, hole depth and its diameter. H-Drill program is quiet user-friendly and follows the same basic stress calculation procedure

described in ASTM E837 [89] with its extensions for non-uniform residual stress calculation using power and integral method.

6.8.2 Hole drilling for Non-uniform residual stress distribution

In many cases of manufacturing process, the distribution of residual stress is non-uniform along the depth, such as in the shot peening of the material causes the compressive stress close to the surface. Therefore, in such scenarios the hole drilling method is used which makes it possible to choose from various functions that represents the stress state. The functions can be piecewise constant spline, linear spline, cubic spline, power series or Fourier series. Different mathematical procedures have been developed for calculating non-uniform residual stress by incorporating the influence functions in order to construct the experimental measurements. These methods identify the interior residual stress as the evolution of the strains measured as the depth of the drilled hole is increased gradually. The stress sensitivity creates the difficulty for evaluating the interior stresses. The reliability of stress decreases with depth as the sensitivity is correspondingly reduced. Therefore, small errors in the experimental measurement can cause significant induction of errors in the calculated residual stress. This is the fundamental limitation in hole drilling method. Thus, different mathematical methods use various approaches to minimize the noise and disturbance of the experimental errors. The acceptable approaches for non-uniform stress field with least sensitive to experimental errors for calculating the unknown distribution in the specimen can be power series method and integral method [90]. The later method is used for

rapidly varying stress field and severely sensitive to the small experimental errors while the former method assumes the residual stress varies linearly with depth.

6.8.3 Power series method for stress calculation

For calculating the non-uniform stress field, power series method is an acceptable procedure for estimation of the residual stresses from the incremental strain data recorded after the gradual drilling. This method is an approximate approach and firstly introduced by Schajer [88,90]. In this method, the unknown residual stress field is approximated by the terms of the power series.

$$\sigma(h) = b_0 + b_1 h + b_2 h^2 + \dots$$

The strain response using power series variation with depth i.e. $\sigma^0(h) = 1$, $\sigma^1(h) = h$, $\sigma^2(h) = h^2$, etc. is calculated for the incremental drilled hole into the stress field using coefficients $\bar{a}^0(h)$, $\bar{a}^1(h)$, $\bar{a}^2(h)$ and $\bar{b}^0(h)$, $\bar{b}^1(h)$, $\bar{b}^2(h)$. These series coefficients are estimated through finite element calculation by Schajer [90] and shown in Table 6.2 and Table 6.3.

Table 6.2: Coefficients of $\bar{a}^o(h)$ and $\bar{b}^o(h)$ for a stress field, $\sigma^o(h) = 1$ [90]

		Coefficients \bar{a}^o						Coefficients \bar{b}^o			
Hole Depth z/r_m	Hole Radius, r_a/r_m				Hole Depth z/r_m	Hole Radius, r_a/r_m					
	0.30	0.35	0.40	0.45		0.30	0.35	0.40	0.45		
.00	.000	.000	.000	.000	.00	.000	.000	.000	.000		
.05	-.011	-.015	-.021	-.028	.05	-.021	-.028	-.037	-.048		
.10	-.027	-.036	-.049	-.063	.10	-.050	-.067	-.088	-.111		
.15	-.043	-.059	-.079	-.102	.15	-.082	-.111	-.145	-.181		
.20	-.058	-.080	-.107	-.137	.20	-.115	-.155	-.201	-.250		
.25	-.072	-.099	-.131	-.167	.25	-.147	-.196	-.252	-.312		
.30	-.084	-.114	-.150	-.190	.30	-.175	-.232	-.297	-.366		
.35	-.093	-.127	-.165	-.208	.35	-.200	-.264	-.335	-.410		
.40	-.100	-.135	-.176	-.221	.40	-.220	-.290	-.367	-.447		
.45	-.105	-.142	-.184	-.230	.45	-.237	-.312	-.392	-.476		
.50	-.108	-.146	-.189	-.236	.50	-.251	-.329	-.413	-.499		
.60	-.112	-.149	-.193	-.241	.60	-.271	-.352	-.441	-.530		
.70	-.112	-.150	-.193	-.240	.70	-.282	-.367	-.457	-.548		
.80	-.111	-.150	-.190	-.236	.80	-.288	-.376	-.466	-.558		
.90	-.108	-.145	-.187	-.233	.90	-.290	-.378	-.471	-.563		
1.00	-.106	-.141	-.183	-.228	1.00	-.291	-.379	-.472	-.564		

Table 6.3: Coefficients of $\bar{a}^1(h)$ and $\bar{b}^1(h)$ for a stress field, $\sigma^1(h) = h$ [90]

		Coefficients \bar{a}^1						Coefficients \bar{b}^1			
Hole Depth z/r_m	Hole Radius, r_a/r_m				Hole Depth z/r_m	Hole Radius, r_a/r_m					
	0.30	0.35	0.40	0.45		0.30	0.35	0.40	0.45		
.00	.0000	.0000	.0000	.0000	.00	.0000	.0000	.0000	.0000		
.05	-.0003	-.0004	-.0005	-.0007	.05	-.0005	-.0007	-.0009	-.0012		
.10	-.0012	-.0017	-.0022	-.0029	.10	-.0024	-.0032	-.0042	-.0052		
.15	-.0029	-.0039	-.0052	-.0066	.15	-.0058	-.0077	-.0100	-.0123		
.20	-.0050	-.0068	-.0089	-.0112	.20	-.0105	-.0139	-.0178	-.0218		
.25	-.0075	-.0101	-.0130	-.0161	.25	-.0163	-.0214	-.0270	-.0328		
.30	-.0100	-.0132	-.0169	-.0208	.30	-.0226	-.0295	-.0368	-.0442		
.35	-.0123	-.0162	-.0203	-.0248	.35	-.0292	-.0377	-.0466	-.0556		
.40	-.0143	-.0186	-.0232	-.0281	.40	-.0356	-.0457	-.0560	-.0662		
.45	-.0159	-.0205	-.0254	-.0305	.45	-.0416	-.0532	-.0647	-.0760		
.50	-.0169	-.0219	-.0269	-.0321	.50	-.0469	-.0599	-.0725	-.0846		

The measured strains are decomposed into components in such a way that corresponds to the power series stress field. The actual stress field is determined by

summing the stress fields corresponding to the individual strain relaxation components. For calculation purpose, the only first two terms of power expansion series are considered. The main reason is that the hole drilling method is not reliable for the higher order terms of the series. Therefore, the function values of $\bar{a}^o(h)$, $\bar{b}^o(h)$ and $\bar{a}^1(h)$, $\bar{b}^1(h)$ are considered, as the above power series terms for stresses are not well adapted for accurate results. The maximum depth of the hole below the surface is limited to the $0.5 R_m$, where R_m is the radius of the gage circle.

The transformed strains are calculated by defining as $p(h) = (\varepsilon_1(h) + \varepsilon_3(h))/2$; $q(h) = (\varepsilon_3(h) - \varepsilon_1(h))/2$; $t(h) = (\varepsilon_3(h) + \varepsilon_1(h) - 2\varepsilon_2(h))/2$. The transformed stress variables are defined as $P(h) = (\sigma_3(h) + \sigma_1(h))/2$; $Q(h) = (\sigma_3(h) - \sigma_1(h))/2$ and $T(h) = \tau_{13}(h)$. The transformed variable decouples the stress/strain equations which make it possible to consider transformed stresses or strains independently. The least square analysis is best to perform using "normal equations" [90] to each of the defined transformed strain. The transformed stresses $P(h)$ are calculated from the strains $p(h)$ using:

$$\begin{bmatrix} \Sigma \bar{a}^o(h) \bar{a}^o(h) & \Sigma \bar{a}^o(h) \bar{a}^1(h) \\ \Sigma \bar{a}^1(h) \bar{a}^o(h) & \Sigma \bar{a}^1(h) \bar{a}^1(h) \end{bmatrix} \begin{bmatrix} P^o \\ P^1 \end{bmatrix} = \frac{E}{1+\nu} \begin{bmatrix} \Sigma \bar{a}^o(h) p(h) \\ \Sigma \bar{a}^1(h) p(h) \end{bmatrix} \quad (6.1)$$

The stress function is given by $P(h) = P^o + P^1 h$, where P^o and P^1 , are the first two power series components of the "P" stress field, Σ sign in the equation representing the

summation of the product of the values corresponding to each hole depth of strain measurement. The calculation procedure is performed again for other transformed stresses $Q(h)$ and $T(h)$ using strains $q(h)$ and $t(h)$ respectively, by replacing $\bar{a}(h)$ coefficients with $\bar{b}(h)$ and further omitting the factor $(1+\nu)$ in the equation. The Cartesian stress field components are recovered by using following set of equations.

$$\begin{aligned}\sigma_1(h) &= P(h) - Q(h) \\ \sigma_3(h) &= P(h) + Q(h) \\ \tau_{13}(h) &= T(h)\end{aligned}\tag{6.2}$$

Finally, the principal stresses can be evaluated in terms of the transformed stresses which is given by

$$\sigma_{\max}, \sigma_{\min} = P \pm \sqrt{Q^2 + T^2}\tag{6.3}$$

The advantage of power series is that it uses least square method which offers the best fit curve among the measured strain data. This method is suitable when numbers of strain measurements are made at many increments of hole in depth. The major limitation of this procedure is that it suitable for smoothly varying stress field.

6.8.4 Integral method for stress calculation

In the integral method, it considers that the total strain relaxations of stresses contribute simultaneously at all depths. The application of the integral method is practically possible because of the use of finite element calculations as a calibration procedure. Bijak-Zochowski, Niku-Lari et al. Flaman and Manning [90] did work for its

initial development in this area. Let $\sigma(H)$, is the stress at the depth of H from surface and also assume that biaxial stress field exists i.e. stresses are present in same direction parallel to the surface at all depths. The strain relaxation is measured on each rosette grid for installed strain gages. The measured strain relaxation $\varepsilon(h)$ is the integral of infinitesimal strain relaxation components from the stresses at all range of depths due to the drilling hole depth of h .

$$\varepsilon(h) = \frac{1+\nu}{E} \int_0^h \hat{A}(H, h) \sigma(H) dH, \quad 0 \leq H \leq h \quad (6.4)$$

Since the use of transformed variables decouples the stress/strain equations which make it possible to consider the each transformed stress or strain independently of the others. It is convenient to work with the transformed stress and strain variables. Consider the transformed strain $p(h)$, measured after drilling of hole depth h and the corresponding transformed stress $P(H)$ within the range of $0 \leq H \leq h$ is calculated by the use of integral method as.

$$p(h) = \frac{1+\nu}{E} \int_0^h \hat{A}(H, h) P(H) dH \quad (6.5)$$

where $\hat{A}(H, h)$ is the strain relaxation per unit depth caused by a unit stress at depth H , when the hole depth is h . The strain relaxation function $\hat{A}(H, h)$ is very difficult to calculate experimentally. However, it is possible to evaluate the function with the aid of finite element method. The unknown transformed stress field $P(H)$ can be determined by

the solving the integral Eq. (6.5). It is assumed that solution exists and unique. Since the strain relaxation are measured in the discrete increments of depth, $h_i=1,2,\dots,n$ so the discrete form of Eq. (6.5) is given below.

$$\sum_{j=1}^{j=i} \bar{a}_{ij} P_j = \frac{E}{1+\nu} p_i, \quad 1 \leq j \leq i \leq n \quad (6.6)$$

where, n is the total hole depth increments, \bar{a}_{ij} strain relaxation due to a unit stress within increment j of a hole i increments deep, p_i transformed strain after i^{th} increment hole depth, P_i transformed stress within the j^{th} hole depth increment. The relationship between the coefficients and the strain relaxation function $\hat{A}(H, h)$ is

$$\bar{a}_{ij} = \int_{H_{j-1}}^{H_j} \hat{A}(H, h_i) dH \quad (6.7)$$

The transformed stress and strain vectors, \mathbf{P} , \mathbf{Q} , \mathbf{T} and \mathbf{p} , \mathbf{q} , \mathbf{t} are written in the matrix notation. Similarly, Eq.(6.6) and the other two transformed stresses become

$$\begin{aligned} \bar{a}\mathbf{P} &= E\mathbf{p}/1+\nu \\ \bar{b}\mathbf{Q} &= E\mathbf{q} \\ \bar{b}\mathbf{T} &= E\mathbf{t} \end{aligned} \quad (6.8)$$

where, the matrix \bar{b} contains the coefficient of pure shear stress field corresponding to strain relaxation function $\hat{B}(H, h)$ for a hole drilling. A step wise approximate solution for the stress variation along the depth can be found using this method. The non- uniform strain response is captured within increments on the basis of increased sensitivity to the

stresses closer to the surface. The discrete strain relaxation matrices \bar{a} and \bar{b} are lower triangular. The Cartesian stress components are calculated by using the Eq.(6.2) and corresponding principal stress field is determined by Eq.(6.3).

The measured residual stresses at different locations using uniform, power and integral method are shown in Fig. 6.10. Few positions on the inner and outer side are selected. It is observed that the calculated residual stresses through uniform method are same along depth and does not provide the spatial resolution. The measured stresses using power method vary linearly along depth. The observed variation is either increasing or decreasing in the depth. However, at the location of 4 and 5, the calculated minimum principal stress distribution using power and uniform method are found to be almost same along depth. The distributions of stresses using integral method are fluctuating in the depth. The calculated stresses with this method are randomly varying about the power method stress distribution. The close observation gives the idea that the power method provides the mean variation of the integral method. In the estimation of non-uniform residual stress distribution, power series is an appropriate choice as it less sensitive to experimental errors than the integral method and provide smooth variation in depth.

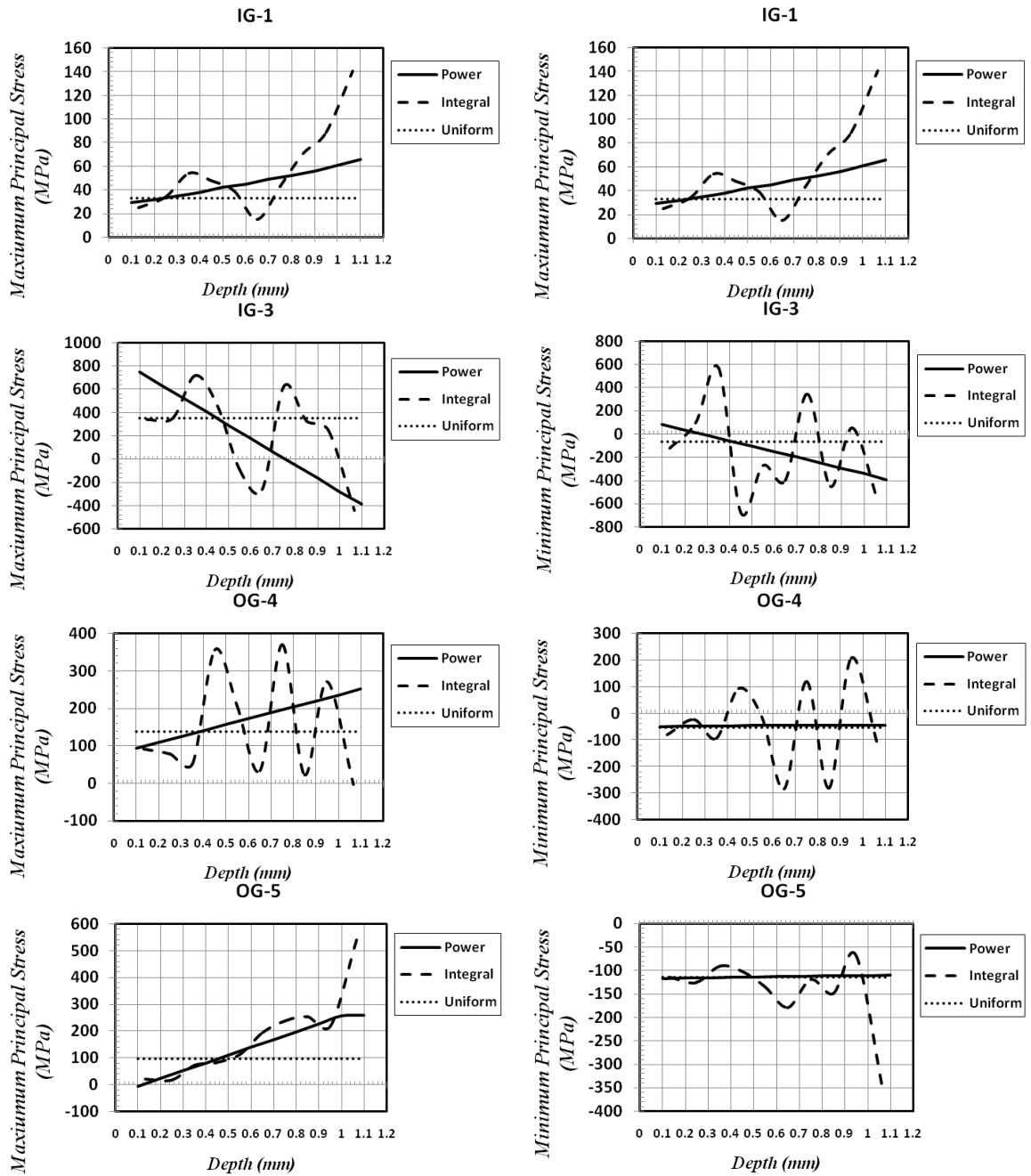


Fig. 6.10: Residual stress using different methods

6.9 RESULTS AND DISCUSSION

The principal stress distribution at different location of gages is anticipated by using the power series method from the measured strain data of the respective gage. The interior stress distributions are calculated below the surface from the depth of 0.1 *mm* to 1.1 *mm*. The maximum and minimum principal stresses are for the inner gages at the location of 1, 2, 4 and 5 are plotted. The word IG stands for the gages mounted on the inner side of the pipe. The maximum and minimum principal stress distribution can be seen in the Fig. 6.11. The trend of maximum principal stresses for IG-1 and IG-5 are increasing. At IG-1, the stress is varying linearly from 29 MPa to 66 MPa while for IG-5, the stress is varying along depth from 24 MPa to 264 MPa. The maximum stresses at both locations are observed at their maximum depth. The observed slope of stress distribution at IG-5 is comparatively higher than the location IG-2. Therefore, at maximum depth both have different magnitudes while starting from minimum depth having almost same magnitude. The location IG-2 and IG-4 are relative nearer to the weld line. The opposite trends are observed at these positions. At location IG-2, the stress is decreasing linearly from 133 MPa to -13 MPa as with increase of depth. The sharp increasing trend is found at IG- 4 from 7 MPa to 411 MPa with continuous increase in depth. The stresses are comparatively different near to the surface and at the full depth on these positions.

The minimum residual principal stress at location IG-1 and IG-5 are exhibiting the same trend. The nature of stresses changes along depth from highly compressive to

relatively low compressive or tensile stress. The stresses are compressive of magnitude -111 MPa and -121 MPa at depth of 0.1 mm while at full depth it is found to be 19MPa and -25MPa at IG-1 and IG-5 respectively. The stress value at location IG-2 and IG-4 are varying oppositely with the increasing depth. The stress values of IG-2 vary -63 MPa to -27 MPa while at IG-4 these values are changing from 29 MPa to -103 MPa. The nature of stresses at these locations is compressive at depth of 1.1 mm while near to the surface stresses are converse to each other.

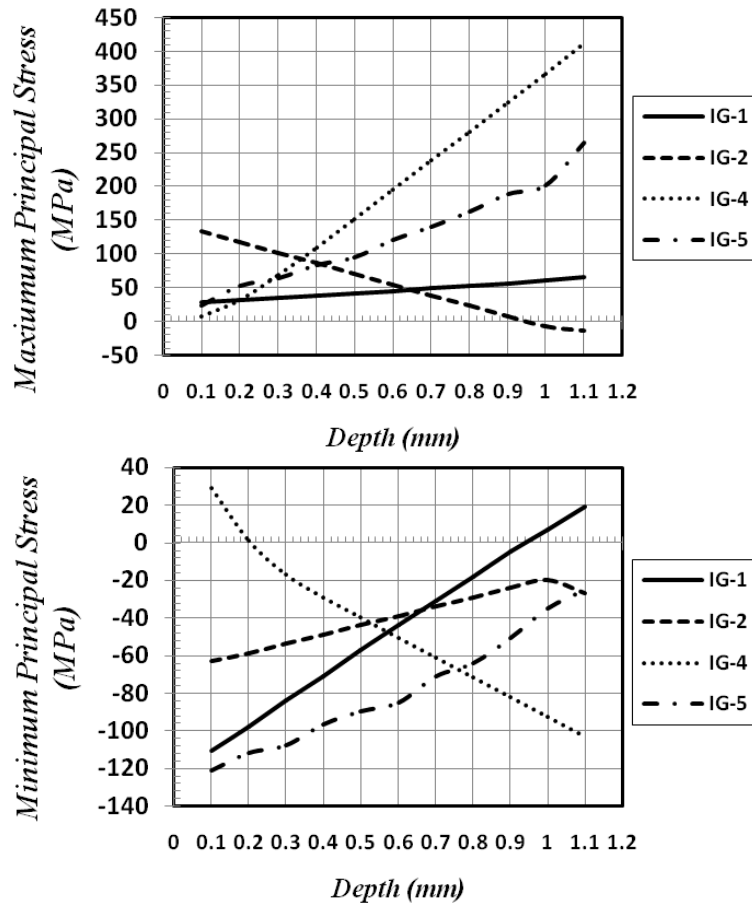


Fig. 6.11: Principal stresses along depth for Inner gages

For outer gages maximum and minimum principal stresses along depth are calculated and shown in the Fig. 6.12. The word OG stands to represent outer gages. The linearly increasing trend for all location is observed. The maximum stresses are found at the full depth. The stress range values along depth of OG-1 and OG- 5 are almost similar. The stress at OG-1 varies from 25 MPa to 240 MPa and at OG-5 it varies from -5 to 258 MPa. The stress variation for location OG-2 and OG-4 are also increasing which is in contrast with the observed trend on the inner side. The stress values for OG-2 and OG-4 at depth of 0.1 *mm* are found to be 64 MPa and 94 MPa while at their full depth they have been increased to 225MPa and 253 MPa respectively. The maximum principal stress on inner side is seen at IG-4 at its complete depth is 411 MPa which is comparatively higher to all positions. However, on the outer side these values are marginally close at full depth.

The minimum principal stresses for OG-4 and OG-5 are slightly increasing with small slope. Therefore very small variation in stress is observed along depth. The stress variation is seen at OG-4 is -49 MPa to -44 MPa and at OG-5 is -118MPa to -110 MPa. The linearly decreasing trend is observed for location OG-1 and OG-2. On these positions, compressive stress of -70 MPa is found at maximum depth. However, at 0.1 *mm* depth stresses are different in values which are -23 MPa and 2 MPa respectively. The minimum principal stresses on outer side are compressive in nature for all location at their full depth.

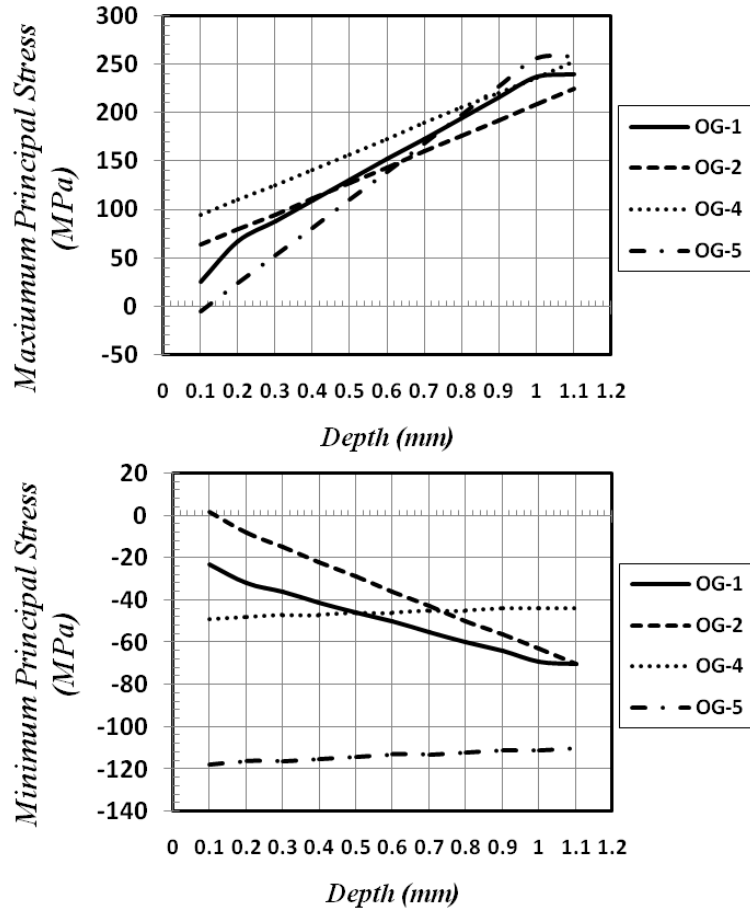


Fig. 6.12: Principal stresses along depth for Outer gages

The maximum and minimum principal stresses are shown in Fig. 6.13 presenting the variation along depth at location 3 for both inner and outer sides. The maximum principal stresses are decreasing linearly for IG-3 and OG-3 positions with the increase of drilled depth. The tensile stresses are present near to the surface while near to depth are compressive. For IG-3, the stress changes tensile to compressive at the depth of 0.75 mm but for OG-3 it changes at 0.9 mm . The value of stresses at 0.1 mm and 1.1 mm for IG-3 and OG-3 are 746 MPa , -385 MPa and 551 MPa , -136 MPa respectively. The slope of IG-3 is sharp as compared to OG-3. Therefore, stresses at OG-3 are less tensile and less compressive than IG-3, near to surface and at full depth respectively.

The minimum principal stresses are also decreasing with the increasing depth for both locations. The compressive nature of stress is observed at full depth of IG-3 and OG-3 with value of -393 MPa and -397 MPa respectively. The stress value at 0.1 mm is tensile for IG-3 and compressive for OG-3 with value of 81 MPa and -21 MPa respectively. The tensile to compressive stress of IG-3 changes at depth of 0.27 mm. The decreasing slope of OG-3 is sharp after 0.5 mm as compared to IG-3 but before this depth it is not decreasing significantly.

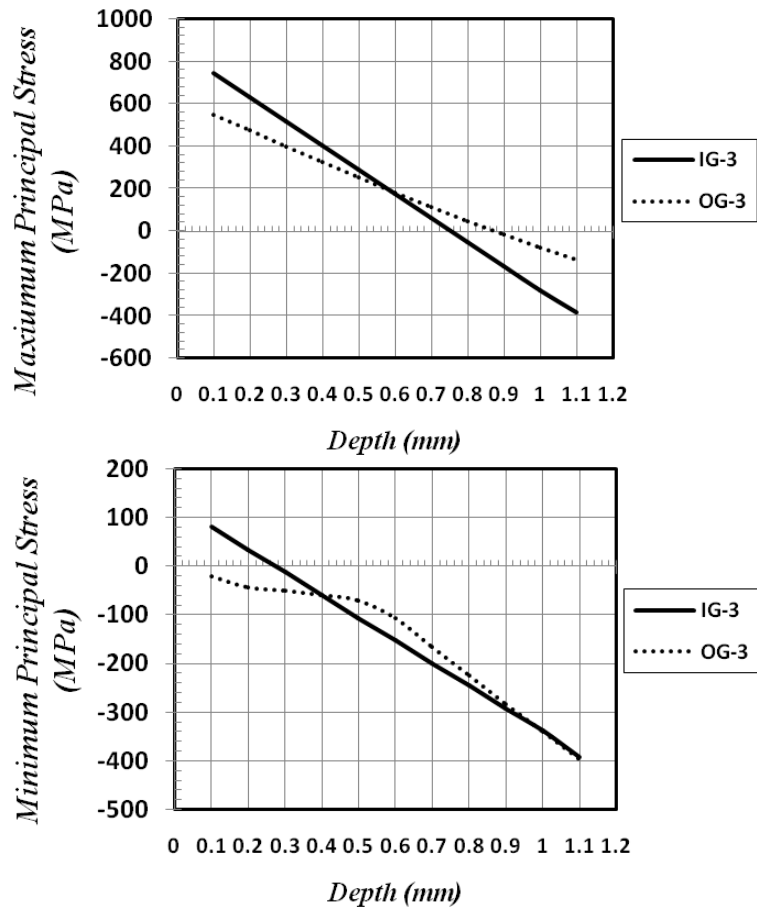


Fig. 6.13: Principal stresses along depth for IG-3 and OG-3

6.10 COMPARISON WITH FE RESULTS

6.10.1 Finite element with uniform method

The finite element and experimental results are plotted for inner and outer side. The maximum and minimum principle stresses are shown for each side in Fig. 6.14 and Fig. 6.15. It is found that 1st principal stress values on both sides are high near to the welding region which shows that tensile residual stress exist on the weld line. The 1st principal residual stress decreases on both side of weld line as moving away from it which shows that the tensile nature of stress vanishes away from the weld line. These tensile stress approaches to the yield strength of the material on the both inner and outer side of the weld line near to the weld bead. Therefore, these stresses are the major cause of cold cracking and stress corrosion cracking in the welded components. On the outer side, more tensile stress exists on the weld toe than the weld centre which is because of metal shrinkage between the weld bead and the groove face. However, on the inner side such peak is not observed because of the reheating of second arc unit and redistribution of stresses.

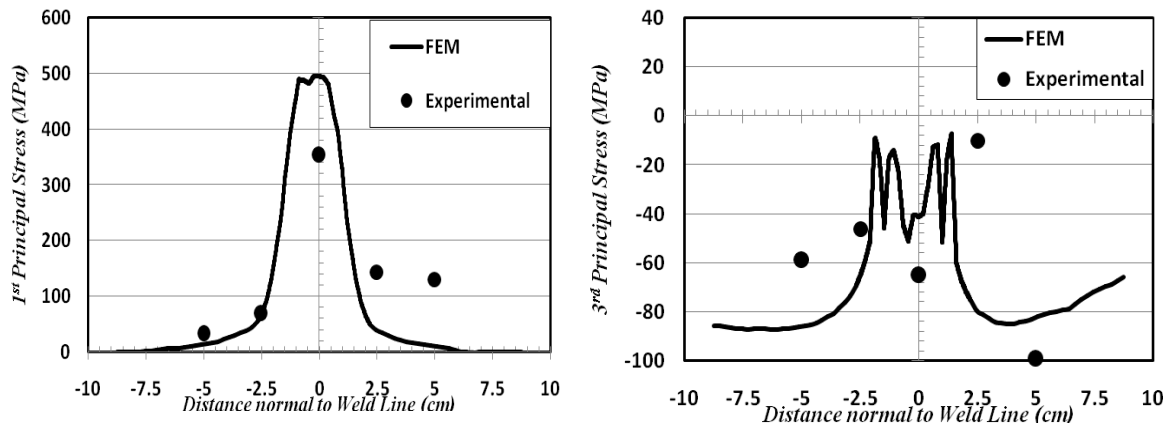


Fig. 6.14: Residual stress distribution on inner side using uniform method

The compressive 3rd principal stress of high magnitude exists in the weld and away from the weld. On the outer side, the compressive stress value in the weld line is relatively more than the inner side. The compressive stress on inner side is about -40 MPa while on outer side it is found to be -120 MPa. The reheating during the top welding has considerably reduced the stress on the inner side. The far away from the weld centre line, the tensile 1st principal stresses have low value while the compressive 3rd principal stresses have dominant influence. On both sides of the welded zone, the 3rd principal stresses are compressive in nature but beyond 2.5 cm distance from the centre line on inner side, more compressive stress is observed than weld.

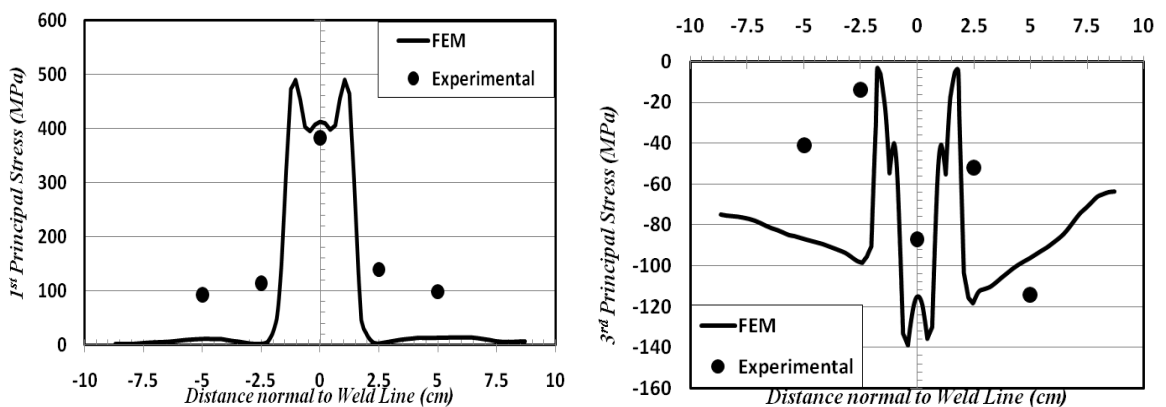


Fig. 6.15: Residual stress distribution on outer side using uniform method

The experimental calculated stresses are plotted for each strain gage. It can be seen that the trend of the experimental results seem to follow the outcomes of simulation. However, the difference in the values is due to the absence of forming process of sheet bending into pipe in FE model. The pipe forming strain is the basis of variation between the results. The other causes of variation can also be due to the machining and cutting processes after welding such as grinding, flame cutting of pipe ring etc. Beside all of these, experimental uncertainty errors and human intervention may also be the reason of the difference between the results. It is observed that variation between the FE results and experimental results are in the range of 20 to 100MPa. However, the overall trend is clearly depicted by the experimental results, which shows the agreement of weld stresses in the pipe. Therefore, it is evident that the current model has been validated on basis of experimental data.

The comparison between the FE prediction and experimentally calculated values has been made for inner and outer side gages in the Table 6.4 and Table 6.5 respectively.

Table 6.4: Inner gage FE and experimental data

Strain Gage on Inner side	1 st Principal Stress (MPa)			3 rd Principal Stress (MPa)		
	FE Prediction	Experimental	Absolute Diff.	FE Prediction	Experimental	Absolute Diff.
IG-1	13.20	33	19.8	-85.98	-59	26.98
IG-2	67.10	69	1.9	-65.13	-46	19.13
IG-3	494.61	353	141.61	-41.03	-65	23.97
IG-4	39.99	144	104.01	-79.62	-10	69.62
IG-5	10.05	131	120.95	-81.93	-99	17.07

Table 6.5: Outer gage FE and experimental data

Strain Gage on Inner side	1 st Principal Stress (MPa)			3 rd Principal Stress (MPa)		
	FE Prediction	Experimental	Absolute Diff.	FE Prediction	Experimental	Absolute Diff.
OG-1	11.08	92	80.92	-87.09	-41	46.09
OG-2	4.30	114	109.7	-95.83	-14	81.83
OG-3	408.83	383	25.83	-120.88	-87	33.88
OG-4	3.94	139	135.06	-112.66	-52	60.6
OG-5	13.23	98	84.77	-94.58	-114	19.42

The magnitude comparison between the FE prediction and experimental results for inner and outer gages can be seen in Fig. 6.16 and Fig. 6.17. It can be seen that the variation between their results is least for IG-3 and OG-3 than the other location of gages.

This is due the reason that at this location the gage is mounted on the welded position. The weld residual stresses have the dominant influence on all other manufacturing processes at this site. Since the other locations are not sufficiently affected due to the heat of welding. Therefore, considerable errors are present between the simulation results and experimental measurements. The marginal influence of other manufacturing processes causes the variation between the results.

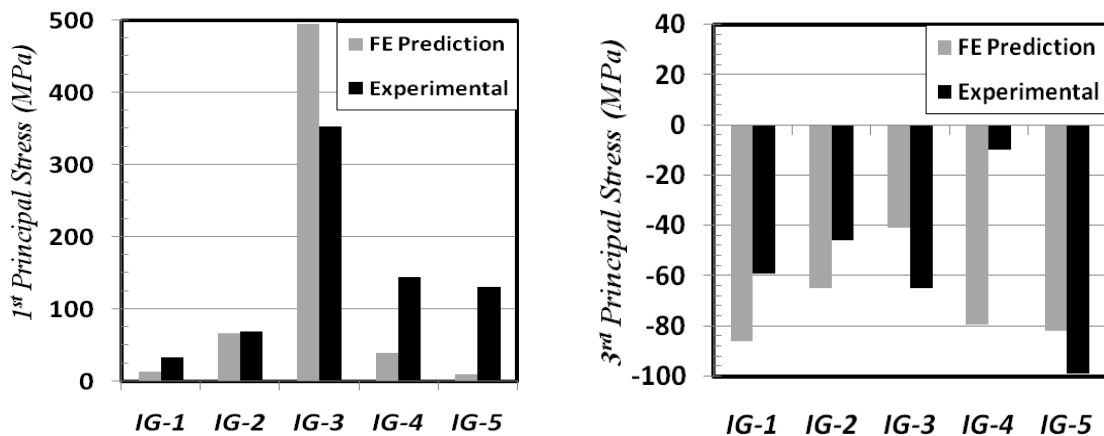


Fig. 6.16: Comparison for inner gages

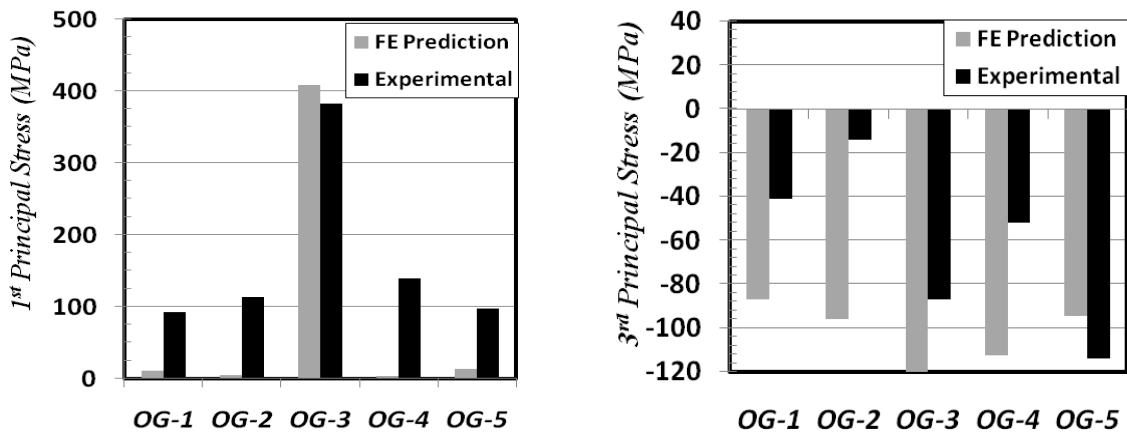


Fig. 6.17: Comparison for outer gages

The von Mises yield criterion suggests whether the yielding in the material has been initiated under the stress state or not. According to von Mises yield criteria, yielding

occurs at any point in material when the distortion energy per unit volume for a state of combined stresses equals that is associated with yielding in simple tension test [92].

Mathematically, the von Mises criterion for plane stress condition is given by

$$\sigma_{von}^2 = \sigma_{max}^2 - \sigma_{max}\sigma_{min} + \sigma_{min}^2 \quad (6.9)$$

The von Mises residual stress is calculated for FE and experimental results for both inner and outer gages as shown in Table 6.6 and

Table 6.7 respectively using plane stress condition. The maximum von Mises stress is found at the IG-3 for inner side and OG-3 for the outer side. The experimentally calculated von Mises stress value reaches 80% and 90% of the yield strength of the material for inner and outer side respectively. The large local plastic deformation occurs due to thermal heating and subsequent cooling at the weld the location. Therefore, von Mises stresses are high at these positions. The other locations are not significantly affected due to the thermal heating, relatively lower values of von Mises stresses are observed.

Table 6.6: von Mises stress comparison for Inner gages

Stain Gage	FE Von Mises stress (MPa)	Experimental Von Mises stress (MPa)	Absolute Difference (MPa)
IG-1	93.29	80.73	12.56
IG-2	114.52	100.25	14.27
IG-3	516.35	389.59	126.76
IG-4	105.47	149.25	43.78
IG-5	87.39	199.83	112.44

Table 6.7: von Mises stress comparison for Outer gages

Stain Gage	FE Von Mises stress (MPa)	Experimental Von Mises stress (MPa)	Absolute Difference (MPa)
OG-1	93.13	117.97	24.84
OG-2	98.06	121.61	23.54
OG-3	480.80	433.10	47.70
OG-4	114.69	171.04	56.35
OG-5	101.85	183.77	81.92

6.10.2 Finite element with power method

Using the power series method, the residual stresses are calculated near to the surface at 0.1 mm and the comparison has been made with FE results. It can be seen in the Fig. 6.18 and Fig. 6.19. The experimental 1st principal stress values on the inner and outer side are over estimated at the weld line. The calculated values on inner and outer side are found to be 746 MPa and 551 MPa respectively. However, good agreement can be seen far away from the weld line on both sides as the stresses are not high. The 3rd principal stresses on the weld line on both sides and also at 2.5 cm distance on the inner side are over predicted in comparison to the FE results. This is due to the reason that the power

series method forms the best fit curve to the measured strains after drilling with the least square procedure which in results gives over estimated values at the weld. In uniform method, the trend is observed to be predicted more reasonably than power series method. However, this method doesn't provide any spatial variation in depth. Using power series method, the results are observed to be deteriorated due to over estimation of stresses at few locations. Therefore, the uniform method is the reasonable choice for validation purpose with FE results.

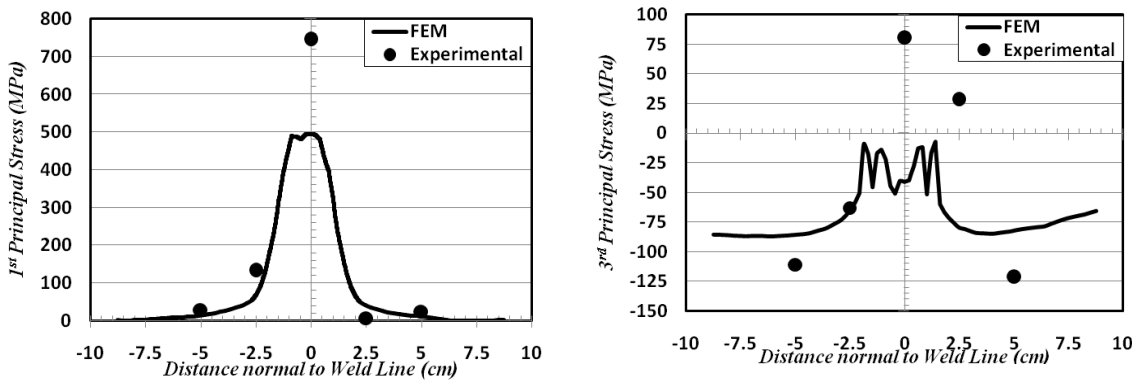


Fig. 6.18: Residual stress distribution on inner side using power series method

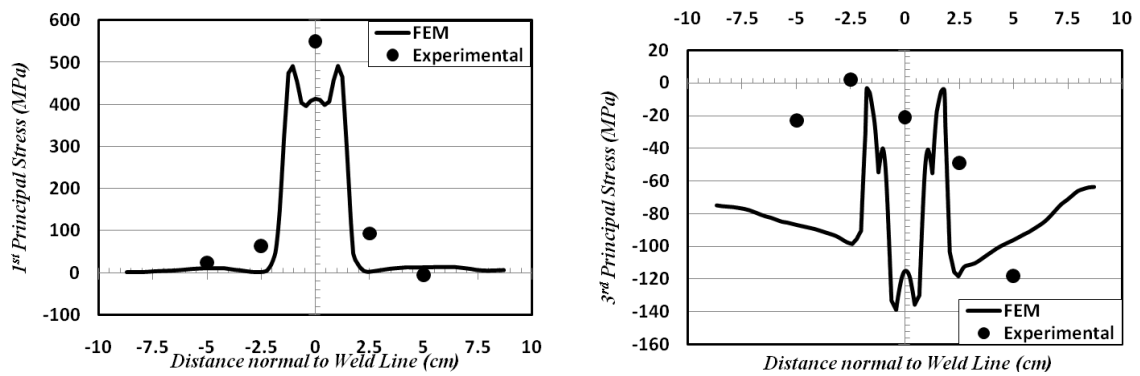


Fig. 6.19: Residual stress distribution on outer side using power series method

6.11 CONCLUSION

An experimental setup has been arranged for measuring the residual stresses in the API 5L X70 grade steel using hole drilling strain gage method. The following conclusions can be drawn after the investigation of the residual stresses.

- The calculated von Mises stresses using plane stress, are higher on the weld location, than any of other location because of local plastic deformation due nonlinear thermal heating and cooling.
- The observed variation at different locations between the FE model and experimental results are in the range of 20 to 100 MPa because of the absence of all other process in the current FE model such as forming, flame cutting etc.
- The 1st principal stresses are highly tensile at the weld and nearby while it is diminished far away from the weld centre line.
- The 3rd principal stresses are highly compressive at the weld centre and beyond the 2.5 cm distance from the weld centre.
- The power series method is suitable as it provide smooth linear variation along depth while the integral method is observed to be fluctuating. The uniform method doesn't provide any variation in depth.
- At the weld location, the power series method estimate the over predicted values of 1st and 3rd principal stresses while reasonable predicts the stresses away from weld.

- The uniform method is good choice for validation of FE results as the power method deteriorates the results due to over estimation of stresses.

CHAPTER 7 CONCLUSION AND RECOMMENDATIONS

Spiral welded pipes are manufactured through the coiled skelp, continuously fed into spiral forming unit, bended into a tube with abutting edges of strip are progressively welded. These pipes are effectively meeting the industrial purposes. The increase in their demand is due to high production rate, which is characterized due to the fact the various pipe diameters can be prepared from single strip just by modifying the approach angle of strip into roller. These pipes find their application in water supply, gas transmission, oil industry, petrochemical plants. The major problem associated in these pipes is due to welding which makes the weld zone to be susceptible and critical region. The high residual stresses are generated in pipes which are the causes of detrimental effects in the pipe. These effects can decrease performance and strength of the pipe, minimize its fatigue life and initiate stress corrosion cracking. The reduction of residual stresses in the pipe will enhanced its acceptance worldwide even for the critical services. Therefore, consideration has been made to the residual stress in spiral pipes as it play important role on the working condition and the integrity of the pipe.

The effort in the current study is also made for the reason to understand the distribution of residual stresses due to welding in the manufacturing of the spiral pipes and analyze their consequences. The residual stresses in the pipes are dependent upon the

various process parameters which influence the distribution of stresses. Therefore, to control the residual stresses, it is necessary to control the process variables. Some parameters are weld speed, heat input, dimension of pipe, material grade, weld root geometry and welding type. To analyze the effects of welding on the spiral, a comprehensive Finite Element model is developed. The three dimensional computational model can efficiently predict residual stresses associated due to welding. The non-uniform temperature and complex stress distribution are obtained from the model. For obtaining accurate stress distribution in the model, filler metal addition is also implemented. The thermo-mechanical and metallurgical processes are occurring in welding, cause localized plastic deformations and plastic strains, are governed by material behavior formulation with associated strain hardening law. A new methodology for implementation of distributed flux using Goldak heat source model is adopted. FE method is found as a reliable tool for investigation of residual stress, temperature evolution, deformation, distortion and shrinkage in the pipe. However, the computational cost is required for solving the nonlinear three dimensional large deformation problem of welding.

Double submerged arc welding (DSAW) is most commonly used in the production of spiral pipes. The welding is performed on the both side of pipes. Prior to welding on the outer side of pipe, it has already been started on the inner side. The difference in the time between the outer and inner side welding is present which referred as time lag in the fabrication of the pipe. The highly tensile stress region occurs on cooling near to weld because of intense thermal heating. The welding of mild steel is performed in the time lag

analysis. In the vicinity of the weld the stress level is reached to 280 MPa which close to the material yield strength. However, the residual stresses on the inner side are found lower than the outer side. The major reason is that the welding on outer side served as the purpose of mitigation of stresses on the inner side because of generated reheating temperature. The observed distribution of temperature, fusion zone (FZ), HAZ dimension and residual stresses are verified through manufacturer weld data sheet and literature. The established model is found in good agreement. The study also shows that the maximum plastic strain is observed at the wall of groove adjoining with base metal. The time lag analysis showed that the highly stressed area can expand or contract due to variation in the difference of time. However, the insignificant variation is found in the value of residual stress and plastic strains.

The hoop stress are playing significant role in the performance of pipes. The combined stress state exists, generated due to number of process involved in the manufacturing of spiral pipes. However, in the current study only weld induced imperfections are analyzed. The hoop residual stress distribution is investigated in the X70 grade pipe. It is found that the major portion of pipe has insignificant residual hoop stress except in the vicinity of weld. The split ring test is modelled and analyzed in the current work. The major contribution is to explore that whether the split ring test can estimate the weld induced thermal stresses. It is observed that the split ring test has certain limitation and it is not successfully applicable for determining the weld residual stresses. However, the stress release due to longitudinal splitting in split ring test reasonable agrees with FE and theoretical calculated stress. It is also analyzed that the

maximum stress release occurs at the weld location. The hoop membrane and hoop bending stress are calculated along the thickness of the pipe for comparison and discussion. This is because that the theoretical equations are based on the linear stress distribution along thickness. The linearization of finite element calculated stress is possible by decomposing its distribution into structurally equivalent membrane and hoop stress components.

The experimentation has been performed on X70 grade steel pipe using a semi-destructive technique that is hole drilling strain gage method. A small blind hole is drilled into the specimen through the exact centre of gage and the strains are measured due relaxation of stresses. The purpose of this study is to validate the model using experimental data and analyze the stress distribution along drilled hole depth. The model is successfully validated through experiments with the variation of 20 to 100 MPa because of other processes involved in the manufacturing of stresses. Different stress calculation procedure such as uniform method, power series method, and integral method are used for examining the stresses. It is observed that the calculated residual stress using uniform method don't provide any spatial resolution along depth but it is suitable choice for validation purpose because of average residual stress calculated along the depth. The discrepancy is observed at few locations due to overestimation of stresses using power series method. Therefore, this method is not found suitable for verification. In the study it is observed that the integral method gives fluctuating stresses at each location. Therefore, the power series method is found most appropriate choice as it fits least square curve to the measured strains and provides linearly varying stress distribution along depth. This

method has the capability to identify the localized stress in weld which can't be captured by split ring test. In general, it is observed that the weld residual stresses can be estimated accurately using hole drilling method which make it a successful tool for research.

Still spiral pipe industry is facing challenges to overcome the residual stresses. The most appropriate way is to develop the technologies to avoid or reduce the residual stresses during manufacturing. For more accurate modelling, it is possible to consider phase transformation, chemical composition of alloy steel, plasticity transformation and include volumetric change due heating. The forming strains in spiral pipes due bending by rollers can be considered in FE model for improvement in stress distributions. The development in the work can be extended to overcome the limitation in split ring test by finding appropriate the calibration coefficients and make it useful test for residual stress measurement at weld. During service, the pipes are subject to loading and high pressure. The life prediction and crack propagation can be estimated using strain based fatigue life models or through fracture mechanics approach. The advent ways for mitigation of stresses can be found by analyzing the cold expansion of pipes by introducing the concept of autofrettage. The stress corrosion cracking (SCC), sulfide stress cracking (SSC), and corrosion resistance can also be focused.

REFERENCES

- [1] “3E Methods of Manufacturing Steel Tubes and Pipe” [Online]. Available: http://www.jfe-21st-cf.or.jp/chapter_3/3e_1_img.html. [Accessed: 13-Apr-2013].
- [2] ArcelorMittal, Spirally welded steel pipes, Mannesmannweg 5, 4794 SL Heijningen, The Netherlands.
- [3] Argyris J., Szimmat J., and Willam K., 1982, “Computational aspects of welding stress analysis,” *Comput. Methods Appl. Mech. Eng.*, **33**(1-3), pp. 635–665.
- [4] Teng T.-L., and Lin C.-C., 1998, “Effect of welding conditions on residual stresses due to butt welds,” *Int. J. Press. Vessel. Pip.*, **75**(12), pp. 857–864.
- [5] Zhu X. K., and Chao Y. J., 2002, “Effects of temperature-dependent material properties on welding simulation,” *Comput. Struct.*, **80**(11), pp. 967–976.
- [6] Teng T.-L., Chang P.-H., and Tseng W.-C., 2003, “Effect of welding sequences on residual stresses,” *Comput. Struct.*, **81**(5), pp. 273–286.
- [7] Mahapatra M. M., Datta G. L., Pradhan B., and Mandal N. R., 2006, “Three-dimensional finite element analysis to predict the effects of SAW process parameters on temperature distribution and angular distortions in single-pass butt joints with top and bottom reinforcements,” *Int. J. Press. Vessel. Pip.*, **83**, pp. 721–729.
- [8] Lindgren L.-E., 2006, “Numerical modelling of welding,” *Comput. Methods Appl. Mech. Eng.*, **195**(48-49), pp. 6710–6736.
- [9] Wang J., Rashed S., and Murakawa H., 2011, “Investigation of Buckling Deformation of Thin Plate Welded Structures,” *Proceeding of 21st International Society of Ocean and Polar Engineering*, Hawaii, USA, pp. 125–31.
- [10] Deng D., and Murakawa H., 2008, “Prediction of welding distortion and residual stress in a thin plate butt-welded joint,” *Comput. Mater. Sci.*, **43**(2), pp. 353–365.

- [11] Long H., Gery D., Carlier a., and Maropoulos P. G., 2009, "Prediction of welding distortion in butt joint of thin plates," *Mater. Des.*, **30**(10), pp. 4126–4135.
- [12] Zhang H. J., Zhang G. J., Cai C. B., Gao H. M., and Wu L., 2009, "Numerical simulation of three-dimension stress field in double-sided double arc multipass welding process," *Mater. Sci. Eng. A*, **499**(1-2), pp. 309–314.
- [13] Zhang Y. M., and Zhang S. B., 1998, "Double-sided arc welding increases weld joint penetration," *Weld. J.*, **77**(6), pp. 57–61.
- [14] Yilbas B. S., Arif a. F. M., and Abdul Aleem B. J., 2010, "Laser welding of low carbon steel and thermal stress analysis," *Opt. Laser Technol.*, **42**(5), pp. 760–768.
- [15] Attarha M. J., and Sattari-Far I., 2011, "Study on welding temperature distribution in thin welded plates through experimental measurements and finite element simulation," *J. Mater. Process. Technol.*, **211**(4), pp. 688–694.
- [16] Deng D., and Kiyoshima S., 2011, "FEM analysis of residual stress distribution near weld start/end location in thick plates," *Comput. Mater. Sci.*, **50**(8), pp. 2459–2469.
- [17] Kumaresan D., Asraff a. K., and Muthukumar R., 2011, "Numerical Investigation on Heat Transfer and Residual Stress in a Butt Welded Plate," *J. Press. Vessel Technol.*, **133**(4), p. 041206.
- [18] Smith M. C., Bouchard P. J., Turski M., Edwards L., and Dennis R. J., 2012, "Accurate prediction of residual stress in stainless steel welds," *Comput. Mater. Sci.*, **54**, pp. 312–328.
- [19] Jiang W., Zhang Y., and Woo W., 2012, "Using heat sink technology to decrease residual stress in 316L stainless steel welding joint: Finite element simulation," *Int. J. Press. Vessel. Pip.*, **92**, pp. 56–62.
- [20] Heinze C., Schwenk C., and Rethmeier M., 2012, "The effect of tack welding on numerically calculated welding-induced distortion," *J. Mater. Process. Technol.*, **212**(1), pp. 308–314.
- [21] Javadi Y., Akhlaghi M., and Najafabadi M. A., 2013, "Using finite element and ultrasonic method to evaluate welding longitudinal residual stress through the thickness in austenitic stainless steel plates," *Mater. Des.*, **45**, pp. 628–642.
- [22] Josefson B. L., and Karlsson C. T., 1989, "FE-calculated stresses in a multi-pass butt-welded pipe—A simplified approach," *Int. J. Press. Vessel. Pip.*, **38**(3), pp. 227–243.

- [23] Teng T.-L., and Chang P., 1997, "A study of residual stresses in multi-pass girth-butt welded pipes," *Int. J. Press. Vessel. Pip.*, **74**(1), pp. 59–70.
- [24] Teng T., and Chang P., 1998, "Three-dimensional thermomechanical analysis of circumferentially welded thin-walled pipes," *Int. J. Press. Vessel. Pip.*, **75**(3), pp. 237–247.
- [25] Brickstad B., and Josefson B. L., 1998, "A parametric study of residual stresses in multi-pass butt-welded stainless steel pipes," *Int. J. Press. Vessel. Pip.*, **75**(1), pp. 11–25.
- [26] Yang Y.-S., and Lee S.-H., 1997, "A study on the mechanical stress relieving in a butt-welded-pipe," *Int. J. Press. Vessel. Pip.*, **73**(3), pp. 175–182.
- [27] Basavaraju C., 2000, "Simplified analysis of shrinkage in pipe to pipe butt welds," *Nucl. Eng. Des.*, **197**(3), pp. 239–247.
- [28] Runnemalm H., and Hyun S., 2000, "Three-dimensional welding analysis using an adaptive mesh scheme," *Comput. Methods Appl. Mech. Eng.*, **189**(2), pp. 515–523.
- [29] Sabapathy P. N., Wahab M. A., and Painter M. J., 2001, "Numerical models of in-service welding of gas pipelines," *J. Mater. Process. Technol.*, **118**(1-3), pp. 14–21.
- [30] Abid M., and Siddique M., 2005, "Numerical simulation to study the effect of tack welds and root gap on welding deformations and residual stresses of a pipe-flange joint," *Int. J. Press. Vessel. Pip.*, **82**(11), pp. 860–871.
- [31] Yaghi A. H., Hyde T. H., Becker A. A., Williams J. A., and Sun W., 2005, "Residual stress simulation in welded sections of P91 pipes," *J. Mater. Process. Technol.*, **167**(2-3), pp. 480–487.
- [32] Deng D., and Murakawa H., 2006, "Numerical simulation of temperature field and residual stress in multi-pass welds in stainless steel pipe and comparison with experimental measurements," *Comput. Mater. Sci.*, **37**(3), pp. 269–277.
- [33] Deng D., Murakawa H., and Liang W., 2008, "Numerical and experimental investigations on welding residual stress in multi-pass butt-welded austenitic stainless steel pipe," *Comput. Mater. Sci.*, **42**(2), pp. 234–244.
- [34] Lee C., and Chang K., 2008, "Three-dimensional finite element simulation of residual stresses in circumferential welds of steel pipe including pipe diameter effects," **487**, pp. 210–218.

- [35] Sattari-Far I., and Javadi Y., 2008, "Influence of welding sequence on welding distortions in pipes," *Int. J. Press. Vessel. Pip.*, **85**(4), pp. 265–274.
- [36] Barsoum Z., 2008, "Residual stress analysis and fatigue of multi-pass welded tubular structures," *Eng. Fail. Anal.*, **15**(7), pp. 863–874.
- [37] Malik A. M., Qureshi E. M., Ullah N., and Khan I., 2008, "Thin-Walled Structures Analysis of circumferentially arc welded thin-walled cylinders to investigate the residual stress fields," *Thin-Walled Struct.*, **46**, pp. 1391– 1401.
- [38] Akbari D., and Sattari-Far I., 2009, "Effect of the welding heat input on residual stresses in butt-welds of dissimilar pipe joints," *Int. J. Press. Vessel. Pip.*, **86**(11), pp. 769–776.
- [39] Lee C.-H., Chang K.-H., and Park J.-U., 2013, "Three-dimensional finite element analysis of residual stresses in dissimilar steel pipe welds," *Nucl. Eng. Des.*, **256**, pp. 160–168.
- [40] Chang K.-H., Lee C.-H., Park K.-T., You Y.-J., Joo B.-C., and Jang G.-C., 2010, "Analysis of residual stress in stainless steel pipe weld subject to mechanical axial tension loading," *Int. J. Steel Struct.*, **10**(4), pp. 411–418.
- [41] Deng D., and Kiyoshima S., 2010, "FEM prediction of welding residual stresses in a SUS304 girth-welded pipe with emphasis on stress distribution near weld start/end location," *Comput. Mater. Sci.*, **50**(2), pp. 612–621.
- [42] Deng D., and Kiyoshima S., 2010, "Numerical simulation of residual stresses induced by laser beam welding in a SUS316 stainless steel pipe with considering initial residual stress influences," *Nucl. Eng. Des.*, **240**(4), pp. 688–696.
- [43] Liu C., Zhang J. X., and Xue C. B., 2011, "Numerical investigation on residual stress distribution and evolution during multipass narrow gap welding of thick-walled stainless steel pipes," *Fusion Eng. Des.*, **86**(4-5), pp. 288–295.
- [44] Chen X. M., 2005, "Springback Prediction on Slit-Ring Test," *AIP Conference Proceedings*, AIP, pp. 222–227.
- [45] Foecke T., and Gnaeupel-Herold T., 2006, "Robustness of the sheet metal springback cup test," *Metall. Mater. Trans. A*, **37**(December), pp. 3503–3510.
- [46] Micari F., Forcellese A., Fratini L., Gabrielli F., and Alberti N., 1997, "Springback Evaluation in Fully 3-D Sheet Metal Forming Processes," *CIRP Ann. - Manuf. Technol.*, **46**(1), pp. 167–170.

- [47] Li K. P., Carden W. P., and Wagoner R. H., 2002, "Simulation of springback," *Int. J. Mech. Sci.*, **44**(1), pp. 103–122.
- [48] Greze R., Laurent H., and Manach P. Y., 2007, "Springback study in aluminum alloys based on the Demeri Benchmark Test : influence of material model," *AIP Conf. Proc.*, **907**(2007), pp. 1512–1517.
- [49] Testing M., "Standard Test Method for Evaluating Springback of Sheet Metal Using the Demeri Split Ring Test 1," pp. 1–6.
- [50] Gnaeupel-Herold T., Prask H. J., Fields R. J., Foecke T. J., Xia Z. C., and Lienert U., 2004, "A synchrotron study of residual stresses in a Al6022 deep drawn cup," *Mater. Sci. Eng. A*, **366**(1), pp. 104–113.
- [51] Kessler L., Gerlach J., and Aydin M., 2008, "Springback Simulation with Complex Hardening Material Models," *Proceedings of LS-DYNA Conference, Bamberg, Germany*.
- [52] Laurent H., Grèze R., Manach P. Y., Coër J., Andrade-Campos A., Oliveira M. C., and Menezes L. F., 2009, "Springback of an aluminium alloy in warm forming conditions using the split-ring test," *7th EUROMECH Solid Mech. Conf.*, (September).
- [53] Laurent H., Coër J., Grèze R., Manach P. Y., Andrade-Campos a., Oliveira M. C., and Menezes L. F., 2011, "Mechanical Behaviour and Springback Study of an Aluminium Alloy in Warm Forming Conditions," *ISRN Mech. Eng.*, **2011**, pp. 1–9.
- [54] Laurent H., Grèze R., Oliveira M. C., Menezes L. F., Manach P. Y., and Alves J. L., 2010, "Numerical study of springback using the split-ring test for an AA5754 aluminum alloy," *Finite Elem. Anal. Des.*, **46**(9), pp. 751–759.
- [55] Laurent H., Grèze R., Manach P. Y., and Thuillier S., 2009, "Influence of constitutive model in springback prediction using the split-ring test," *Int. J. Mech. Sci.*, **51**(3), pp. 233–245.
- [56] Niu C., Zang S. L., and Zhang Y., 2012, "Springback Prediction Using the Split-Ring Test Based on a Combined Anisotropic Hardening Model," *Appl. Mech. Mater.*, **217-219**(28), pp. 1375–1380.
- [57] Xia Z. C., 2004, "Springback Behavior of AA6111-T4 with Split-Ring Test," *AIP Conference Proceedings*, AIP, pp. 934–939.

- [58] Wagoner R. H., Lim H., and Lee M.-G., 2012, “Advanced Issues in springback,” *Int. J. Plast.*, pp. 1–18.
- [59] Gnaeupel-Herold T., Foecke T., Prask H. J., and Fields R. J., 2005, “An investigation of springback stresses in AISI-1010 deep drawn cups,” *Mater. Sci. Eng. A*, **399**(1-2), pp. 26–32.
- [60] Kyriakides S., and Corona E., 2007, *Mechanics of Offshore Pipelines*, Elsevier Ltd, Oxford, UK, Burlington, MA.
- [61] Steel F. C. S., 1928, “Estimating the Approximate Residual Circumferential Stress in Straight Thin-walled Tubing 1,” pp. 5–7.
- [62] Totten G. E., Bates C. E., and Clinton N. ., 1993, *Handbook of Quenchants and Quenching Technology*, ASM International, Materials Park.
- [63] Dong P., Hong J. K., Leis B. N., Lopez P. S., Chavela R. G., and Ghenno C. S., 2006, “Computational Simulation of Line-Pipe Fabrication Processes,” Volume 3: Materials and Joining; Pipeline Automation and Measurement; Risk and Reliability, Parts A and B, ASME, pp. 603–612.
- [64] Knoop D.-I. F. M., 2004, “Two-step spiral welded pipe for pipeline applications,” (January), pp. 3–6.
- [65] Arif A. F. M., Al-omari A. S., Yilbas B. S., and Al-nassar Y. N., 2011, “Journal of Materials Processing Technology Thermal stress analysis of spiral laser-welded tube,” *J. Mater. Process. Tech.*, **211**(4), pp. 675–687.
- [66] Forouzan M. R., Nasiri S. M. M., Mokhtari A., Heidari A., and Golestaneh S. J., 2012, “Residual stress prediction in submerged arc welded spiral pipes,” *Mater. Des.*, **33**, pp. 384–394.
- [67] Ginsberg J. H., *Advanced Engineering Dynamics*, Cambridge university press.
- [68] Goldak J., Chakravarti A., and Bibby M., 1984, “A new finite element model for welding heat sources,” *Metall. Trans. B*, **15**(2), pp. 299–305.
- [69] API Line Pipe 01-SAMSS-035, 2010, Saudi Aramco Materials System Specification.
- [70] Masbuschi K., and Martin D. ., 1966, Investigation of residual stresses in steel weldment, Ship Structure Committee Report, SSC-174.

- [71] Tada H., and Paris P. C., 1983, “The stress intensity factor for a crack perpendicular to the welding bead,” *Int. J. Fract.*, **21**(4), pp. 279–284.
- [72] Mollicone P., Camilleri D., Gray T. G. F., and Comlekci T., 2006, “Simple thermo-elastic–plastic models for welding distortion simulation,” *J. Mater. Process. Technol.*, **176**(1-3), pp. 77–86.
- [73] Rosenthal D., 1946, “The Theory of Moving Sources of Heat and Its Application to Metal Treatments,” *Trans. ASME*, **68**, pp. 849–866.
- [74] Kashani M., and Young R., 2008, “Hoop stress approximation in offshore design codes,” *Mar. Struct.*, **21**(2-3), pp. 224–239.
- [75] AWWA Manual, 2004, *Steel pipe: a guide for design and installation*.
- [76] “A Guide To Water Well Casing and Screen Selection - page 7” [Online]. Available: http://www.roscoemoss.com/tech_manuals/gwwc/p7.html. [Accessed: 15-Sep-2013].
- [77] Knoop F. M., and Sommer B., 2004, “Manufacturing and Use of Spiral Welded Pipes for High Pressure Service: State of the Art,” 2004 International Pipeline Conference, Volumes 1, 2, and 3, ASME, pp. 1761–1769.
- [78] Dong P., 2001, “A structural stress definition and numerical implementation for fatigue analysis of welded joints,” *Int. J. Fatigue*, **23**(10), pp. 865–876.
- [79] Rossini N. S., Dassisti M., Benyounis K. Y., and Olabi a. G., 2012, “Methods of measuring residual stresses in components,” *Mater. Des.*, **35**, pp. 572–588.
- [80] Timoshenko S. P., and Goodier J. N., 1970, *Theory of Elasticity*, McGraw-Hill Book Company, New York, USA.
- [81] Amirat A., Mohamed-chateaneuf A., and Chaoui K., 2006, “Reliability assessment of underground pipelines under the combined effect of active corrosion and residual stress,” **83**, pp. 107–117.
- [82] Petrucci G., and Zuccarello B., 1998, “A new calculation procedure for non-uniform residual stress analysis by the hole-drilling method,” *J. Strain Anal. Eng. Des.*, **33**(1), pp. 27–37.
- [83] Wang H., 1979, “The alignment error of the hole-drilling method,” *Exp. Mech.*, pp. 23–27.

- [84] Ajovalasit a, 1979, "Measurement of residual stresses by the hole-drilling method: Influence of hole eccentricity," *J. Strain Anal. Eng. Des.*, **14**(4), pp. 171–178.
- [85] Olabi a. G., Casalino G., Benyounis K. Y., and Rotondo a., 2007, "Minimisation of the residual stress in the heat affected zone by means of numerical methods," *Mater. Des.*, **28**(8), pp. 2295–2302.
- [86] Mathar J., 1934, "Determination of Initial Stresses by Measuring the Deformations Around Drilled Holes," *Trans. ASME* 56, pp. 249–254.
- [87] Measurement of Residual Stresses by the Hole-Drilling Strain Gage Method, Application Note TN-503-6, Document No. 11053, Revision November 2010, Vishay Micro-Measurement Group.
- [88] Schajer G. S., 1981, "Application of Finite Element Calculations to Residual Stress Measurements," *J. Eng. Mater. Technol.*, **103**(2), p. 157.
- [89] ASTM International, 2003, Standard Test Method for Determining Residual Stresses by the Hole-Drilling Strain, ASTM Standard E837, West Conshohocken, PA.
- [90] Schajer G. S., 1988, "Measurement of Non-Uniform Residual Stresses Using the Hole-Drilling Method. Part I—Stress Calculation Procedures," *J. Eng. Mater. Technol.*, **110**(4), p. 338.
- [91] Aoh J.-N., and Wei C.-S., 2002, "On the Improvement of Calibration Coefficients for Hole-Drilling Integral Method: Part I—Analysis of Calibration Coefficients Obtained by a 3-D FEM Model," *J. Eng. Mater. Technol.*, **124**(2), p. 250.
- [92] Park M. K., Sindhu R. A., Lee S. J., Zai B. A., and Mehboob H., 2010, "A residual stress evaluation in laser welded lap joint with hole drilling method," *Int. J. Precis. Eng. Manuf.*, **10**(5), pp. 89–95.

VITAE

Name: Khalid Naseem

Date of Birth: July 12, 1988

Present Address: P.O. Box 8638, King Fahd University of Petroleum and Minerals,
Dhahran 31261, Saudi Arabia

Permanent Address: Ittehad Colony, Street no. 7 near Ittefaq Factory, Kot Lakhpat,
Lahore, Pakistan

Email Address: khalidnasim@kfupm.edu.sa
khalidnasim123@gmail.com

Educational Qualification:

M.S (Mechanical Engineering)
November, 2013
King Fahd University of Petroleum & Minerals,
Dhahran, Saudi Arabia.

B.Sc. (Mechanical Engineering)
July, 2010
University of Engineering and Technology,
Lahore, Pakistan.